

AD 670 191

**TIME DOMAIN STUDIES OF SHORT PERIOD TELESEISMIC P
PHASES**

Peter William Basham

**Arctic Institute of North America
Washington, D. C.**

September 1967

16102901

AFOSR Accession Number - AFOSR 67-2519

TIME DOMAIN STUDIES OF SHORT PERIOD TELESEISMIC P PHASES

Peter William Basham

September 1967

AF - AFOSR - 702 - 67

Project Task 8652

FINAL REPORT

DDC
JUN 14 1968
B

supported by the Advanced Research
and was monitored by the Air Force
research under Grant AF-AFOsr-702-67

document is unlimited

Reproduced by the
CLEARINGHOUSE
for Federal Scientific & Technical
Information Springfield Va. 22151

TIME DOMAIN STUDIES OF SHORT PERIOD TELESEISMIC P PHASES

by

PETER WILLIAM BASHAM

B.A.Sc. University of British Columbia, 1964

A THESIS SUBMITTED IN PARTIAL FULFILMENT
OF THE REQUIREMENTS FOR THE DEGREE OF
MASTER OF APPLIED SCIENCE

in the Department of Geophysics
University of British Columbia

September 1967

ARPA Order Number:	292-63
Project Code Number:	8652
Name of Grantee:	Arctic Institute of North America
Date of Grant:	January 1, 1967
Amount of Grant:	\$15,700
Grant Number:	AF-AFOSR-702-67
Termination of Grant:	August 31, 1967
Project Scientist:	Dr. John C. Reed Washington, D.C. NO 7-1716

Project Title: Effects of Location of Seismographs on
the Records Obtained

Qualified requestors may obtain additional copies from the Defence Documentation Center; All others should apply to the Clearinghouse For Federal Scientific and Technical Information.

ABSTRACT

Forty-one seismic events recorded on the plains of western Alberta are subjected to a detailed study in the time domain. A "P-detection" time-varying polarization filter is described and applied to the events to detect segments of strong P motion in the first 25 seconds of the P phase coda.

On seismograms of 23 events, 12 of which have reported depths shallower than 40 km, pP phases have been identified; sP phases have been identified on 9 of the events. Considering estimated accuracies of observed and calculated pP-P times, assigned focal depths are accurate to within ± 15 km.

A varying upper crustal structure is found to make a similar contribution to the vertical components of the P phase for stations at separations up to 160 km. The radial components at these stations are similar only during time segments of strong P motion. The dissimilarity in other time segments of the radial components is attributed to different amplitudes and time-delays for PS converted phases generated at crustal layer interfaces. The largest PS converted phase, with amplitude up to about 1.5 that of P, is generated at the base of the sediments.

A small number of PS converted phases generated at the base of the crust have been identified.

TABLE OF CONTENTS

CHAPTER I	INTRODUCTION	
1-1	The AINA Seismic Project	1
1-2	Scope of the Present Study	2
CHAPTER II	DATA ACQUISITION	
2-1	Instrumentation	5
2-2	The Field Program	7
2-3	Events Recorded	11
2-4	Digital Records	15
CHAPTER III	PRELIMINARY FILTERING AND ROTATION	
3-1	Bandpass Filtering	16
3-2	Seismogram Rotation about the Vertical Component	17
3-3	Seismogram Rotation about the Transverse Component	22
CHAPTER IV	DETECTION OF RECTILINEAR MOTION	
4-1	Cross-correlation Filter Functions	25
4-2	Normalized and Phase Selective Filters	33
4-3	General Discussion of Filter Response	35
4-4	Selection of Appropriate Processor	37
4-5	Description of P-Detection (P-D) Processor	40
4-6	Results of P-D Processing	42

CHAPTER V	GENERAL RECORD CHARACTER	
5-1	Strength and Character of Onset	47
5-2	Effects of the Source Radiation Pattern	47
5-3	Some Observed Radiation Pattern Effects	52
5-4	Duration of the P Phase	57
5-5	Period of Motion	60
CHAPTER VI	COMPARISON OF STATION RECORDS	
6-1	Introductory Remarks	63
6-2	Comparison of Vertical Records	64
6-3	Comparison of Radial Records	72
6-4	Significance of Results	76
CHAPTER VII	SECONDARY SOURCE PHASES	
7-1	Introductory Remarks	85
7-2	Amplitude Considerations	88
7-3	Crustal Columns at the Source	91
7-4	The Path of pP Above the Source	93
7-5	Picking and Timing Secondary Phases	96
7-6	Summary of pP Results	100
7-7	Summary of sP Results	103
7-8	Other Possible Early-Arriving Phases	105
CHAPTER VIII	SOURCES OF PHASE DISTORTION	
8-1	Introductory Remarks	111
8-2	Times and Amplitudes of Locally Generated SV	112
8-3	Examples of Locally Generated SV	117
8-4	Examples of Transverse Motion	123

CHAPTER IX	SUMMARY AND CONCLUSIONS	
9-1	Summary	128
9-2	Conclusions	130
CHAPTER X	SUGGESTIONS FOR FURTHER RESEARCH	
10-1	Bandpass and Polarization Filtering	134
10-2	pP and Focal Depth Assignment	135
10-3	PS Cconverted Phases	136
REFERENCES		137
APPENDIX A	THE LANCZOS NUMERICAL FILTER	140
APPENDIX B	LISTING OF FORTRAN IV SUBROUTINE "REMODE"	143

LIST OF TABLES

TABLE I	Description of Stations	10
TABLE II	Summary of Earthquake Locations and Other Pertinent Data	12
TABLE III	R.M.S. Amplitude Signal/Noise Ratios	66
TABLE IV	Errors in pP-P Time Resulting from Assumption of Vertical Reflection	95
TABLE V	Summary of pP-P Calculations	101
TABLE VI	Summary of sP-P Calculations	104
TABLE VII	Wavelengths of Compressional Waves in the Layers of the Alberta Crust	115
TABLE VIII	Velocity Ratios in the Alberta Crust	115

LIST OF FIGURES

FIGURE 1	Laboratory layout of FM magnetic tape recording seismograph.	6
FIGURE 2	Displacement sensitivity of recording system at 6 db amplifier input attenuator setting.	8
FIGURE 3	Alberta recording locations	9
FIGURE 4	81 point bandpass filter	18
FIGURE 5	Seismogram rotation: (a) about vertical component, (b) about transverse component.	20
FIGURE 6	Example of rotation of horizontal motion into radial and transverse components.	21
FIGURE 7	Epicentral distance vs. angle of incidence of P wave at the base of the crust (after Ichikawa, personal communication).	23
FIGURE 8	Detection of P and SV motion by product of vertical and radial component of motion.	26
FIGURE 9	Sample filter functions and corresponding response functions for input sinusoids.	32
FIGURE 10	Half-cycle cosine function illustrating approximate response of normalized REMODE processors.	33
FIGURE 11	An example of the effect of the P-Detection Processor.	43
FIGURE 12	An example of an event with strong P motion which does not require P-Detection Processing for identification.	45
FIGURE 13	An example of the P-D processor detecting a common secondary phase in dissimilar signals.	46

FIGURE 14	Theoretical P wave displacement pattern (right) for each of three mechanism force systems: (a) single couple, (b) double couple, and (c) double dipole (after Stevens, 1966).	49
FIGURE 15	Orientations of source P radiation patterns which will produce: (a) strong P and weak pP, (b) weak P and strong pP, and (c) strong P and strong pP.	51
FIGURE 16	Two New Britain events with opposite radiation pattern effects.	55
FIGURE 17	Two North Atlantic earthquakes showing weak onset relative to secondary arrival.	56
FIGURE 18	Effects of focal depth and crustal type on appearance of P phase.	59
FIGURE 19	Average period of 20 seconds of P motion vs. epicentral distance.	62
FIGURE 20	VERT components of three similar events.	65
FIGURE 21	VERT components of three events distorted by noise.	68
FIGURE 22	VERT components of two near events with distinct difference in signal character.	69
FIGURE 23	VERT components of two similar near events.	71
FIGURE 24	RAD components of four short-period events.	74
FIGURE 25	RAD components of three long-period events.	75
FIGURE 26	Sedimentary columns under Alberta recording sites showing P velocities in km/sec.	78
FIGURE 27	Extrapolated crustal structure under Alberta sites (after Cumming and Kanasevich, 1966) showing P and S ray paths.	80

FIGURE 28	Precambrian basement under recording area (after Garland and Burwash, 1959).	83
FIGURE 29	Four crustal columns used for calculating pP-P and sP-P delay times (after Menard, 1957). Thicknesses in km are shown on the left and P velocities in km/sec on the right of each layer. W, the water depth, was determined from bathometric maps for each event.	92
FIGURE 30	Simulated pP path above the source.	95
FIGURE 31	High quality P-D records showing secondary phases arriving at an identical time on two stations.	98
FIGURE 32	Three events with PcP arriving about 5 seconds after P.	106
FIGURE 33	Three events with multiple secondary arrivals.	108
FIGURE 34	Examples of possible PS_4 phases.	118
FIGURE 35	Vertical-radial particle motion plots of P phases. Each plot contains 2.4 seconds of motion. The beginning of each plot is denoted by a heavy dot. θ is the approximate angle of incidence at the surface.	120
FIGURE 36	Horizontal onset orbital motion.	125

ACKNOWLEDGEMENTS

The author would like to thank Dr. R.M. Ellis for many valuable discussions during the AINA Seismic Project in Ottawa and throughout the research for this thesis at the University of British Columbia. Dr. Ellis also gave a critical appraisal of the manuscript. Gratitude is expressed to Dr. K. Whitham, Chief, Seismology Division, Observatories Branch, Department of Energy, Mines, and Resources for stimulating discussions, to Dr. R.W. Yole, Department of Geology, Carleton University for providing the geological information, and to Dr. J.A. Jacobs, Head of the Department of Geophysics, University of British Columbia for the use of departmental facilities.

The author is indebted to the Arctic Institute of North America for extending financial support during educational leave.

This research was sponsored by the Air Force Office of Scientific Research, Office of Aerospace Research, United States Air Force under AFOSR Grant AF-AFOSR-702-67 to the Arctic Institute of North America.

CHAPTER I

INTRODUCTION

1-1 The AINA Seismic Project

In 1962 the Arctic Institute of North America received from the Air Force Office of Scientific Research, United States Air Force, a grant to undertake a project entitled "Effects of Location of Seismograph Stations on the Records Obtained". This constituted a part of the United States Department of Defense, Advanced Research Projects Agency's program "Vela Uniform", the program undertaken to improve the capability of distinguishing underground nuclear explosions from natural earthquakes. This project will be referred to as the "AINA Seismic Project" throughout this thesis.

The broad aim of the AINA Seismic Project was to examine seismograms from the stations of the Canadian seismograph network, to define station to station and earthquake to earthquake differences, and to search for an explanation of any differences which may be found. The ultimate aim was to determine local effects in sufficient detail to allow their removal from the seismogram; this would enable a study to be made of seismic

signals from a distant source without the added complications due to crustal layering at the recording site.

The principal early work of the AINA Seismic Project has been reported in two papers: Ichikawa and Basham (1965) and Utsu (1966). These dealt with unified magnitude residuals and spectral analysis studies of P phases using data hand-digitized from photographic seismograms. The second phase of the project used data automatically digitized from records of a specially constructed seismograph system operated at four locations in Alberta. The seismograph system has been described by Bancroft and Basham (1967), who also present details of the virtually simultaneous digitization of the three components of motion of the events recorded.

The Alberta Experiment was designed to test procedures for detecting the effect in the short-period range of the crust for a seismic recording area where the upper crust was geologically simple and well defined. At the time of writing, a report on the results of frequency analysis of the events of the Alberta Experiment (see Section 2-3) is in preparation by R.M. Ellis and the present author (Ellis and Basham, 1967).

1-2 Scope of the Present Study

The work undertaken for this thesis was a detailed study of the Alberta Experiment events, restricted to the time

domain, and directed toward answering the question: what is the nature and origin of the seismic signals which contribute to the short-period recording of a teleseismic event within about 25 seconds of the onset of the P phase? This question is pertinent to crustal effect studies and to the fundamental problem of seismogram composition.

As an aid to identification of the types of seismic wave motion present on the seismograms, all events have been processed with a specially designed time-varying polarization filter. This processor, denoted "P-D", for P-detection, is an adaptation of the REMODE processor developed by a group of researchers at the Seismic Data Laboratory, Teledyne, Inc. (Mims and Sax, 1965, Griffin, 1966a and 1966b, and Sax, 1966). Passage of P motion by the P-D processor is dependent on its amplitude and degree of rectilinearity; all motion which is predominantly of S type is rejected.

Before presenting the principal results of these studies, the identification of wave motion in the P wave coda, two chapters are presented in which general seismogram appearance is considered. The first, Chapter V, deals with the features of a P phase which constitute its general character; the second, Chapter VI, gives a comparison of P phase records at various pairs of stations at which they were recorded.

The P-D processor detects much strong P motion

within the 25 second P phase coda of most of the events. Most of this signal energy can be attributed to secondary source phases, i.e., phases which arise in the general earthquake source region but which are delayed varying amounts and arrive at a distant station after the main P wave. The strongest phases of this type are pP, which is a reflection of the main P wave from the surface of the earth above the source, and sP, which is a reflection from the surface as P of the source-generated S wave. pP phases have been tentatively identified on 23 of the 40 earthquake seismograms in the suite. Twelve of these earthquakes had reported focal depths shallower than 40 km. In addition, sP phases have been identified on 9 of the same seismograms. These and other results of the study of secondary source phases are described in Chapter VII.

Although the detection of P motion by the P-D processor is dependent on the rectilinearity of the P orbital motion, vertical-radial particle motion diagrams of the P phase exhibit a high degree of ellipticity. The source of the ellipticity can be ascribed to PS converted phases generated within the crust near the recording station. The strongest PS converted phase is found to be that resulting from P to SV conversion at the interface between the sediments and the crystalline basement rock. This and other sources of distortion of the P phase away from its rectilinearity are discussed in Chapter VIII.

CHAPTER II

DATA ACQUISITION

2-1 Instrumentation

For purposes of recording short-period seismological data, a slow-speed FM magnetic tape recording seismograph (Bancroft and Basham, 1967) was assembled by the AINA Seismic Project staff in cooperation with the personnel of the Seismology Division, Observatories Branch, Department of Energy, Mines, and Resources. Because this seismograph system was used to collect the data discussed in this thesis, for purposes of completeness a brief description of the instrumentation will be given here.

A laboratory layout of the seismograph is shown in Figure 1. Frequency-modulated signals are written by a slow-speed (3/32 ips) IRIG standard magnetic tape recorder on 7-track tape. Using 10 1/2 inch reels of 1.0 mil tape the recording period is 5.3 days. Three components of seismic ground motion are detected by seismometers with a natural frequency of 0.5 Hz, amplified with phototube-galvanometer amplifiers with a natural frequency of 5 Hz, and presented to the recorder at two gain levels separated by 12 db. The

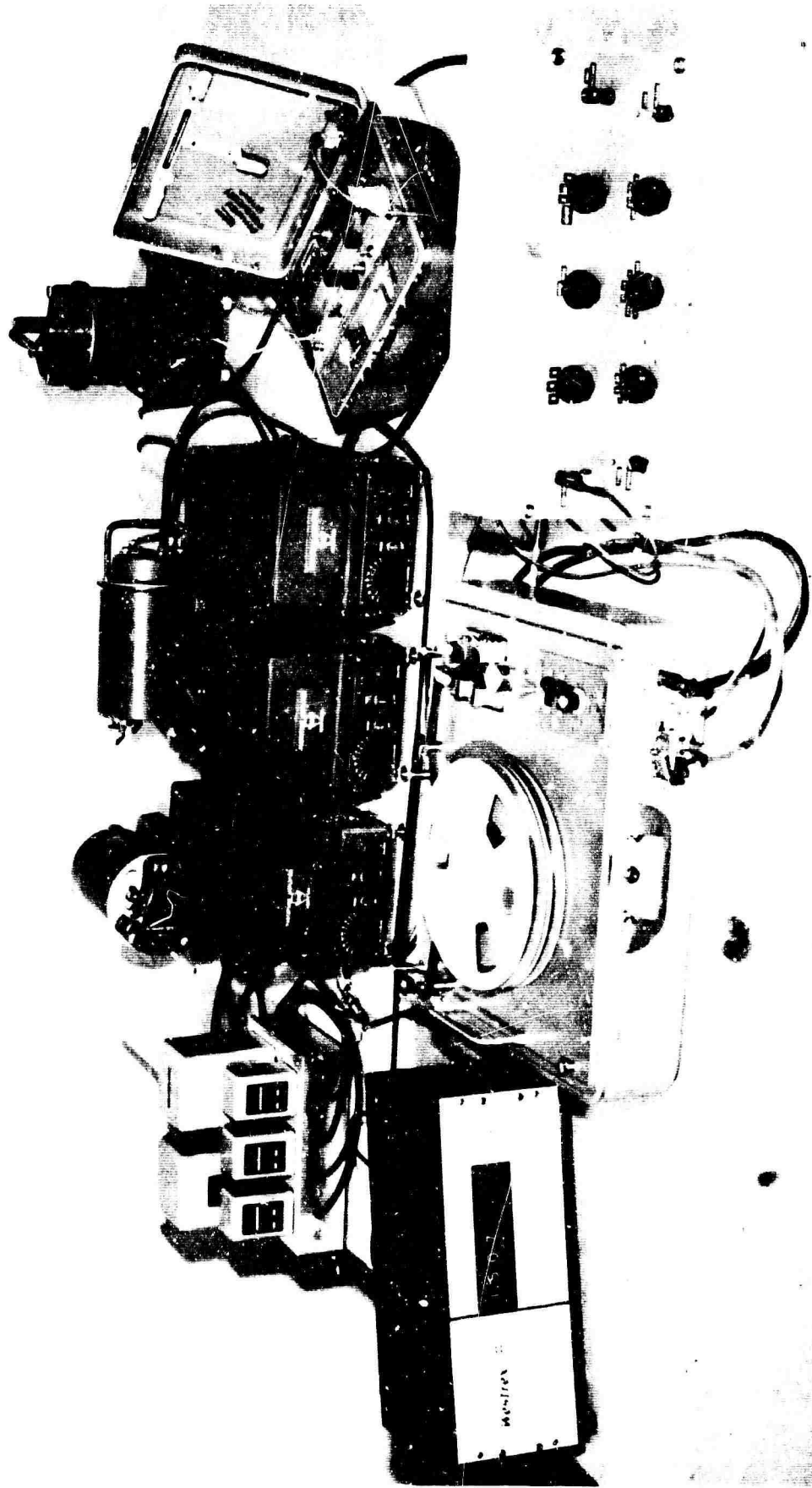


Figure 1. Laboratory layout of FM magnetic tape recording seismograph.

seismic signals require 6 tape tracks; the seventh is used to record time signals. Overall gain is set with the amplifier input attenuators.

A sample 6 db level (amplifier input attenuation) displacement sensitivity curve for the system is shown in Figure 2. As each component amplifier has a slightly different overall gain, and may be set at a different input attenuation, a normalization factor can be applied during playback to standardize all signals to the response shown in Figure 2. The inverse of the curve of Figure 2 can be applied to any signal when actual ground displacement is required.

2-2 The Field Program

During the period June to October, 1965, two of the seismograph systems described in section 2-1 were operated at four sites in western Alberta. The recording sites, Leduc, Warburg, Alder Flats, and Rocky Mountain House are shown on the map in Figure 3 by name abbreviation and station number. The location and site description of each station is given in Table I. One system was operated throughout the entire recording period at Leduc. The other system was operated successively for approximately 6 week periods at Warburg, Alder Flats, and Rocky Mountain House.

The Leduc site is on sandstone and shale bedrock

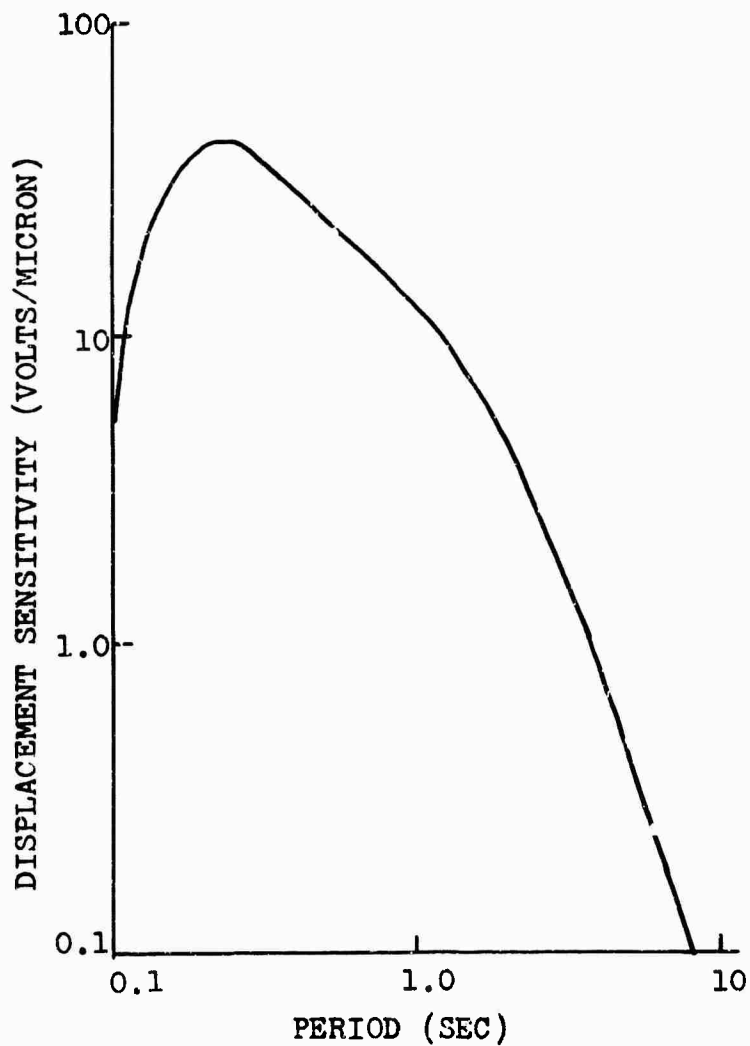


Figure 2. Displacement sensitivity of recording system at 6 db amplifier input attenuator setting.

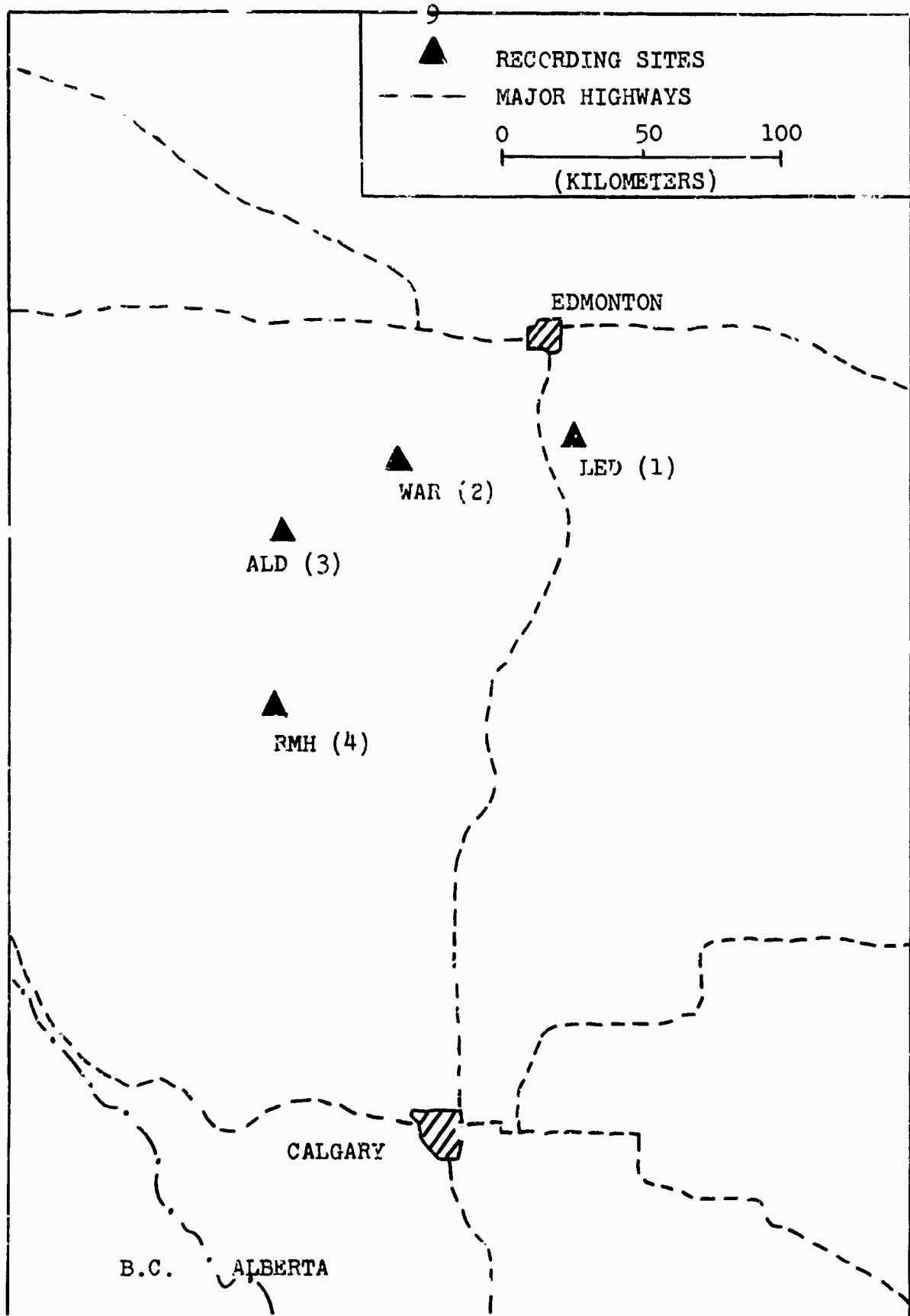


Figure 3. Alberta recording locations.

TABLE I DESCRIPTION OF STATIONS

STATION NAME	STATION NUMBER	LATITUDE	LONGITUDE	SITE DESCRIPTION
LEDUC (LED)	1	53° 13' N	113° 21' W	University of Alberta seismograph vault, 8 miles east of Leduc town.
WARBURG (WAR)	2	53° 10' N	114° 19' W	Concrete basement of vacant house within Warburg town.
ALDER FLATS (ALD)	3	52° 56' N	114° 57' W	Concrete basement of vacant house within Alder Flat, town.
ROCKY MOUNTAIN HOUSE (RMH)	4	52° 24' N	114° 57' W	Concrete floor of vehicle garage 3 miles northwest of Rocky Mountain House.

of the Edmonton (Upper Cretaceous) formation. The Warburg, Alder Flats, and Rocky Mountain House sites are, respectively, on approximately 10, 100, and 30 feet of unconsolidated drift and soil above the shale and sandstone of the Paskapoo (Tertiary) formation. Geophysical surveys and well logs provide good control of the sedimentary section in the recording area. Further details of the total crustal section will be given in a later chapter.

2-3 Events Recorded

During any five-month period many significant earthquakes occur throughout the world. Compared to many of the world seismograph stations the recording stations were seismically quiet sites; seismic background noise near 1 Hz was approximately 20 millimicrons peak-to-peak at each of the four stations. A number of earthquakes occurred during the recording period which were large enough to over-load the FM tape and were, therefore, unusable. Many small events were detected but were not sufficiently above the background noise to constitute good quality records. Forty-one events were chosen as suitable for analysis; these consisted of 40 earthquakes and the nuclear explosion LONG SHOT. A summary of the event locations and other pertinent data is given in Table II.

The first two columns of Table II give the event number and the number of the second station on which it was

TABLE II SUMMARY OF EARTHQUAKE LOCATIONS AND OTHER PERTINENT DATA

EVENT NUMBER	SECOND STATION	REGION	LATITUDE	LONGITUDE	DEPTH (KI)	DATE Y M D	TIME H M S	MAGNITUDE	Δ (deg)
1	2	Aleutians	+52.6	+173.2	25	65 06 09	13 26 52	5.6	42
2	2	Aleutians	+51.8	+174.1	35	65 06 11	02 37 35	5.5	42
3	2	N. Chile	-20.3	- 68.9	103	65 06 12	13 50 11	5.8	83
4	2	Hokkaido	+41.9	+143.4	32	65 06 13	07 06 14	5.7	64
5	2	Aleutians	+52.3	+172.0	54	65 06 19	06 33 13	5.5	43
6	2	Oregon	+42.3	-126.0	33	65 06 20	18 04 36	5.6	13
7	2	S. Alaska	+56.6	-152.9	36	65 06 23	11 09 15	5.7	23
8	2	S. Alaska	+56.6	-152.8	25	65 06 23	12 23 22	6.0	22
9	2	Bouvet Isl.	-54.5	+ 5.6	33	65 06 27	09 45 48	5.9	139
10	2	S. Alaska	+60.3	-141.2	12	65 06 27	11 08 56	5.3	17
11	2	Aleutians	+51.7	+176.5	60	65 06 30	08 33 32	6.0	41
12	2	N. Atlantic	+52.9	- 34.2	33	65 07 05	08 31 59	5.7	45
13	2	Greece	+33.7	+ 22.6	23	65 07 06	03 18 44	5.9	81
14	3	Solomons	- 9.7	+159.8	23	65 07 17	07 20 31	6.4	95
15	3	Aleutians	+53.3	+170.4	26	65 07 21	17 52 31	5.7	43
16	3	New Britain	- 5.3	+151.7	47	65 08 05	00 07 50	6.3	97
17 ^A	3	New Hebrides	-15.4	+166.9	26	65 08 11	03 40 56	6.3	96
18	3	New Hebrides	-15.3	+167.2	33	65 08 11	22 31 49	6.4	96
19	3	New Britain	- 5.3	+152.2	41	65 08 12	12 57 10	5.9	96
20	3	N. Chile	-19.0	- 69.1	129	65 08 20	09 42 49	6.0	82
21	3	Fiji	-22.9	-176.3	77	65 08 20	21 21 51	6.2	93
22	3	Mexico	+15.9	- 96.2	12	65 08 24	00 56 21	5.5	80
23	3	Mexico	+16.2	- 96.2	31	65 08 24	01 01 01	5.6	39

TABLE II. (CONTINUED)

EVENT NUMBER	SECOND STATION	REGION	LATITUDE	LONGITUDE	DEPTH (KM)	DATE			TIME			MAGNI- TUDE	Δ (deg)
						Y	M	D	H	M	S		
24	3	S. Alaska	+59.4	-145.6	19	65	08	24	13	12	19	5.4	18
25	4	S. Alaska	+57.5	-152.1	25	65	09	08	03	26	21	5.6	22
26	4	S. Alaska	+55.7	-155.4	33	65	09	08	11	16	34	5.4	24
27	4	Cent. Am.	+ 6.5	- 84.4	27	65	09	09	10	02	25	5.5	52
28	4	New Britain	- 5.3	+153.0	67	65	09	11	06	53	02	5.3	96
29	4	New Britain	- 6.3	+151.6	48	65	09	12	08	40	13	6.2	98
30	4	California	+40.4	-125.7	33	65	09	16	04	10	23	5.6	15
31	4	S. Alaska	+59.5	-145.1	22	65	09	18	20	46	39	5.3	18
32	4	China Sea	+29.1	+128.2	197	65	09	21	01	38	30	6.0	82
33	4	N. Atlantic	+40.7	- 50.0	23	65	09	21	03	26	37	5.3	44
34	4	Aleutians	+51.9	+175.5	41	65	09	27	05	09	13	5.5	41
35	4	S. Alaska	+59.7	-143.4	19	65	09	30	23	47	41	4.8	13
36	4	Kuriles	+49.5	+156.5	33	65	10	03	14	45	27	5.9	53
37	4	Aleutians	+51.4	-173.9	43	65	10	08	16	32	32	5.2	36
38	4	Aleutians	+51.6	-173.8	32	65	10	20	11	15	11	5.4	36
39	4	Cent. Am.	+12.5	- 87.4	70	65	10	20	23	54	30	5.4	46
40	4	Missouri	+37.5	- 91.0	22	65	10	21	02	09	31	5.2	22
41	4	Long Shot	+51.4	+179.2	1	65	10	29	21	00	00	6.0	40

*The station 1 digital seismogram of event 17 was not available. The wrong section of the analog record had been digitized.

recorded; all of the events were recorded at station 1. Throughout the text and on the illustration; all events will be referred to by event and station number; for example, 17-3 is event 17 recorded on station 3. The location, origin time, and unified magnitude are those given by the United States Coast and Geodetic Survey (U.S.C.G.S.) "Preliminary Determination of Epicenters" cards. If the maximum station separation (1-4) is less than 2° , the epicentral distances (Δ) in Table II are accurate to within 1° for any particular station.

An event is defined to be teleseismic if it occurs within the epicentral distance range 20° to 180° . The Atomic Weapons Research Establishment (A.W.R.E.) (1965), in studies related to nuclear explosion detection, define a narrower range "source window" which extends from 30° to 90° epicentral distance. It is through this "window" that the source can be "seen" almost undisturbed by the transmission path between the source and the recorder. At distances less than 30° the signal is disturbed by the crustal and upper mantle shadow and transition zones, and at distances greater than 90° by the core shadow and transition zones. Twenty-one of the events in Table II fall within this "source window", 11 at smaller distances, and 9 at larger distances.

Eight of the events occurred in a continental environment, the remainder in an oceanic or transitional oceanic-continental environment. Three events have reported depths greater than 100 km, 7 have depths between 45 and 77 km, and

the remaining 31 are shallower than 43 km.

2-4 Digital Records

These 41 events, each with a recording at two stations, were available to this study in digitized form on digital magnetic tape. The digitizing procedure and tape format has been described by Bancroft and Basham (1967).

The digitizing rate was 16.6 samples per second yielding a Nyquist frequency of 8.3 Hz. Eleven minutes of the three components of seismic information plus the time track have been retained for each event at each of the two stations, beginning approximately 1 minute prior to the P arrival time.

The digitization was done on the Department of Energy, Mines, and Resources CDC 3100 computer. All computing for this thesis was done on the University of British Columbia IBM 7044 computer.

CHAPTER III

PRELIMINARY FILTERING AND ROTATION

3-1 Bandpass Filtering

Ellis and Basham (1967) have shown that the P wave signal energy in the recording passband (see Figure 2) for these events is concentrated in the frequency band between 0.3 and 2.5 Hz. It is shown in Chapter V by a study of the period of P phase motion that the dominant period can vary considerably among events within this equivalent frequency range.

Many of the events are contaminated by background noise at both sides of this frequency band. At the low frequency end there are the well-known oceanic microseisms with periods between about 3 and 10 seconds. At the high frequency end of the band there is considerable contamination of many of the events by cultural noise. Although Leduc is the most isolated site (see Table I) there are occasional bursts of noise from farm machinery and a local road in the area. Each of the other three sites is in close proximity to moderately heavy vehicular traffic which contributes noise in this band. The frequency of this cultural noise is generally

3 to 1 Hz.

For a production processing run (P-detection to be described in Chapter IV) it was desirable to use a single bandpass filter on all events before input to the processor. The bandpass filter BP-1, whose response is shown in Figure 4, was used for this purpose. This is an 81-point symmetrical filter of the Lanczos type (Lanczos, 1957) with corners at 0.25 and 2.0 Hz. A general discussion of the Lanczos filter is given in Appendix A. The filter does not completely eliminate either the high or low frequency noise but was considered the best general filter for the production run.

3-2 Seismogram Rotation about the Vertical Component

A plane P wave is a compressional wave with displacement rectilinear in the direction of propagation. When such a wave enters obliquely a horizontally layered crustal system it will undergo reflection and refraction and generate reflected and transmitted P and SV waves at each interface. All incident displacement is in a plane containing the vertical direction and the direction of the great-circle azimuth of approach. The interface boundary conditions require that all P and SV displacements generated during passage through a horizontally layered crust must remain in this same plane. Although this is often far from true in practice, it is useful to rotate the three recorded components so that all signals accountable in terms of plane P wave propagating through a

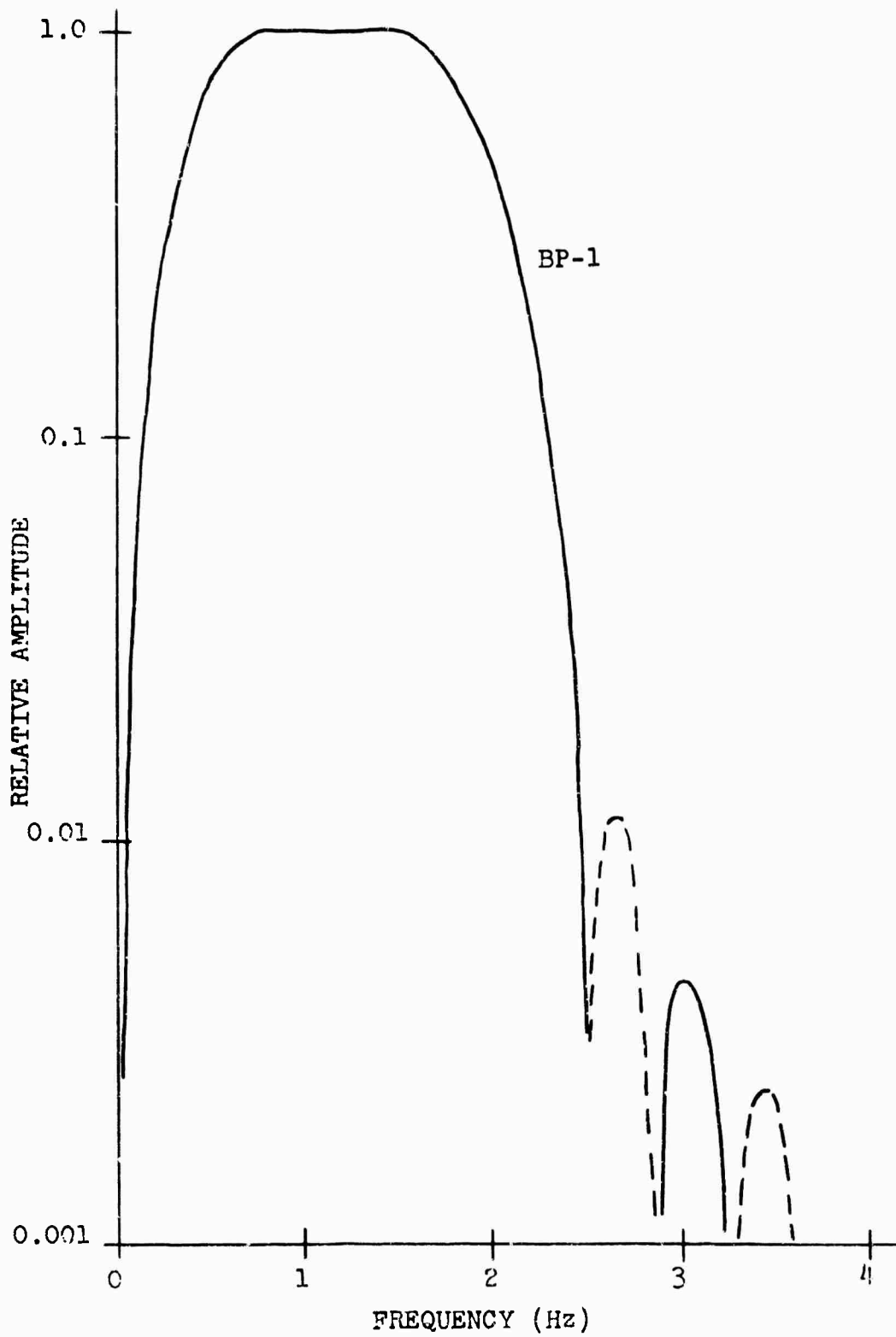


Figure 4 81 point bandpass filter response.

horizontally layered crust are represented on two components, the vertical and radial, the radial being the horizontal direction of the great-circle azimuth. Theoretically, no signal remains on the transverse horizontal.

This rotation about the vertical direction is accomplished as shown in Figure 5(a). The resulting radial and transverse components are given by the relations

$$R = -N \cos \alpha - E \sin \alpha$$

and

$$T = N \sin \alpha - E \cos \alpha$$

where α is the great-circle azimuth from the station to the epicenter measured clockwise from north. N is the recorded north-south component defined as positive toward the north and E is the recorded east-west component defined as positive toward the east. This yields the convention of R being positive away from the epicenter and T positive toward the right.

An example of the effect of this rotation is shown in Figure 6 for event 10-1. Shown are the three original components and the rotated radial and transverse. The onset pick is shown by a broken vertical line through each of the components. It can be seen in Figure 6 that most of the horizontal signal energy is retained by the radial component and very little retained by the transverse. The transverse is not significantly above the background noise until a slow buildup of energy occurs 15 or 20 seconds after the onset.

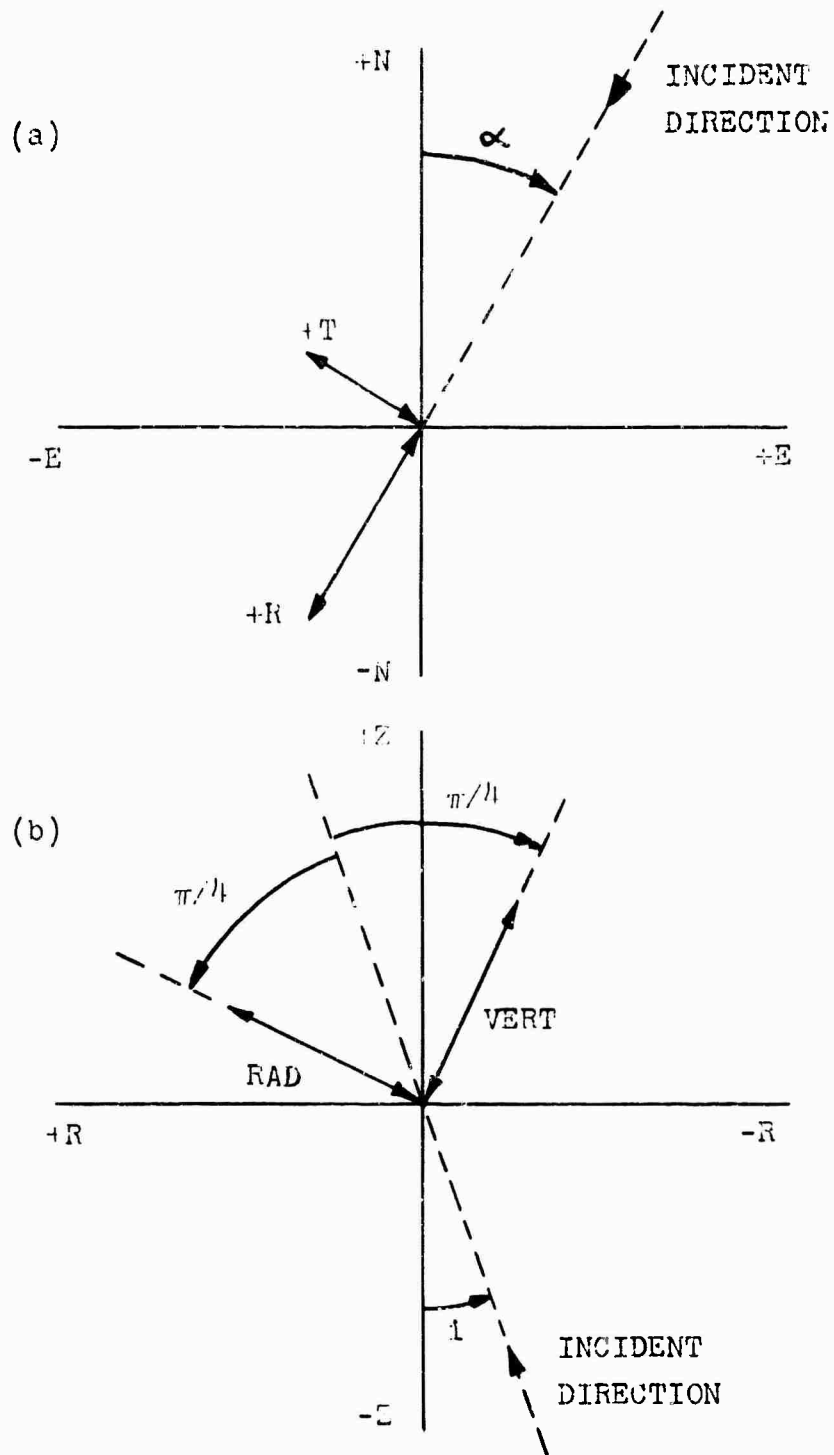


Figure 5. Seismogram rotation: (a) about vertical component, (b) about transverse component.

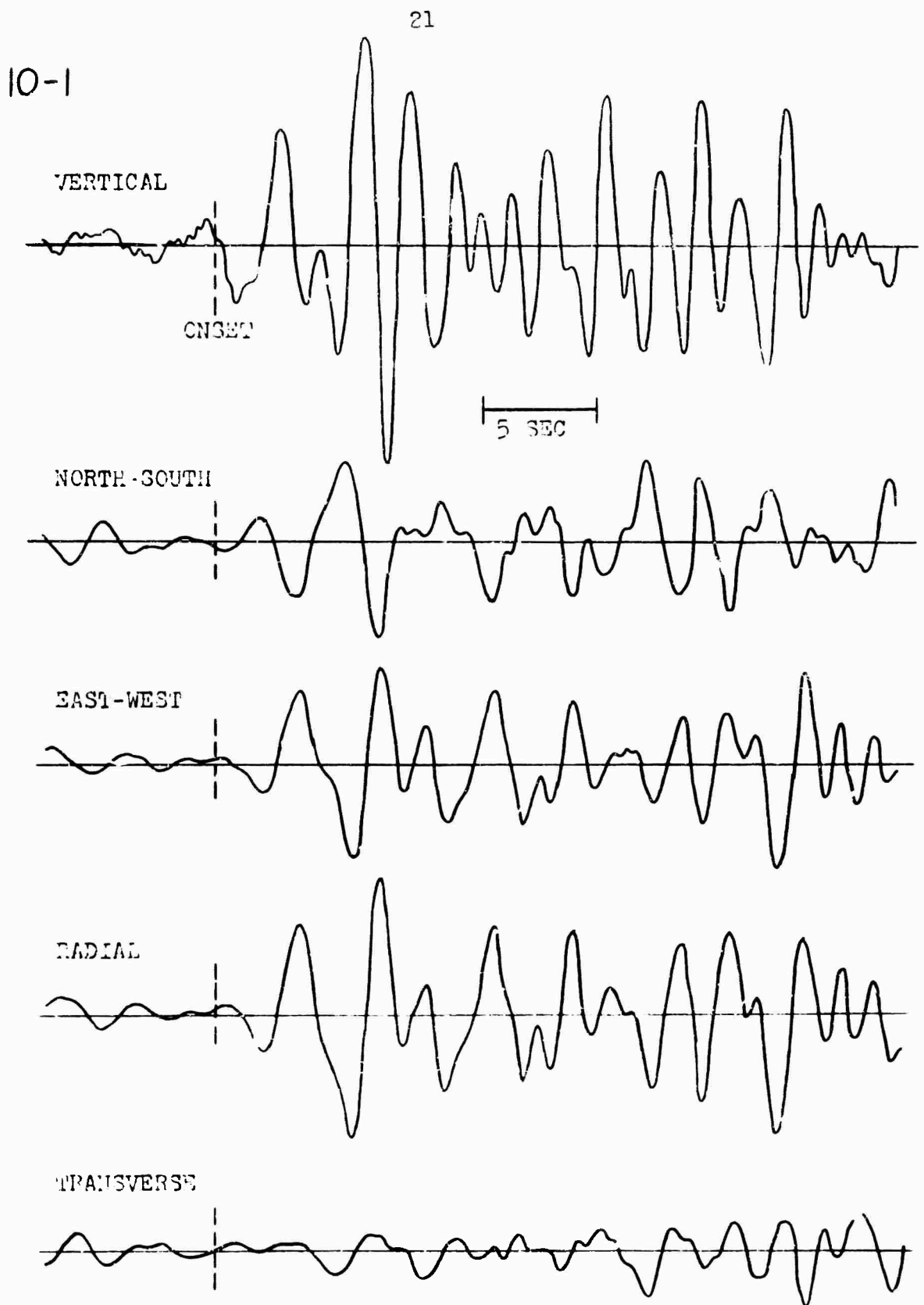


Figure 5. Example of rotation of horizontal motion into radial and transverse components.

This transverse energy will be discussed in some detail in Chapter VIII. It will be seen there that many events show considerably more transverse energy than does this event.

3-3 Seismogram Rotation about the Transverse Component

The specialized filters to be described in Chapter IV require that the signal energy be approximately equally distributed between the vertical and the radial components. This is accomplished as shown in Figure 5(b) by rotating the vertical and radial components about the new transverse component so that each is 45° away from a specified angle of incidence of the P arrival for the particular event.

The rotated vertical and rotated radial as described in Figure 5(b) are given by the relations

$$\text{VERT} = Z \cos(\pi/4 - i) + N \cos\alpha \sin(\pi/4 - i) + E \sin\alpha \sin(\pi/4 - i)$$

$$\text{RAD} = Z \sin(\pi/4 - i) - N \cos\alpha \cos(\pi/4 - i) - E \sin\alpha \cos(\pi/4 - i)$$

where α is the azimuth and i the angle of incidence. These relations give the doubly rotated VERT and RAD in terms of the recorded components. The angle of incidence used in these calculations is the angle at the base of the crust. A curve of this angle versus epicentral distance, after Ichikawa (personal communication), is shown in Figure 7. As the approach path steepens during passage through the crust (see Figure 27), use of the angle of incidence at the base of the crust rather than the apparent angle of emergence

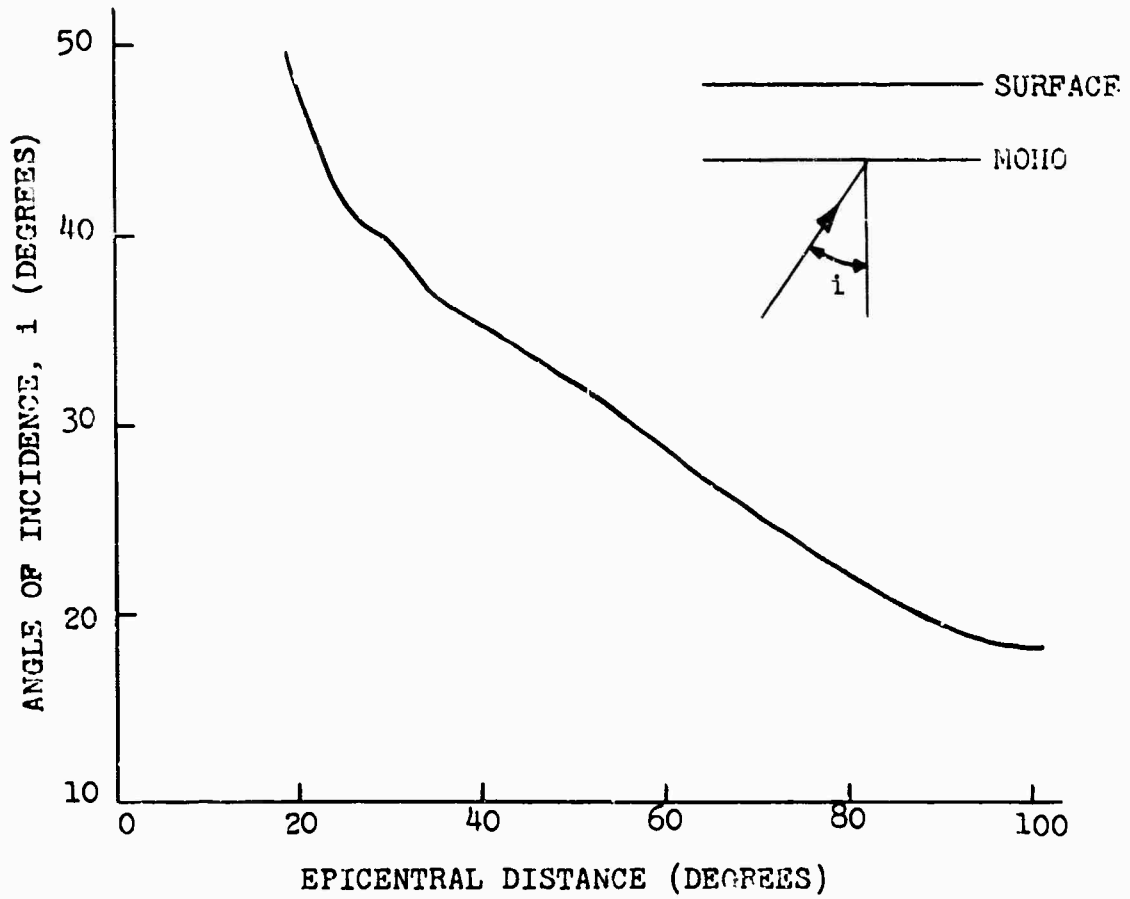


Figure 7. Epicentral distance vs. angle of incidence of P wave at the base of the crust (after Ichikawa, personal communication).

at the surface has the effect of retaining proportionally more of the signal on VERT than on RAD. This does not make a significant difference to the signal processing described in Chapter IV.

All but the nearest events are at epicentral distances greater than 20° (see Table II), hence the angles of incidence given on Figure 7 will be smaller than 45° . The effect of rotation about the transverse will generally be the addition of vertical signal energy to the radial component rather than *visa versa*.

CHAPTER IV

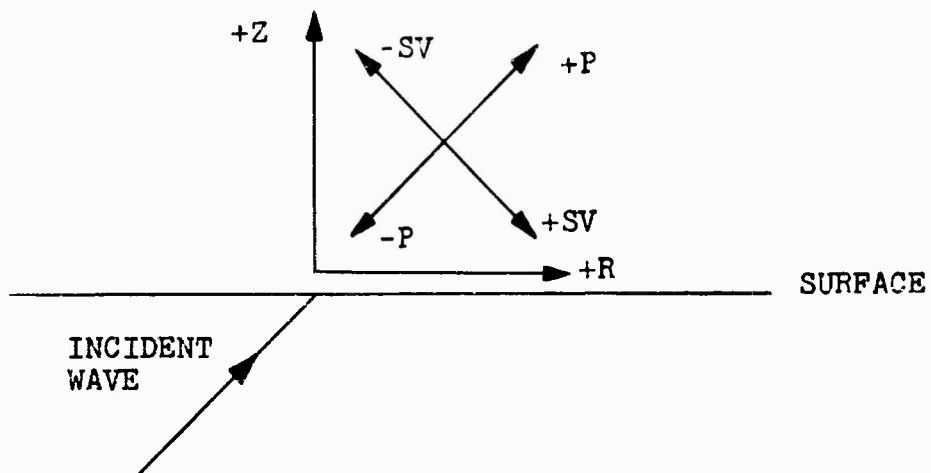
DETECTION OF RECTILINEAR MOTION

4-1 Cross-Correlation Filter Functions

An important characteristic of P and SV seismic signals is their rectilinear polarization; both are in the vertical-azimuthal plane, but P in the direction of propagation and SV orthogonal to this direction. Using the vertical and radial seismograms, operators can be designed which use the rectilinear polarization of the signals compared with elliptical and random polarization of noise to enhance the seismic signals.

The simplest operation of this type uses the difference in phase relations between the vertical and radial components to distinguish P from SV. This is a simple motion product operator described in the diagram and accompanying table in Figure 8. Forming the zero-lag cross-correlation between the vertical and radial component, usually with some smoothing process, the product is positive for a P wave and negative for an SV wave. This operation is easily accomplished with data in either analog or digital form.

Shimshoni and Smith (1964) describe two non-linear



SIGNS OF COMPONENTS

PHASE	Z	R	ZXR
$+P$	+	+	+
$-P$	-	-	+
$+SV$	-	+	-
$-SV$	+	-	-

Figure 8. Detection of P and SV motion by product of vertical and radial component of motion

processes which utilize polarization for signal enhancement. One process uses the product of the time-averaged cross-product and the two components of the original signal to amplify all rectilinearly polarized signals in the seismogram. The output trace amplitude at each point is simply the input trace amplitude multiplied by a time varying constant. The second process fits ellipses to the particle trajectories and displays the parameters of the ellipses as functions of time to separate the rectilinearly polarized waves and to obtain a rough estimate of their angle of incidence.

A class of more general polarization filters, collectively called "REMODE" (for rectilinear motion detection) has recently been developed by a group of researchers at Teledyne Inc.; Mims and Sax (1965), Griffin (1966a, 1966b), Sax (1966). These REMODE filters are based on the following concept. When a large P or SV phase arrives at a recording site, its particle motion orbit will be more rectilinear than elliptical or random. If the segments of the rotated vertical and radial components containing the phase are cross-correlated, the even part of the cross-correlation function will be large relative to its odd part. When the even part of the function is used as a filter on the same segments of the components, the filter will pass with least attenuation the frequency band for which particle motion is most rectilinear.

A cross-correlation function is defined for a segment

of record as

$$C(\tau) = \int_{t - w/2}^{t + w/2} z(t)r(t + \tau)dt \quad (1)$$

where t is the time at the center of the record segment, w is the segment width, and τ is the lag interval. $z(t)$ and $r(t)$ are the rotated vertical and radial input traces. To determine $C(\tau)$ in ideal limiting cases, consider $z(t)$ and $r(t)$ when they are unit-amplitude sinusoids with a phase difference of θ . Equation (1) becomes

$$C(\tau) = \int_{t - w/2}^{t + w/2} \sin(t)\sin(t + \tau + \theta)dt$$

which, after integration and simplification, becomes

$$C(\tau) = 1/2 \sin w \sin 2t \sin (\tau + \theta) \\ - [w - \sin w \cos 2t] \cos (\tau + \theta). \quad (2)$$

The sinusoidal motion will be purely rectilinear when $\theta = 0$, and purely circular when $\theta = \pi/2$. From equation (2) the cross-correlation function for rectilinear motion becomes

$$C_{\text{REC}}(\tau) = 1/2 [\sin w \sin 2t] \sin \tau \\ + 1/2 [w - \sin w \cos 2t] \cos \tau \quad (3)$$

and the cross-correlation function for circular motion becomes

$$C_{\text{CIR}}(\tau) = 1/2 \left[\sin w \sin 2t \right] \cos \tau + 1/2 \left[\sin w \cos 2t-w \right] \sin \tau. \quad (4)$$

These are functions which retain the window length and record time as parameters. If w is large compared to unity then

$$w \gg \begin{cases} \sin w \sin 2t \\ \sin w \cos 2t \end{cases}$$

and $C_{\text{REC}}(\tau) \simeq \frac{w}{2} \cos \tau \quad (5)$

and $C_{\text{CIR}}(\tau) \simeq -\frac{w}{2} \sin \tau. \quad (6)$

Thus, for a long window length the rectilinear cross-correlation function is a cosine (even) and the circular cross-correlation function is a sine (odd).

Now consider using the even parts of these two cross-correlation functions (equations (5) and (6)) as filters for the input sinusoids. The even part of the circular function is identically zero and the input sinusoid will be attenuated completely. Convolution of the even part of the rectilinear function, i.e., the entire $C_{\text{REC}}(\tau)$, with one of the input sinusoids will yield an amplified sinusoid as output.

In the intermediate case of a phase difference $0 < \theta < \pi/2$, or the more practical case where the input sinusoids are distorted by additional random motions, the cross-correlation function will contain both even and odd parts, the even part predominating if the motion is more

nearly rectilinear, the odd part predominating if the motion is more nearly circular. The even part of a general $C(\tau)$ as it varies continually along the records would be an appropriate time varying filter for passing motion in proportion to the degree of rectilinearity. However, it is computationally more efficient to use a slightly different function.

The procedure adopted by the Teledyne researchers for the REMODE processor (Griffin, 1966a) was to use an even function which has the form of equation (5) when the motion is ideally rectilinear. This is accomplished by defining a cross-correlation function for positive lags as

$$C_{t,w} (+\tau) = \int_{t-w/2}^{t+w/2} z(t)r(t-\tau)dt, \quad (7)$$

and by making the function even by reflecting the positive-lag correlations into negative lags by imposing the condition

$$C_{t,w} (-\tau) = C_{t,w} (+\tau). \quad (8)$$

The filter function is then defined as

$${}_{(2)}\bar{\Phi}_{t,w} (\tau) = C_{t,w} (\tau), \quad (9)$$

where the prescript, (2), denotes the Teledyne designation for REMODE 2, and the subscripts t and w denote dependence of the filter function on the record time and window length respectively. For the case of input in-phase sinusoids

equation (7) will be identical to equation (3), and for $w \gg 1$ equation (9) will be identical to equation (5). When the input sinusoids are out-of-phase ($\theta = \pi/2$) the procedure of equation (8), by reflecting the sine function (equation (6)) about the point $\tau = 0$, would place a π phase shift at the center of the filter function. Such a filter function would reject motion having the same period as the circular input sinusoids.

To demonstrate the response of $(z) \Phi_{t,w}(\tau)$ for in- and out-of-phase sinusoids, and to carry the procedure one step closer to the practical case, $(z) \Phi_{t,w}(\tau)$ and its frequency response have been calculated for a particular data sample interval, window length, and total lag length. The results of these computations are shown in Figure 9. The input sinusoids with 16 sample points per cycle are shown on the top of Figure 9. The rectilinear motion is shown with in-phase sinusoids and the circular motion with R lagging Z by $\pi/2$. The rectilinear and circular filter functions shown in the center of Figure 9 were computed using the digital equivalents of equations (7), (8), and (9) with $w = 20$ sample intervals and maximum $\tau = 12$ sample intervals. This value of w , being greater than one period (2π), conforms generally to the requirements for equations (5) and (6) but is not long enough for the filter functions to take the exact form of equations (5) and (6). A maximum lag of only slightly more than half of the window length is used so that the filter functions retain a significant

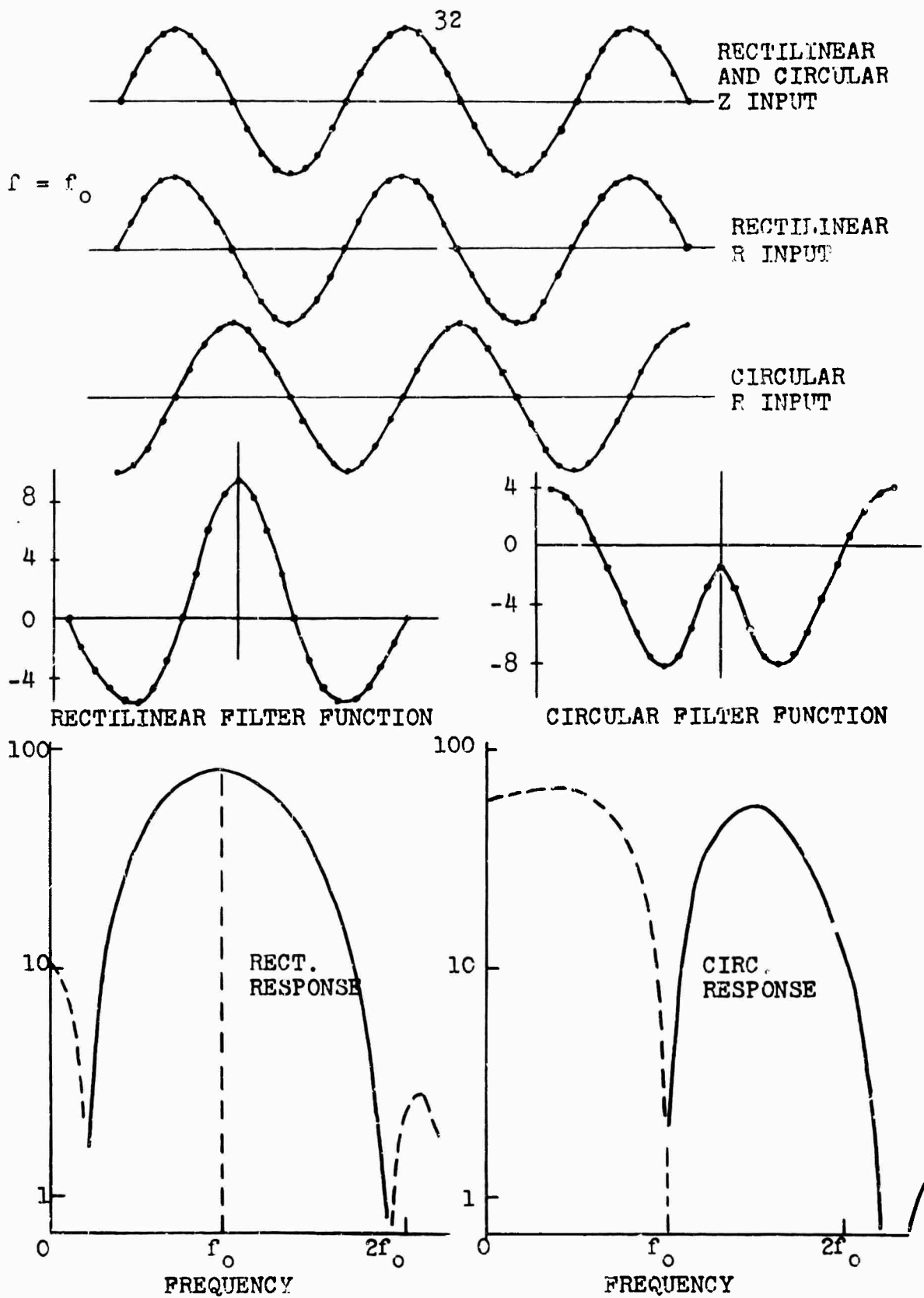


Figure 9. Sample filter functions and corresponding response functions for input sinusoids.

contribution from the input signals at the larger lags. Because of the regularity of the sinusoidal inputs, the parameter t does not appear in this computation; the filter functions are the same at any point in the record.

The effect that these filters will have on the input traces is well demonstrated by their cosine transform response functions which are shown at the bottom of Figure 9. For input sinusoids of frequency f_0 the rectilinear filter has a gain of 80 and the circular filter a gain of 1.2 at a frequency of f_0 . Therefore, if the input records contained successive portions of in- and out-of-phase motion, the in-phase (rectilinear) sections would be amplified by a factor of about 55 relative to the out-of-phase (circular) sections.

The filter responses also demonstrate the necessity of narrow bandpass filtering of experimental input signals. Because of the filter function truncation, the corresponding response function has large side lobes. For the case of input sinusoids shown in Figure 9, which can be considered as experimental signals passed by an infinitely narrow bandpass filter, the rectilinear detection effect applies only within a small range of the input frequency.

4-2 Normalized and Phase Selective Filters

The response of $(2)\bar{F}_{t,w}(\tau)$, the REMODE 2 filter, depends on the amplitudes of, and the phase difference between, input signals. The dependence on amplitude can be eliminated

by normalizing the filter function by time-varying estimates of the average power in the input signals, over the same time window as used in the cross-correlation estimates. The normalization factors are determined from zero-lag auto-correlations as

$$\sigma_t = \left[\int_t^{t+w/2} z^2(t) dt \cdot \int_t^{t+w/2} r^2(t) dt \right]^{-1/2} \quad (10)$$

and the normalized filter function becomes

$${}_{(3)}\bar{\Phi}_{t,w}(\tau) = \sigma_t \cdot {}_{(2)}\bar{\Phi}_{t,w}(\tau) \quad (11)$$

where the prescript, (3), is the Teledyne designation for REMODE 3. The response of the filter function ${}_{(3)}\bar{\Phi}_{t,w}(\tau)$ depends only on the phase difference between the input signals. Some discussion of the form of this response is given in Section 4-3.

The polarity convention for all seismograms is such that the zero-lag cross-correlations between z and r components will have positive values for P phases and negative values for SV phases (see Figure 8). The Teledyne filters REMODE 2A and 3A are modified versions of REMODE 2 and 3 which reject SV motion by setting the filter functions to zero whenever the zero-lag cross-correlations are negative. The REMODE 2A and 3A filter functions can, therefore, be given by the relations

$$(2A) \bar{\Phi}_{t,w}(\tau) = \begin{cases} (2) \bar{\Phi}_{t,w}(\tau) & \text{for } C_{t,w}(0) \geq 0 \\ 0 & \text{for } C_{t,w}(0) < 0 \end{cases} \quad (13)$$

and

$$(3A) \bar{\Phi}_{t,w}(\tau) = \begin{cases} (3) \bar{\Phi}_{t,w}(\tau) & \text{for } C_{t,w}(0) \geq 0 \\ 0 & \text{for } C_{t,w}(0) < 0 \end{cases} \quad (14)$$

These unnormalized and normalized phase selective filters could equally well be defined to reject P rather than SV motion by setting the filter functions to zero when the zero-lag cross-correlation was positive.

4-3 General Discussion of Filter Response

The response of the REMODE 2 filter has been shown in Figure 9 for two ideal limiting cases, pure in-phase and out-of-phase input sinusoids. A filter function defined by equations (7), (8) and (9) with $z(t)$ and $r(t)$ as rotated vertical and radial components of an experimental seismogram will be different at every point along the record. Although such a filter cannot be defined analytically it is important to gain some understanding of its response in the practical application.

Griffin (1966a), in an examination of the case of infinite window lengths, assumes that $(2) \bar{\Phi}_{t,w}(\tau)$ is enough like the even part of the general $C(\tau)$ that the response of

the even part of $C(\tau)$ will be representative of the response of $(2)\bar{\Phi}_{t,w}(\tau)$. Griffin presents the following discussion. Let $z_{t_0}(t)$ and $r_{t_0}(t)$ be two transient functions representing segments of two components of a seismogram within some time window centered on t_0 , and let their cross-correlation function be defined

$$C_{t_0}(\tau) = \int_{-\infty}^{+\infty} z_{t_0}(t) r_{t_0}(t + \tau) dt. \quad (15)$$

If the two record segments have Fourier transforms

$$|z_{t_0}(\omega)| \exp[i\phi_z(\omega, t_0)]$$

and

$$|R_{t_0}(\omega)| \exp[i\phi_r(\omega, t_0)]$$

then $C_{t_0}(\tau)$ has a Fourier Transform given by

$$2\pi |z_{t_0}(\omega)| |R_{t_0}(\omega)| \exp[i(\phi_r(\omega, t_0) - \phi_z(\omega, t_0))] \quad (16)$$

The real part of (16) will be the transform of the even part of $C_{t_0}(\tau)$ in equation (15). Therefore, the frequency response of $(2)\bar{\Phi}_{t,w}(\tau)$ will have the form of

$$2\pi |z_{t_0}(\omega)| |R_{t_0}(\omega)| \cos[\phi_r(\omega, t_0) - \phi_z(\omega, t_0)],$$

i.e., it is both amplitude and phase dependent. Frequency components of the input signals will be passed in proportion to the cosine of the phase difference between $z_{t_0}(t)$ and $r_{t_0}(t)$. When the filter function is normalized with a function

similar to equation (10) the response of $(3)\overline{\Phi}_{t,w}(\tau)$ will have the form of

$$\cos [\phi_r(\omega, t_0) - \phi_z(\omega, t_0)] . \quad (17)$$

Griffin (1966a) presents a graph of the ratio of input to output amplitudes versus the phase difference between the two input records for a narrowly bandpass filtered teleseism processed with REMODE 3A. The graph shows considerable similarity to the cosine function, (17). A half cycle of such a cosine function is shown in Figure 10. The response is +1 and -1 for phase differences of 0 and 180 degrees respectively, i.e., the filter will pass pure P and pure SV with unit gain. The response is +1/2, 0, and -1/2 for phase differences of 60, 90, and 120 degrees respectively. The effect of SV rejection shown by equation (14) is represented by the broken line in Figure 10. The REMODE 3A processor simply has zero response for phase differences between 90 and 180 degrees.

A Fortran IV subroutine with options to process a two-component time series according to REMODE 2, 2A, 3, or 3A is shown in Appendix B. The explicit form of the calculation used in this subroutine is described in Section 4-5.

4-4 Selection of Appropriate Processor

The first half minute after the onset of a tele-

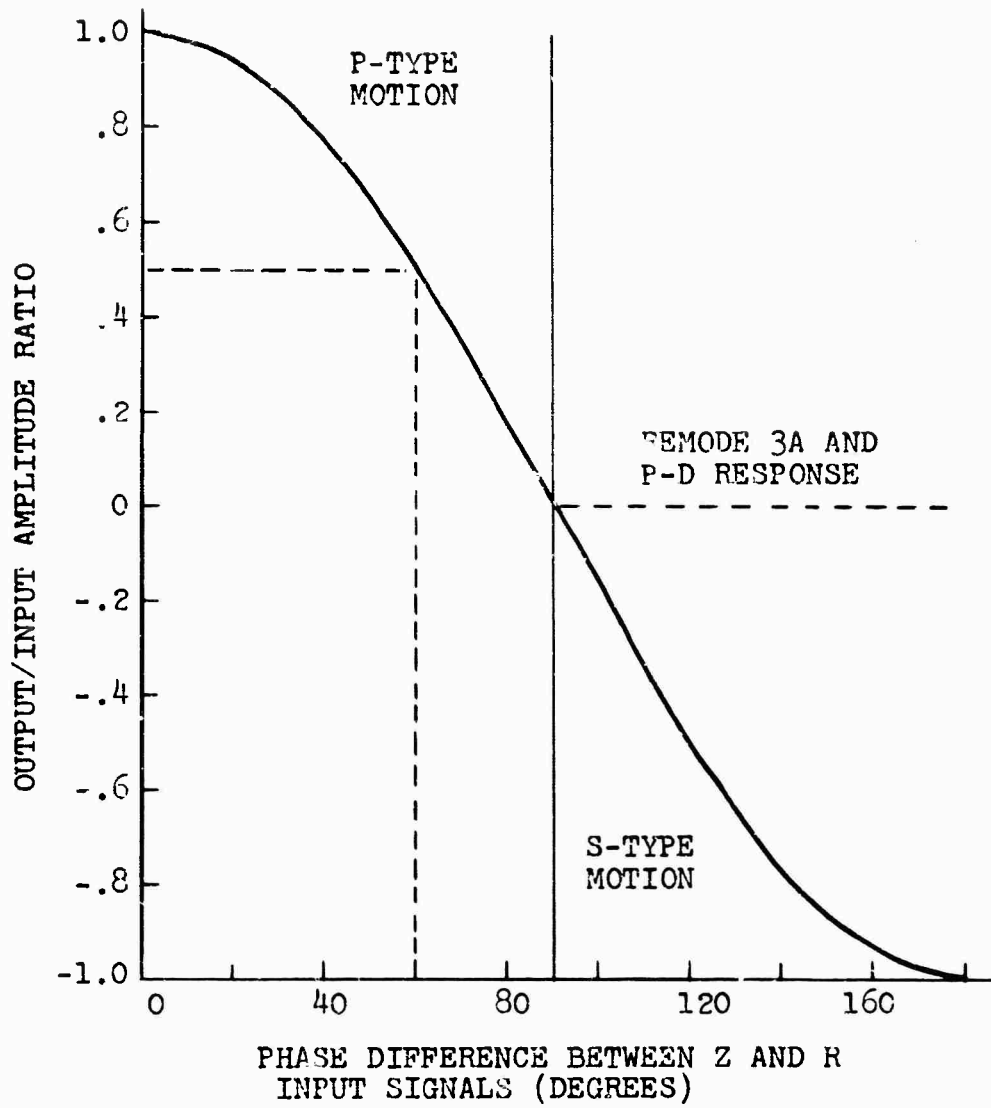


Figure 10. Half-cycle cosine function illustrating approximate response of normalized REMODE processors.

seismic P phase should contain principally P type motion. As can be seen in the one seismogram that has been presented (Figure 6), and will be seen on many to follow, the seismic energy is usually well distributed over this interval. It was decided to use a normalized version of the REMODE processor, i.e., normalized according to the average power in the input traces, to enhance the stronger signal sections in the record interval. It would be expected that there would be more signal in this interval that tends toward rectilinearity than signal which does not. A REMODE 3 processor would, therefore, pass more signal than it would reject, and would pass equally P and SV signals of equal amplitude and rectilinearity. One would have to return to the Z and R input signals to decide on the basis of phase relations alone which part of the input was SV.

By using a REMODE 3A processor, P is passed in amounts proportional to its rectilinearity and total energy, and all SV motion is attenuated completely. Strong SV motions can then be detected by noting which portions of the signal were rejected, and which were distinguishably out-of-phase on the input records. A REMODE 3A type processor, designated "P-D" for P-Detection, was used in a production run for the 41 events in this study. The P-D processor is described in detail in the next section.

4-5 Description of the P-Detection (P-D) Processor

As described in section 4-1, the basic processor is REMODE 2. Applying to a seismogram the filter described by equations (7), (8), and (9), the output in digital form can be described by

$${}^2Fz_k = z_k \sum_{i=k-LW2}^{k+LW2} rz_{i,i} + \sum_{i=1}^L \left\{ (z_{k-i} + z_{k+i}) \sum_{j=k-LW2}^{k+LW2-i} rz_{i+1,j} \right\}$$

for the z component, and (18)

$${}^2Fr_k = r_k \sum_{i=k-LW2}^{k+LW2} rz_{i,i} + \sum_{i=1}^L \left\{ (r_{k-i} + r_{k+i}) \sum_{j=k-LW2}^{k+LW2-i} rz_{i+1,j} \right\}$$

for the r component, with the following variable definitions.

k = sample index

z_k = k^{th} rotated vertical sample

r_k = k^{th} rotated radial sample

$rz_{p,q}$ = cross-product of the q^{th} rotated radial sample with the $(q + p - 1)^{\text{st}}$ rotated vertical sample

p = lag number

LW2 = 1/2 the window length

L = maximum lag

2Fz_k = k^{th} vertical output sample

2Fr_k = k^{th} radial output sample

Using the normalizing factor from equation (10),

$$\sigma_k = \left[\sum_{i=k}^{k+LW/2} z_i^2 \cdot \sum_{i=k}^{k+LW/2} r_i^2 \right]^{-1/2}, \quad (19)$$

the normalized output is given by

$$3^{Fz}_k = \sigma_k \cdot 2^{Fz}_k \quad (20)$$

and

$$3^{Fr}_k = \sigma_k \cdot 2^{Fr}_k$$

for the vertical and radial output respectively. Using the procedure shown in equation (14), the final output becomes

$$\begin{aligned} (\text{P-D VERT})_k &= 3^{Fz}_k && \text{for } rz_{k,k} \geq 0 \\ &= 0 && \text{for } rz_{k,k} < 0 \end{aligned}$$

and

$$\begin{aligned} (\text{P-D RAD})_k &= 3^{Fr}_k && \text{for } rz_{k,k} \geq 0 \\ &= 0 && \text{for } rz_{k,k} < 0, \end{aligned} \quad (21)$$

where the designation P-D (for P-Detection) is given to the final output. Equations (18) to (21) are used in subroutine "REMODE" shown in Appendix B.

Half a minute of signal starting approximately 5 seconds before the onset of P was processed for each of the events listed in Table II using the P-D processor with a window length of 20 sample intervals and $L = 12$. The second

half minute was processed for those events with focal depth greater than 100 km. The window length and L were chosen as suitable after some experiments on seismograms varying these values. The dominant periods of motion were 1 to 2 seconds. With data digitized at 16.6 samples per second, the window length of 20 sample intervals was a compromise for a production run.

Throughout the text and on all illustrations the components will be referred to as VERT and RAD for the doubly rotated vertical and radial input signals respectively, and P-D VERT and P-D RAD for the P-D processed vertical and radial output signals respectively.

4-6 Results of P-D Processing

A few examples of the results of P-D processing will be shown here to demonstrate some of the more important effects. Others will be shown in some of the following chapters as illustrations for particular topics.

Figure 11 gives a comparison of the appearance of the input and output records. The VERT record shows two strong signal bursts, the primary P and another approximately 15 seconds later. As can be seen from the phase relations on VERT and RAD, the first burst is relatively pure P motion, and is passed strongly on P-D VERT and P-D RAD. The second burst is strong on VERT but weaker and distorted on RAD; only half of one cycle of this burst is passed strongly by the

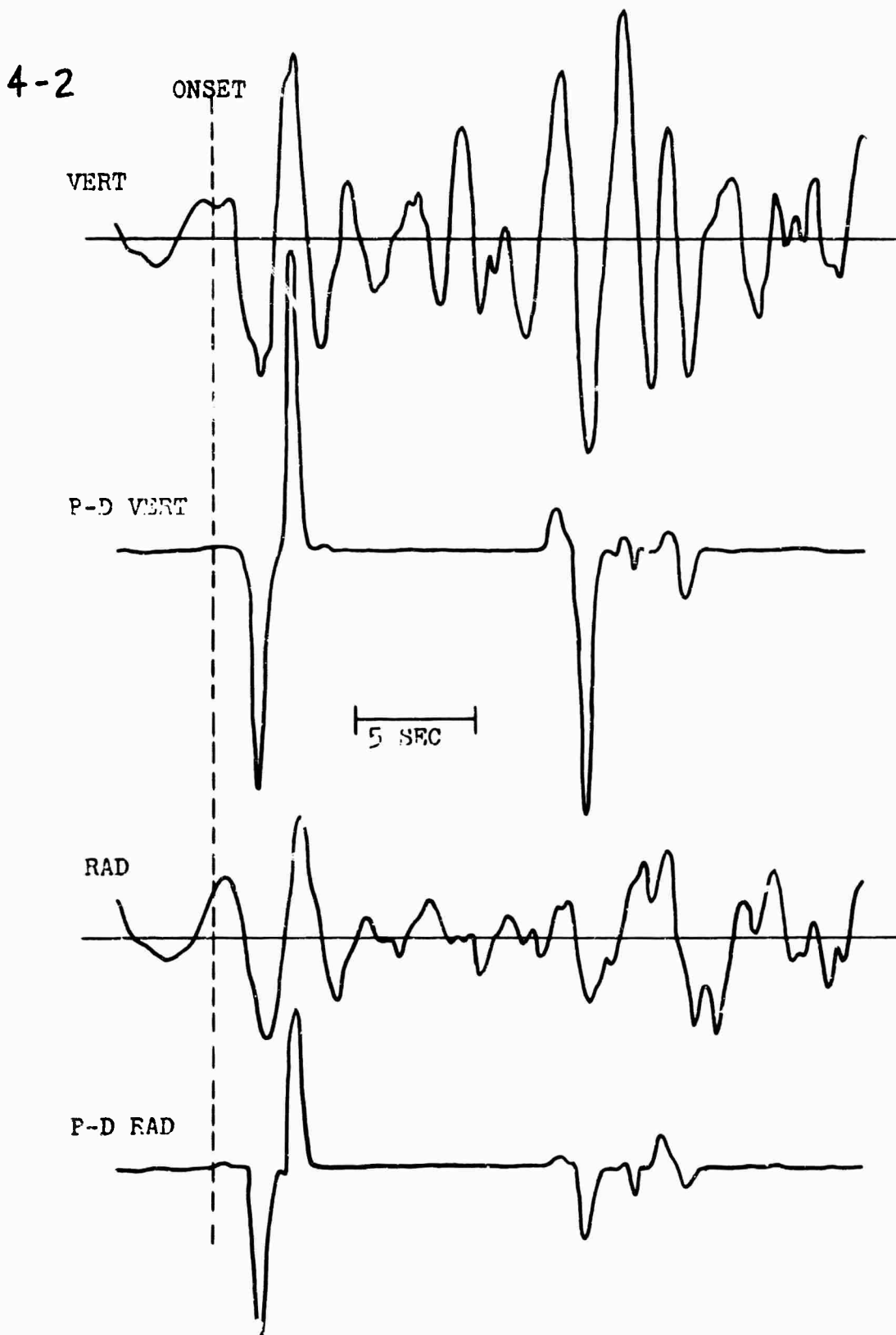


Figure 11. An example of the effect of the P-detection processor.

processor. The processor eliminates completely all other motion on the records. An important effect shown in Figure 11 is the enhancement of the initial onset of the two strong signal bursts.

Figure 12 is included to illustrate that strong P motion does not require P-D processing for identification. The VERT and RAD records are superimposed and the area between the traces shaded to emphasize their similarity. From the coincidence and in-phase relation of the VERT and RAD components all of the energy in the seismogram can be identified as relatively pure P. That this is true is shown by the abundant energy retained on P-D VERT and P-D RAD.

The ability of the P-D processor to detect a common secondary phase at two stations when the seismograms are not similar is shown in Figure 13. The two station records are aligned on the onset pick. The strongest P-D VERT energy burst appears at an identical time (13 seconds after onset) on both of the station records. Although passage of this phase is based partly on the radial components which are not shown in Figure 13, the appearance of the VERT records does not suggest the presence of a single strong phase common to the two seismograms. The ability of the processor to detect such phases is used to identify pP and sP phases which are discussed in Chapter VII.

13-2

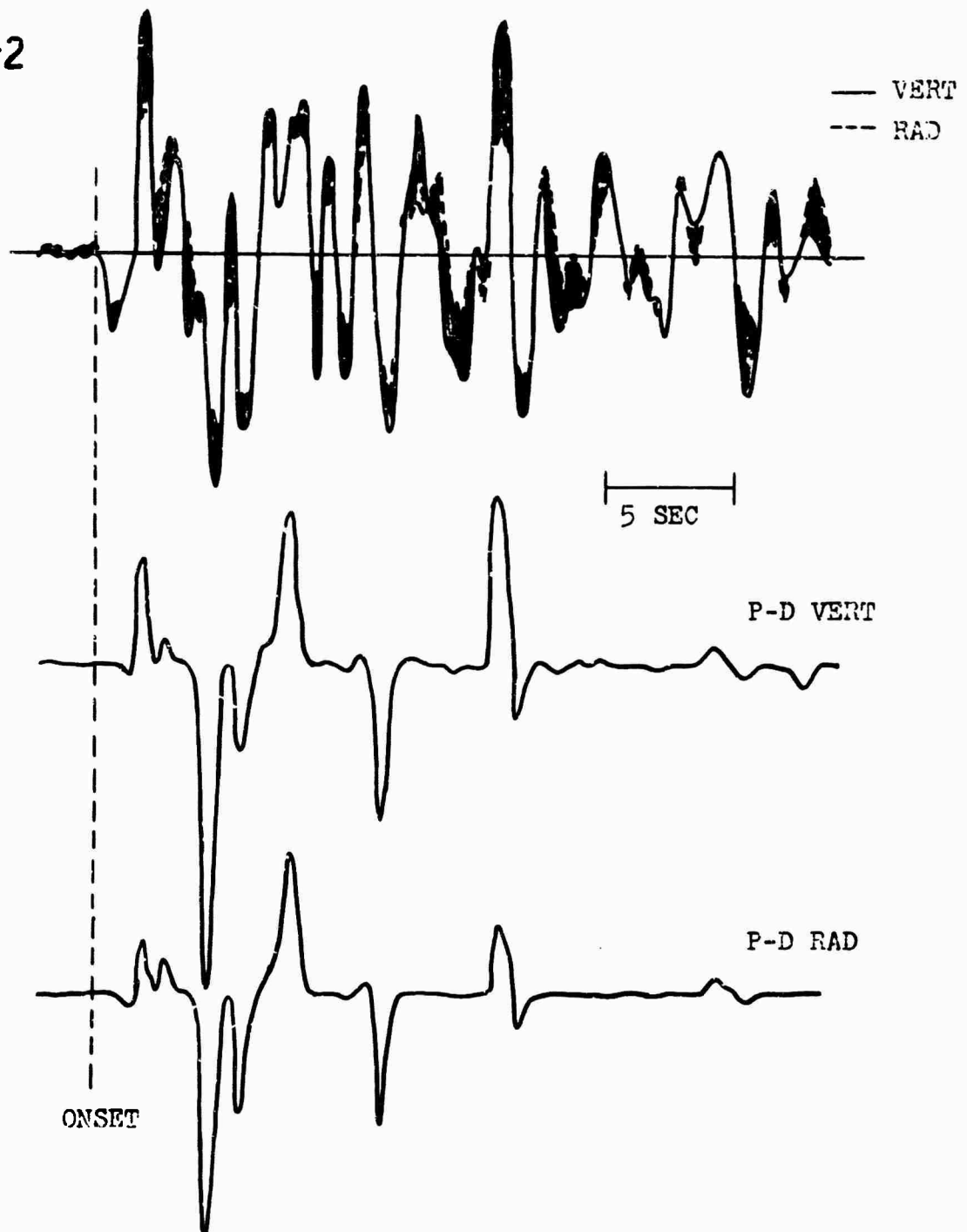


Figure 12. An example of an event with strong P motion which does not require P-Detection processing for identification.

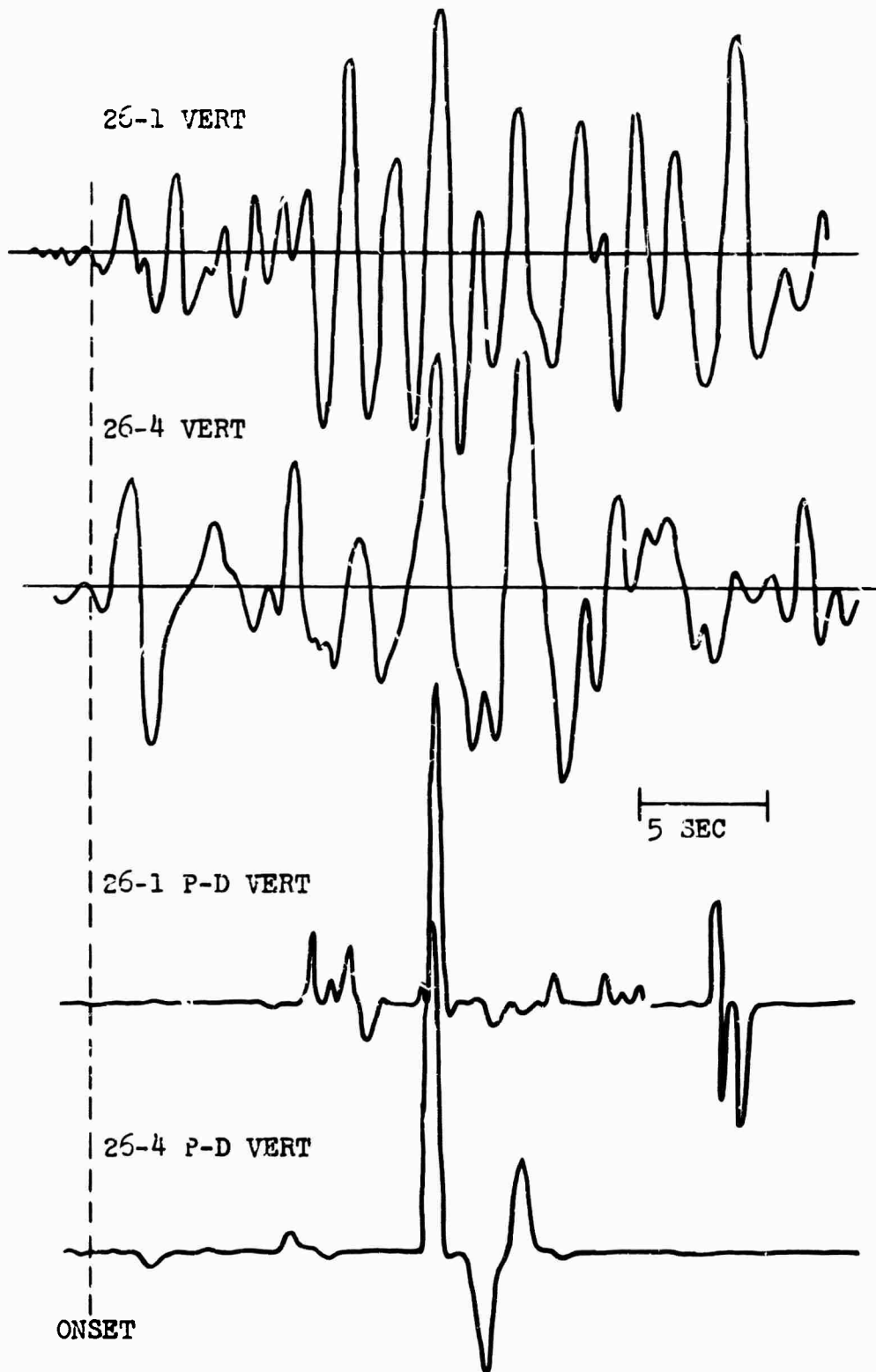


Figure 13. An example of the P-D processor detecting a common secondary phase in dissimilar signals.

CHAPTER V

GENERAL RECORD CHARACTER

5-1 Strength and Character of Onset

Experienced seismologists can often look at a teleseismic P phase and, without the benefit of other information, categorize the earthquake as distant or near, deep or shallow, continental or oceanic, etc. This judgement is made on the basis of the "character" of the P phase. The term "character" is not easily defined in this context but includes such things as the frequency of the oscillations, the degree of sinusoidal regularity of the oscillations, the time of duration of strong motion, the strength of the onset relative to later arriving signals, and the time of arrival of later arriving signals. Some of the parameters of an earthquake which appear to contribute to this general record character will be discussed in this chapter on the basis of the appearance of the P phase of some of the events in Table II.

5-2 Effects of the Source Radiation Pattern

For many large earthquakes source mechanism solutions can be determined which yield information on the stress

system acting in the focal region. For a summary of the theory and procedure see, for example, Stevens (1966). There are believed to be three principal types of force system: the single couple, the double couple, and the double dipole. These three force systems are shown schematically on the left side of Figure 14. Each will produce an identical initial displacement pattern in the P wave. This quadrantal displacement pattern is shown on the right of Figure 14. A pair of orthogonal planes intersecting in the focus are oriented such that there is a separation of areas of compressional P first motion (away from the focus and defined as positive) and dilatational P first motion (toward the focus and defined as negative). The P first motion on these "nodal" planes is zero. The orientation of the force systems, and hence of the radiation patterns, will depend on the tectonics of the source area and can in general be considered to have a random distribution. This first motion displacement pattern expresses itself as an azimuthal variation on world-wide station records; the observed distribution enables the determination of the orientation of the nodal planes. Each of the theoretical force systems leads to a theoretical faulting model for the earthquakes, one of the nodal planes being the fault plane and the other orthogonal to it. An additional feature of faulting is the azimuthal variation which expresses itself not only in a first motion pattern but also in a variation of signal amplitude and shape with azimuth.

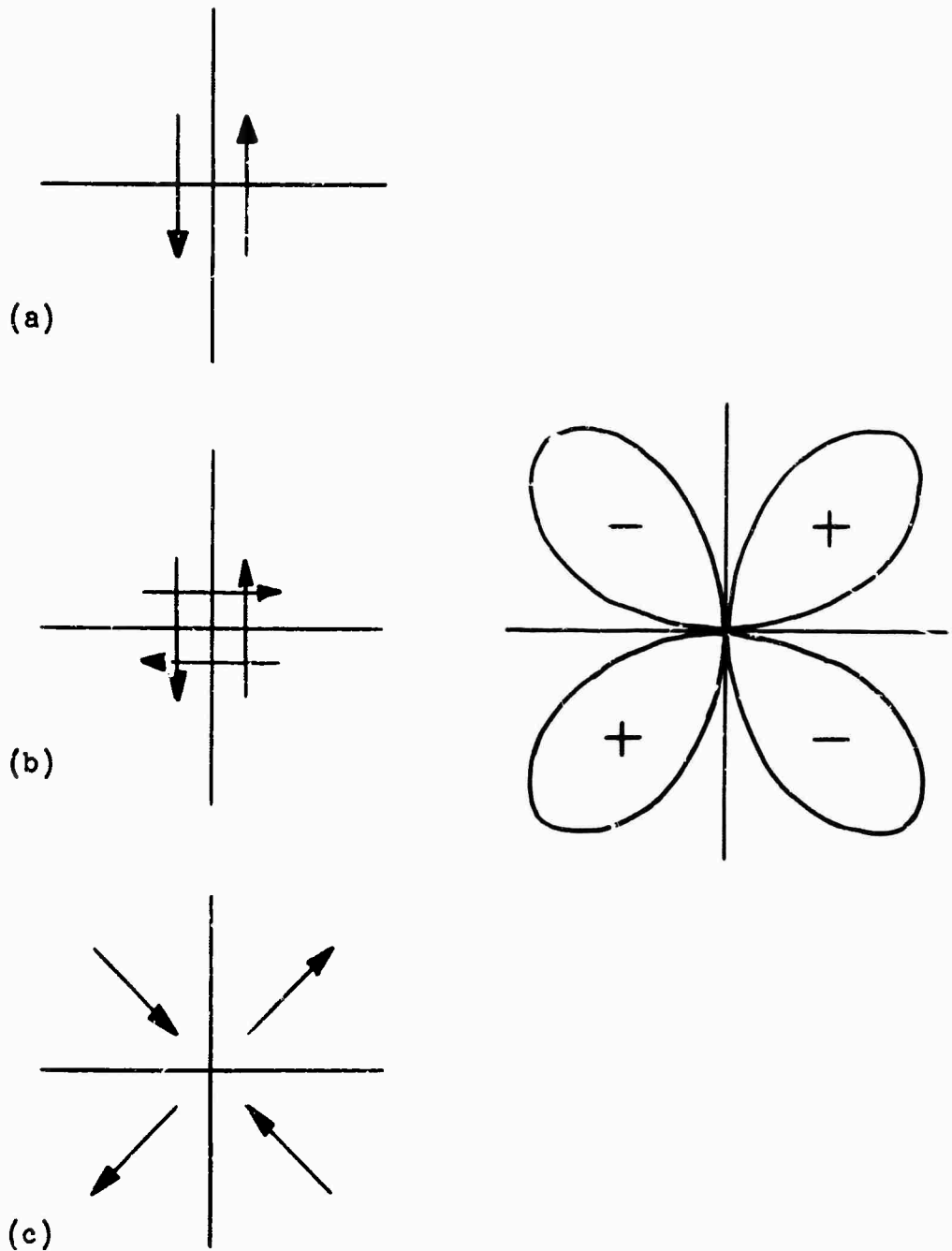


Figure 14. Theoretical P wave displacement pattern (right) for each of three mechanism force systems: (a) single couple, (b) double couple, and (c) double dipole (after Stevens, 1966).

On the world-wide scale of azimuthal variation for such an earthquake mechanism, the entire recording area of western Alberta would virtually constitute a single point. Although there will be no observable variations among stations due to the nodal plane orientations, there is an effect related to the source radiation pattern which would be common to all four stations.

The main P wave is often closely followed by a reflection (pP) from the earth's surface almost directly above the source, the P to pP time separation being dependent on the depth of the source. The complexity of these secondary source phases will be discussed in Chapter VII. The strength of a pP phase on a seismogram is often as great and sometimes greater than that of the primary P phase. On some seismograms pP may be entirely absent. In Figure 15 it is shown how appropriate orientation of the P displacement pattern can cause differences in the relative strength of P and pP.

In Figure 15 P is shown leaving the source region inclined to the vertical at an angle (i) of 30° . As the ray path will travel an approximately symmetrical path from the source to the station, this P will arrive at the base of the crust below the recording station at an angle of incidence of approximately 30° . As the depth of the source is small compared to the total travel path, the minimum time path of pP will be very similar to that of P, and pP will, therefore, reflect from the surface at a point almost directly

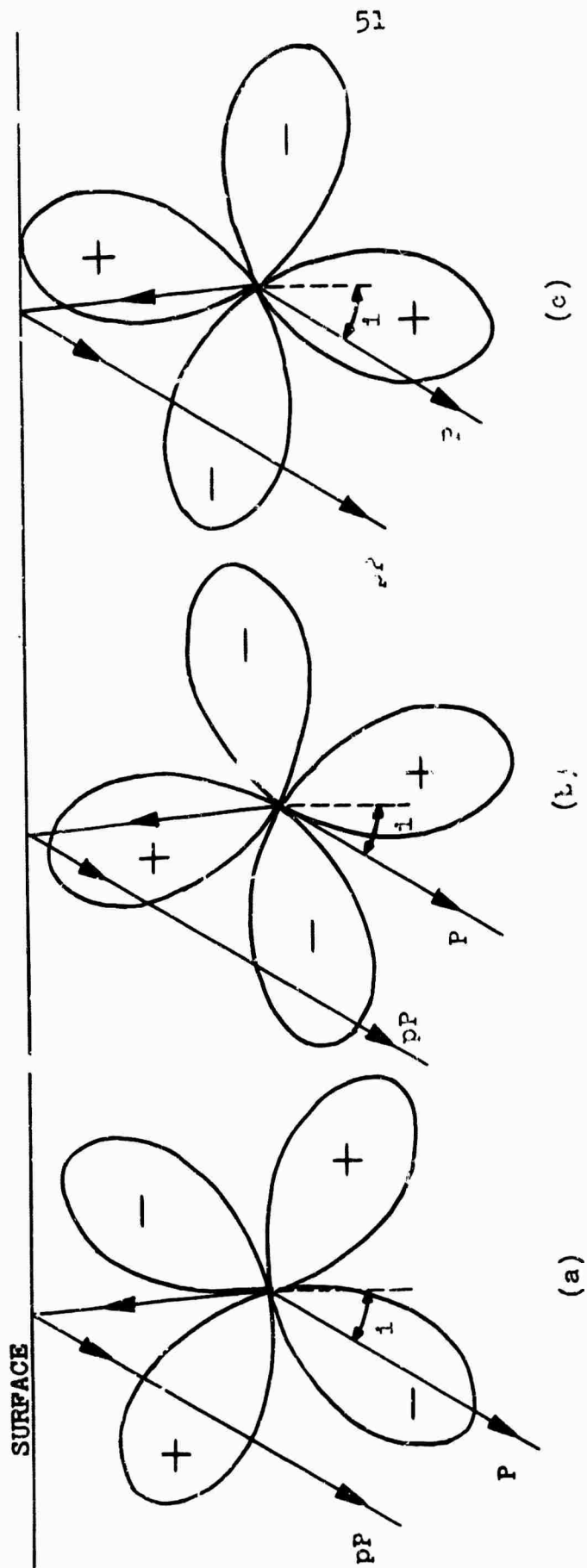


Figure 15. Orientations of source radiation patterns which will produce:
 (a) strong P and weak pP, (b) weak P and strong pP, and
 (c) strong P and strong pP.

above the source. A detailed discussion of the point of reflection of pP is given in Section 7-4. pP, during its upward path is shown on Figure 15 slightly inclined to the vertical. The P and pP rays are shown parallel leaving the source region; because of the scale of the drawings this has the effect of distorting the equality of angles of incidence and reflection of pP at the surface.

The theoretical P wave displacement pattern from Figure 14 has been superimposed on these ray paths in three different orientations. In Figure 15 (a) it is oriented to produce maximum P displacement and minimum pP displacement, in Figure 15(b) the opposite, and in Figure 15(c) P and pP of approximately equal strength. Although, because of the complexity of pP type phases and of source mechanisms themselves, this is a gross over-simplification, it is believed that some of these radiation pattern effects appear on seismograms ^ some of the earthquakes of Table II.

5-3 Some Observed Radiation Pattern Effects

If an earthquake is shallower than about 80 km its pP phase will arrive within about 25 seconds of the primary P phase. The P-D process was run on this length of record and the output plots normalized according to the maximum amplitude in the output record. The P-D VERT records, therefore, show the relative strength of primary P and secondary source phases for earthquakes shallower than 80 km. pP and P

phases for deeper quakes were processed on different runs and were not scaled equally. Earthquakes nearer than 30 degrees tend to show strong motion over much of the 25 second record and identification of secondary phases is more difficult. Consequently, only those events with reported focal depths shallower than 80 km and epicentral distances greater than 30 degrees were studied for radiation pattern effects.

There are 25 earthquakes in this category. Six earthquakes show strong primary P onset with weak or absent secondary, 8 show a weak onset relative to a strong secondary, and 11 show onset and secondary phases of approximately equal strength. No obvious correlation can be found between the grouping of earthquakes in these categories and any of the hypocentral parameters given in Table II. It is proposed that the observed effects may be related to the three orientations of the source radiation pattern shown in Figure 15. Unfortunately, mechanism solutions are not available for any of the earthquakes listed in Table II. In the event that solutions for some of the earthquakes become available at a later date, in order that this proposal might be checked the events in each of the three categories are shown in the following table.

	EVENT NUMBERS (SEE TABLE II)
strong onset, weak secondary	14, 16, 22, 23, 29, 39
weak onset, strong secondary	2, 11, 12, 19, 27, 28, 33, 34
strong onset, strong secondary	1, 4, 5, 13, 15, 17, 18, 21, 36, 37, 38

To demonstrate the criterion of "weak" and "strong" signals, and to show how the P-D processor emphasizes the comparison, two New Britain earthquakes with apparently opposite radiation pattern effects are shown in Figure 16. The two events, 19-1 and 29-1 are aligned on the arrival pick. The relative strengths of the onset and secondary are apparent on the VERT records, but emphasized on the P-D VERT records. 19-1 shows no P-D VERT motion at the onset, but 2 cycles of secondary motion at about 15 seconds. 29-1 shows 3 strong cycles of onset motion, but no secondary motion.

Both North Atlantic earthquakes, events 12 and 33, show weak onset relative to the secondary motion. The VERT and P-D VERT records for 12-2 and 33-4 are shown in Figure 17. The P-D VERT records show very strong secondaries; at 16 seconds for 12-2 and 8 seconds for 33-4. On the basis of the time of arrival of event 12 secondary, the focal depth for this event has been adjusted to 45 km (see Table V and accompanying text).

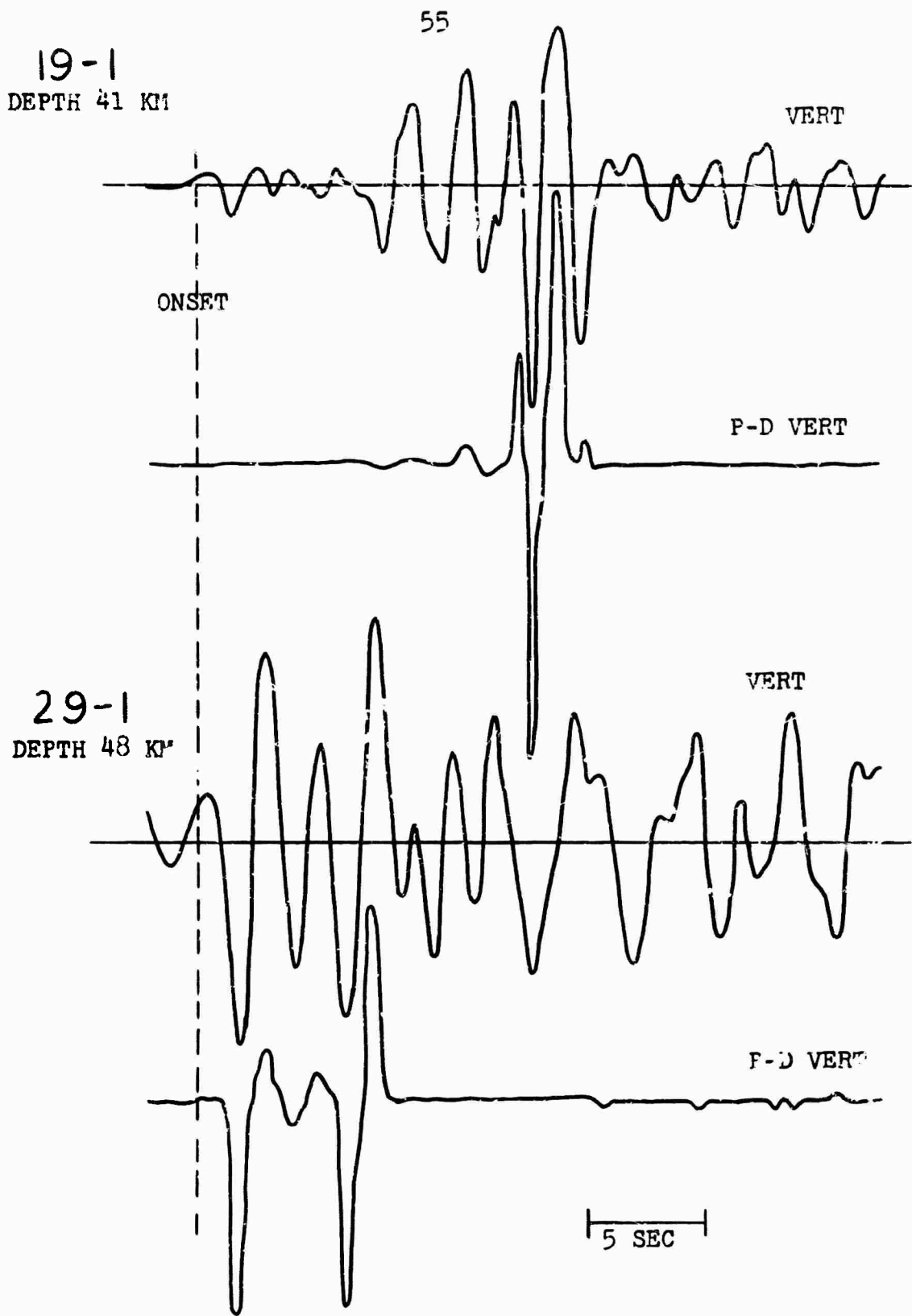


Figure 16. Two New Britain events with opposite radiation pattern effects.

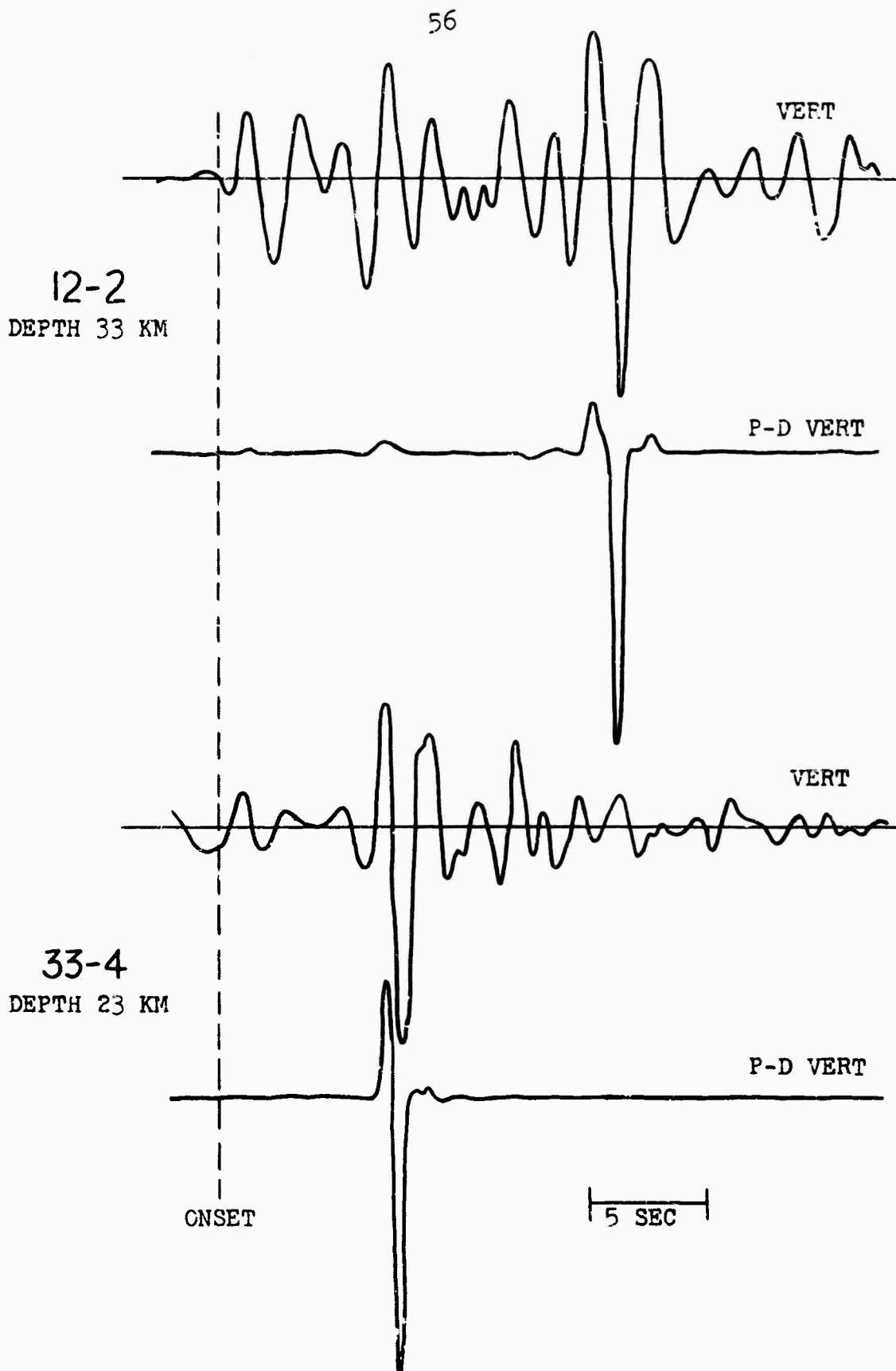


Figure 17. Two North Atlantic earthquakes showing weak onset relative to secondary arrival.

Sykes (1967) gives mechanism solutions for ten earthquakes occurring on fracture zones that intersect the North Atlantic ridge. The mechanism of each of the earthquakes is characterized by predominant strike-slip motion on a steeply dipping plane. Using the fracture zone map of Heezen and Tharp (1965) it is found that event 12 is on a large fracture zone, event 33 is not. There remains the possibility that event 33 is associated with a smaller fracture zone not shown on the large scale map of Heezen and Tharp. The P radiation patterns shown in Figures 14 and 15 are cross sections through the focus in the plane of the force system, and are representative of a point source. For a steeply dipping fault plane, figures of the type shown in Figure 15 would contain the plane of the radiation pattern perpendicular to the plane of the paper. Therefore, this type of radiation pattern cannot be drawn in the same plane as the P and pP rays. Although it might be assumed that events 12 and 33 have mechanism solutions similar to the ten earthquakes studied by Sykes, because of this difficulty it cannot be shown that a steeply dipping fault is (or is not) consistent with weak onset signals relative to strong secondaries. Of possible significance is that the two North Atlantic quakes shown in Figure 17 may have a similar mechanism orientation.

5-4 Duration of the P phase

pP phases for earthquakes at depths greater than 100 km are well separated on the seismogram from the primary

P arrival. As pP is, except in special circumstances, the only strong phase which arrives within a minute of P for teleseismic events, it is easily recognized and an approximate depth for the event easily calculated by assuming a velocity for its extra two-way travel path to the surface. For shallow earthquakes (say, 30 km), pP will follow the primary P phase very closely and may overlap and interfere with the main P signal burst. For very shallow events, for example, underground nuclear explosions at depths of 1 or 2 km (large earthquakes seldom have depths shallower than about 10 km), pP phases will be inseparably mixed with the primary P signal on the seismogram. Therefore, the depth of an event strongly governs the complexity and duration, i.e., part of the "character", of the first arriving signals on a seismogram.

An illustration of this effect is given in Figure 18 which shows VERT records for 4 different events. The portions of each record which, on the basis of P-D VERT, is strong P is shown shaded on Figure 18. Event 32 was 197 km deep and shows about 3 cycles of regular motion with a duration of about 9 seconds. pP for event 32 arrives 52 seconds after the onset and is not shown in Figure 18. Event 41, which is the nuclear explosion LONG SHOT, has about 6 seconds of higher frequency and more irregular motion. Both events 32 and 41 show low signal level after the initial burst. Events 13 and 4 on Figure 18 have reported depths of 28 and 32 km respectively. Event 13 occurred in a continental environment (Greece) and event 4 in a transitional oceanic-continental

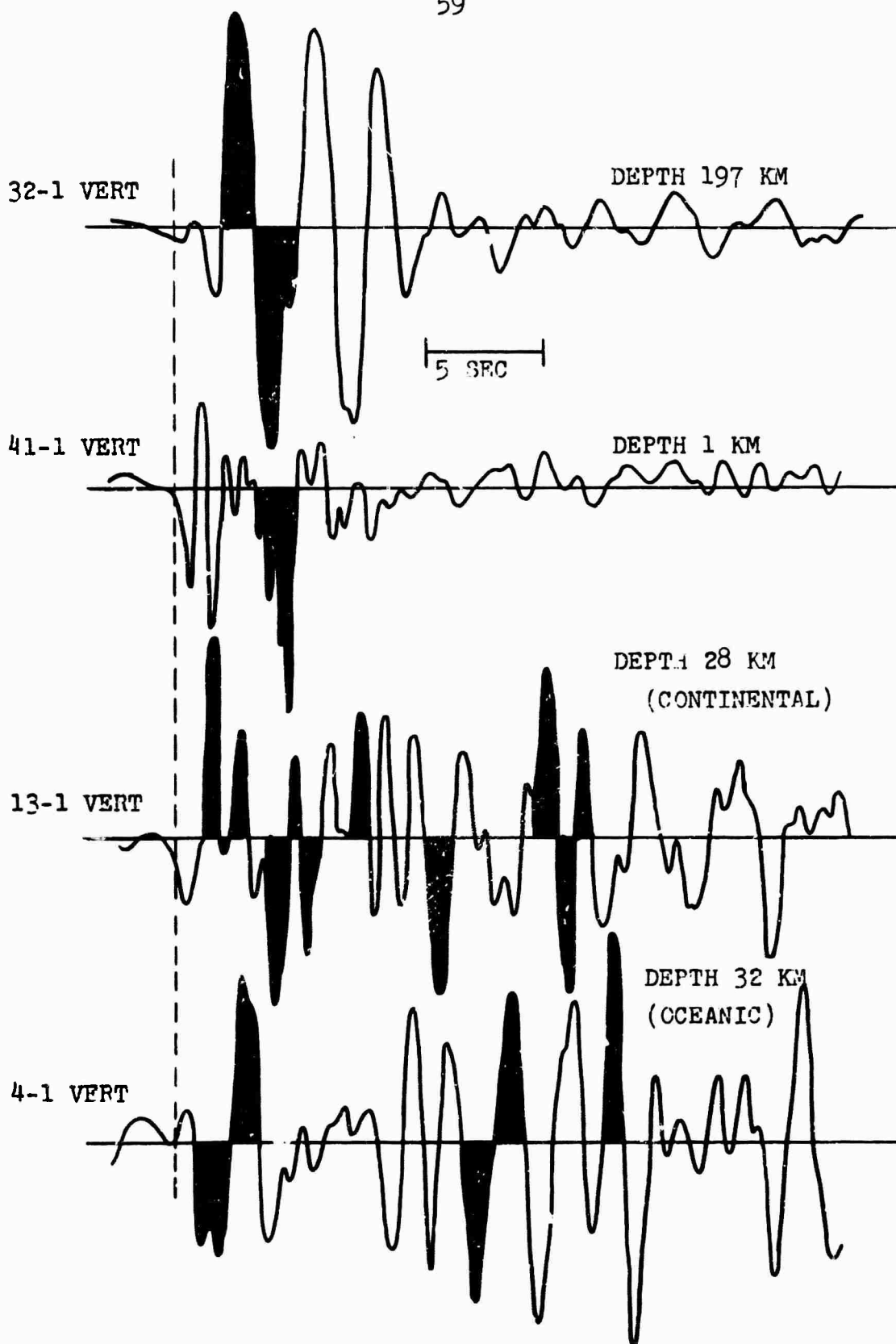


Figure 18. Effect of focal depth and crustal type on appearance of P phase.

environment (Hokkaido); both show strong signal over the entire 25 second record, including more than one contribution of strong P type motion.

Although pP is the dominant phase which contributes to the signal after the primary P, the seismograms are complicated further by additional phases generated both at the source and in the crust near the recording station. Some of these effects will be discussed in Chapters VII and VIII.

5-5 Period of Motion

Another factor contributing to the character of the P phase is the period of the oscillations. The variations in period of oscillation that can occur is well demonstrated by the four events shown in Figure 18. The dominant period in the strong motion of 32-1 is about 3 seconds whereas in 13-1 it is about 1 second. The periods of motion in 41-1 and 4-1 are more variable.

In a search for correlation between the period of P motion and other hypocentral parameters, the average period was determined for the first 20 seconds of the VERT station 1 record for each of the events. Ellis and Basham (1967) show that the dominant period of motion for a particular event can vary from station to station, depending on the crustal transfer function. By studying the periods at one station only it is assumed that variations in the crustal

transfer function among events will not be great. The results of the period measurements are shown in Figure 19 where period is plotted versus epicentral distance using different symbols for each of 3 focal depth ranges.

There is not a strong dependence of period of motion on either epicentral distance or focal depth, although the events with epicentral distance between 80 and 100 degrees, taken as a group, show slightly longer periods than the nearer events. There is a differential attenuation of P waves with period, the shorter periods being more strongly attenuated, as the waves travel through the earth. This phenomena is probably causing the above effect. Also the shorter periods may be relatively more attenuated for shallow events than for deep events because of the greater density of small scale inhomogeneities in the upper layers of the earth. A dependence of period of motion on depth of focus is not seen in Figure 19.

Most of the variation in period of P phase motion among events is probably attributable to variations in source functions. It should be remembered however, that the seismograms being used here have passed through the recording system response shown in Figure 2 and do not represent true ground motion, let alone true source motion.

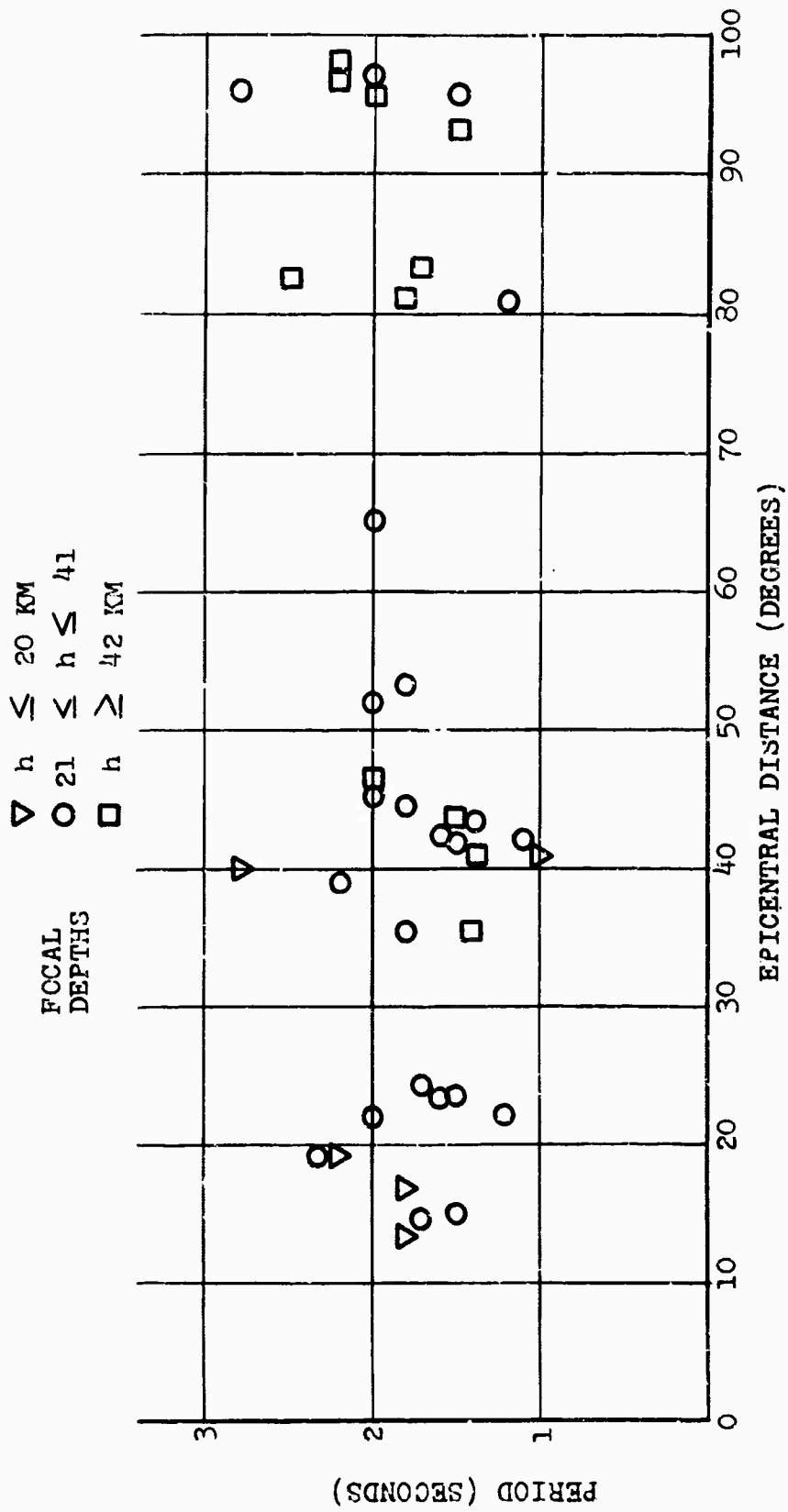


Figure 19. Average period of 20 seconds of P motion vs. epicentral distance.

CHAPTER VI

COMPARISON OF STATION RECORDS

6-1 Introductory Remarks

The principal objective of frequency domain studies of P phases by Ellis and Basham (1967) and others has been to determine if the relative frequency content of horizontal and vertical P signals is in agreement with the wave spectra predicted theoretically from knowledge of the crustal layering. If good agreement could be found the procedure would provide a method of (a) determining local crustal structure from the P phase records of any single seismograph station, and (b) removing local effects from the record to study source signals undisturbed by crustal complexities. To date the method, broadly termed "crustal deconvolution", has been relatively successful at the longer periods, say greater than 10 seconds, but not at shorter periods (authors cited by Ellis and Basham, 1967).

If a P phase has a frequency content which is dependent on the local crustal conditions, some variability among stations should appear in the time domain records.

A search for this variability has been made on the records of events of the Alberta Experiment.

6-2 Comparison of Vertical Records

When the VERT records for the station pairs for the 41 events are superimposed some events can be classified as having similar VERT records at the two stations, and others as having dissimilar VERT records. When the VERT records are similar they are remarkably so. The three events shown in Figure 20 demonstrate this similarity. A total of 26 pairs of VERT components are similar to approximately the degree shown for the events in Figure 20. Of the remaining 14 events (event 17 omitted), one or both VERT components are distorted by noise (12 events) or show a distinct difference in VERT signal character (2 events).

In Table III are listed the signal-to-noise ratios for all events determined from the r.m.s. amplitudes of the first 8 seconds of unrotated vertical signal and the preceding 8 seconds of background noise. The noise and signal sections were filtered with a filter similar to BP-1 in Figure 4 prior to the S/N calculation. As would be expected, the 11 events with noise distortion have low S/N ratios on one or both stations in Table III. However, many of the 26 events showing similar VERT components have S/N ratios lower than 2.0 on one or both stations; three of the events in Figure 20, 12-1, 12-2, and 22-3, have S/N

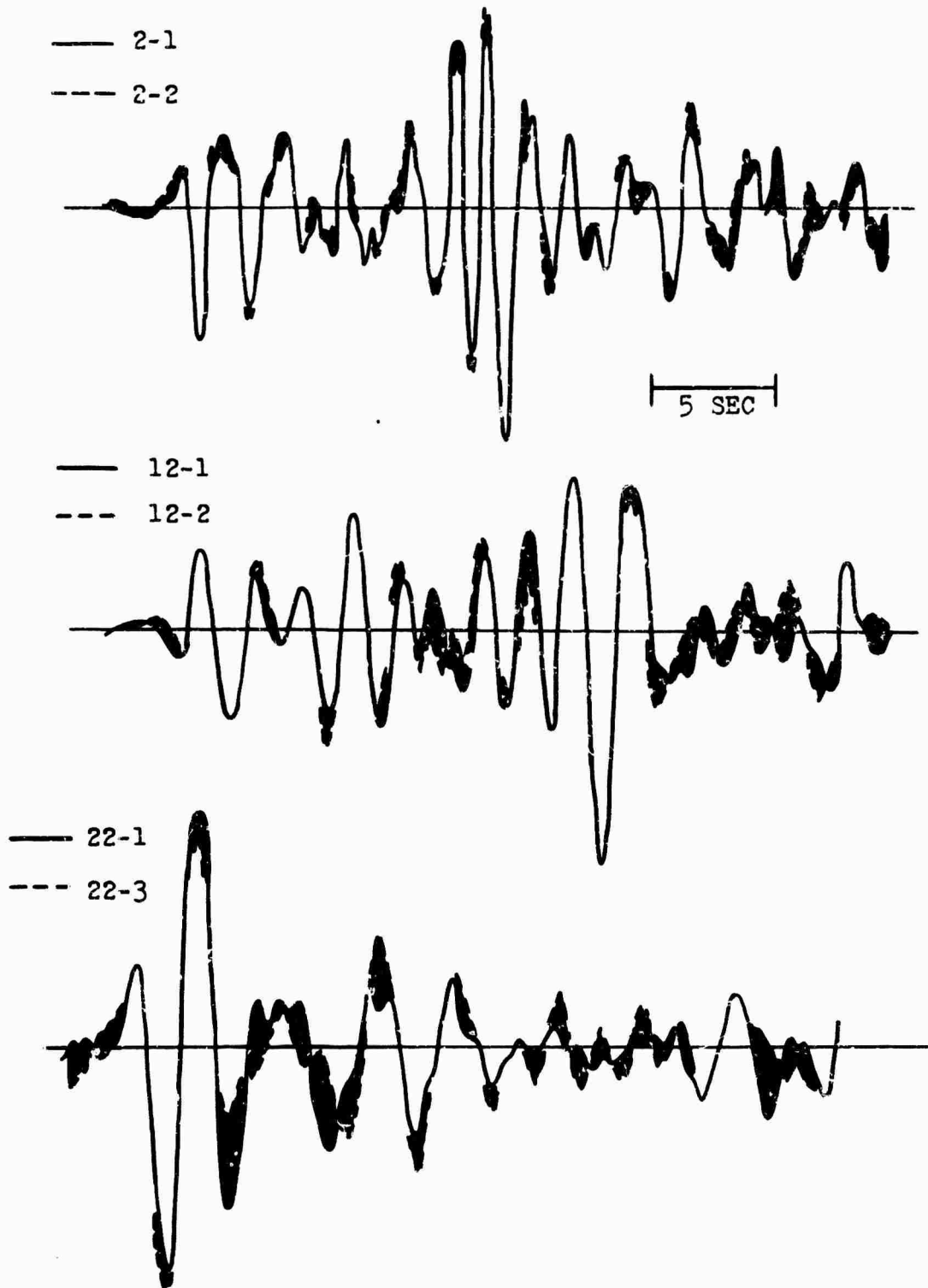


Figure 20. VERT components of three similar events.

TABLE III

RMS AMPLITUDE SIGNAL/NOISE RATIOS

EVENT	STATION			EVENT	STATION	
	1	2	3		1	4
1	2.9	2.3		25	6.8	13.5
2	5.2	5.4		26	3.0	2.4
3	10.6	5.9		27	3.5	5.2
4	2.9	2.0		28	2.2	1.1
5	6.3	8.3		29	1.3	1.8
6	3.7	4.4		30	7.5	5.0
7	5.1	6.7		31	2.7	2.8
8	1.1	2.0		32	19.3	17.6
9	7.8	5.4		33	1.1	3.1
10	2.3	5.4		34	4.5	1.6
11	4.2	2.2		35	1.7	1.7
12	2.0	2.1		36	6.9	2.4
13	11.9	8.0		37	4.1	1.4
14	6.2		1.8	38	1.2	0.9
15	8.5		7.7	39	3.6	3.0
16	3.4		3.6	40	9.8	4.1
17	-		1.2	41	8.4	2.4
18	1.6		1.0			
19	4.0		2.9			
20	23.3		8.5			
21	5.3		1.2			
22	4.6		1.9			
23	5.3		2.3			
24	3.9		4.0			

STATION	MEAN S/N
1	5.1
2	4.6
3	3.3
4	4.1

ratios near 2.0.

Three examples of events showing noise distortion on the VERT records are shown in Figure 21. Comparing the events of Figure 21 with those of Figure 20, the approximate noise level throughout the records can be judged by the clearness of onset of the signal; events 2 and 12 in Figure 20 show a very clean onset, whereas all events in Figure 21 show onset distortion. When background noise contaminates these events its frequency band is usually very near to that of the signal and cannot be eliminated by the filter BP-1. However, some of the unfiltered records contained excessive long and short period noise which passed the filter in sufficient amounts to contaminate the VERT records; the station-pair similarity of these would be improved by a slightly narrower bandpass filter.

The general sources of background noise were outlined in Section 3-1. In that section it was stated that station 1 was the quietest of the four sites. An approximate measure of the background noise level at the four stations is shown in the table of average S/N ratios for the three station pairs in Table III. For each station-pair group of events station 1 has a slightly higher S/N ratio.

The two events showing a distinct difference in VERT signal which is not attributable entirely to noise contamination are shown in Figure 22. Both of these are

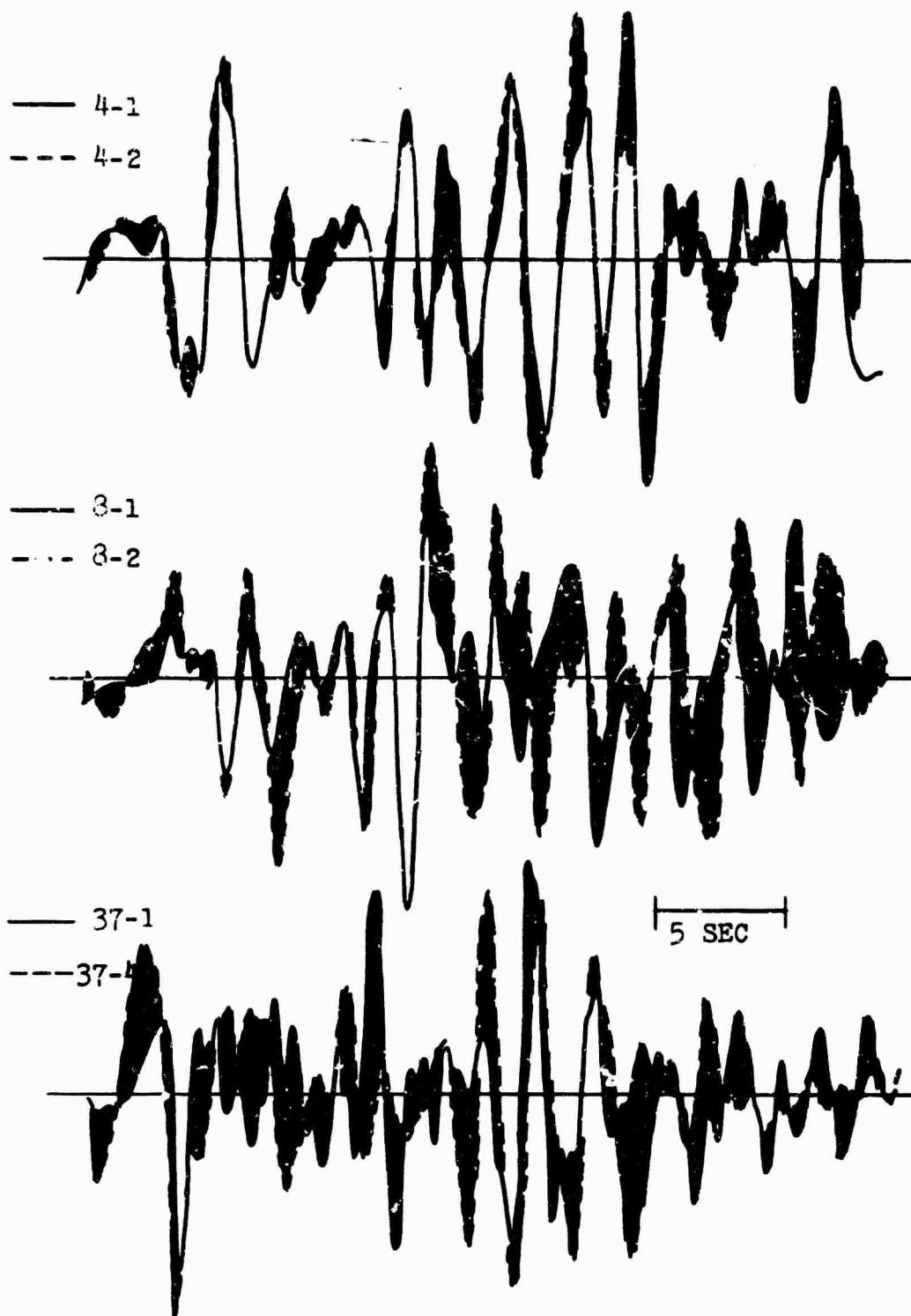


Figure 21. VERT components of three events distorted by noise.

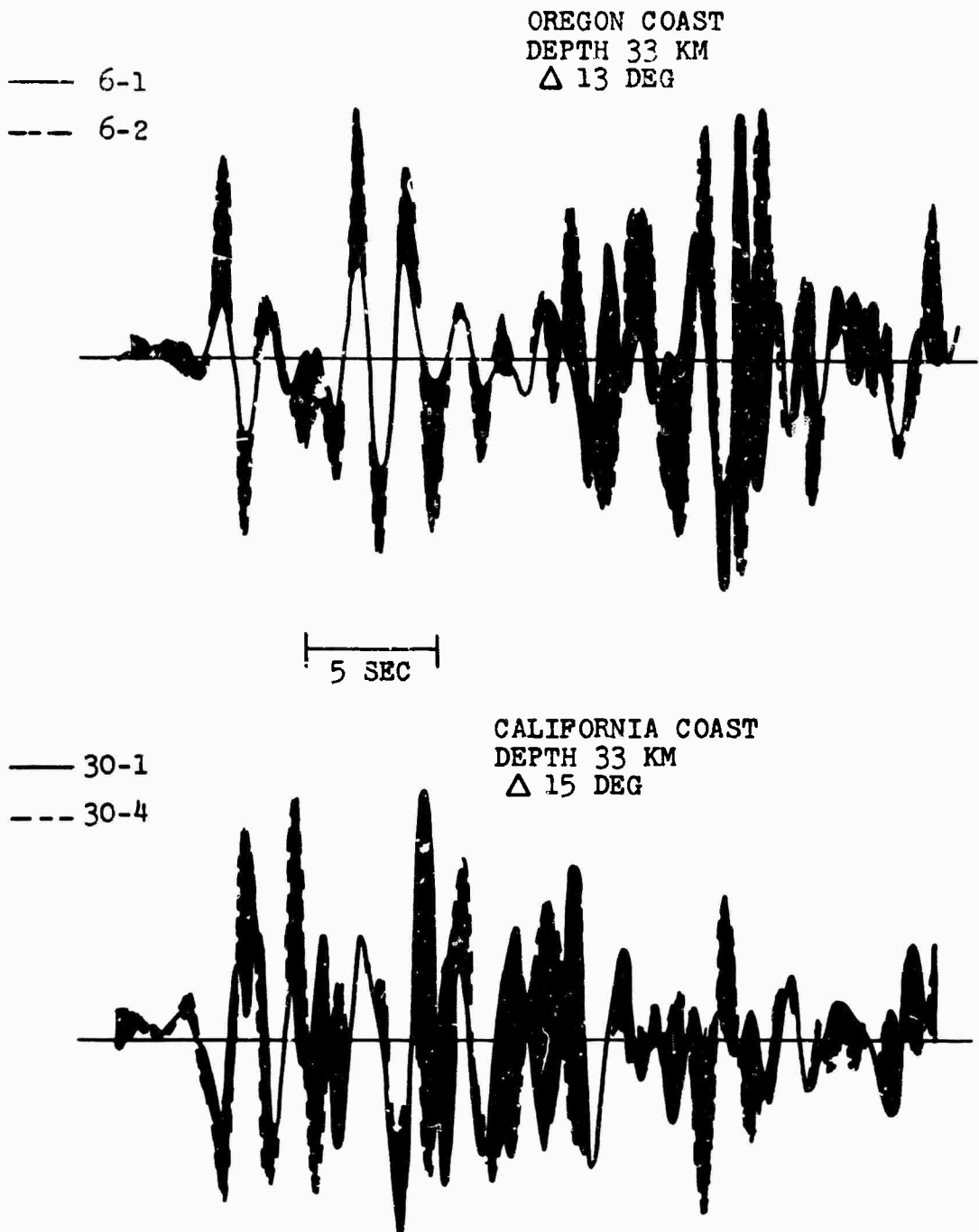


Figure 22. VERT components of two near events with distinct difference in signal character.

near events on the Pacific coast of United States. Event 6 has a difference in signal amplitude throughout the first half of the 25 second record, and a relative shift in phase throughout the second half. Event 30 shows amplitude and phase differences throughout the record.

With epicentral distances of 13 and 15 degrees for events 6 and 30 respectively, neither is teleseismic (as defined in Section 2-3). However, there are four southern Alaska events (10, 24, 31, and 35) which are not teleseismic but which show remarkably similar VERT components on the station pairs. It may then be assumed that the degree of difference is in some manner related to the azimuth of approach. There are five events with epicentral distances slightly larger than 20 degrees. Two in southern Alaska (7 and 25) having similar station-pair VERT components, two in southern Alaska (8 and 26) with noise distortion, and one in Missouri (40) with noise distortion. For comparison with the dissimilar near events in Figure 22, two similar southern Alaska near events are reproduced in Figure 23.

The phases which constitute the P signal for events of this epicentral distance range (13 to 24 degrees) are not well understood. It is within this distance range that P_n and P_r (the wave refracted below a low velocity discontinuity in the mantle) travel time curves intersect (see, for example, Lehmann, 1962), but the time difference

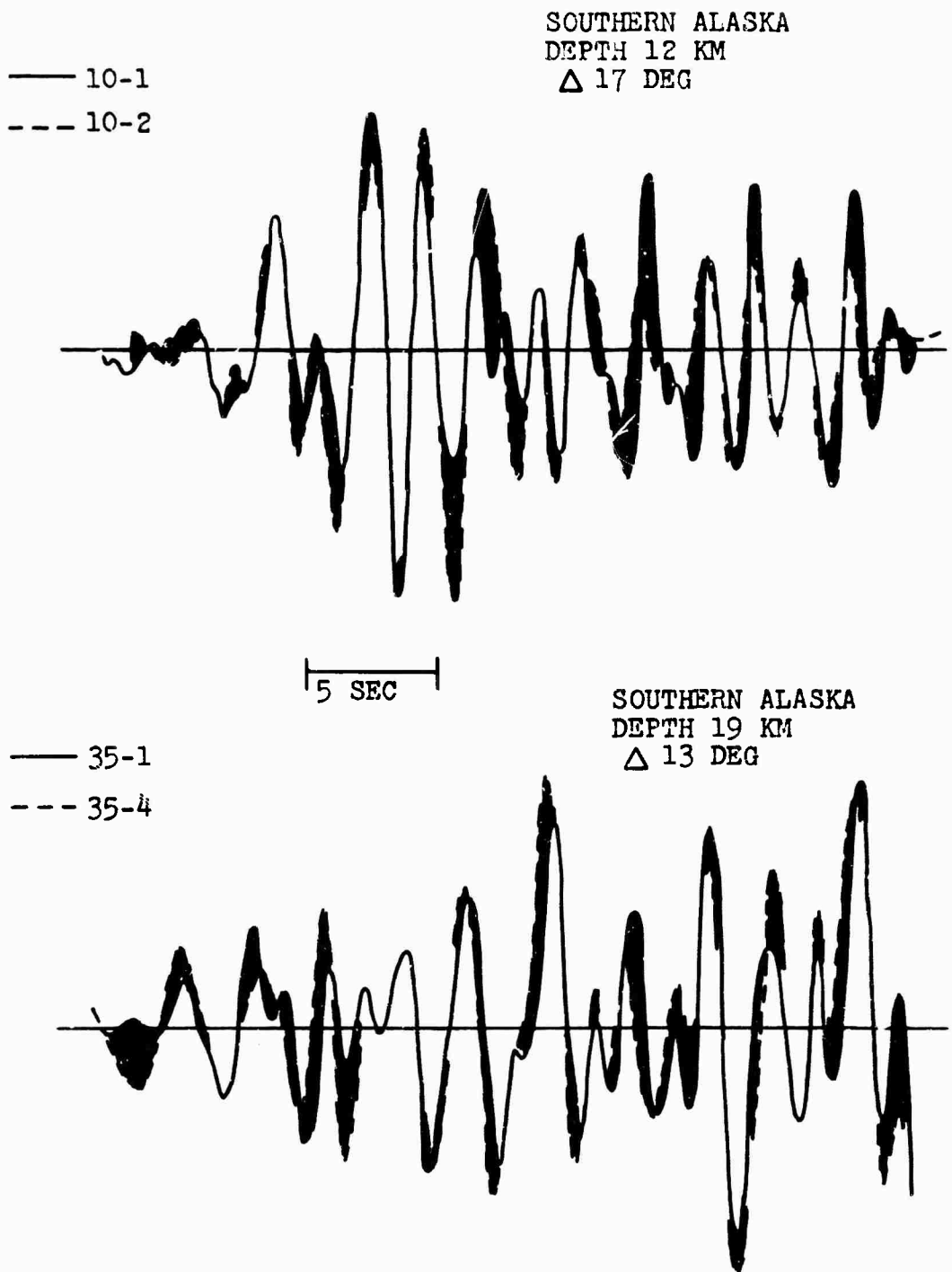


Figure 23. VERT components of two similar near events.

between P_n and P_r will depend on a number of other factors including the focal depth of the event, the thickness and velocity structure of the crust, and the velocity structure of the upper mantle. In addition there can be amplitude shadow zones caused by reversals in sign of the velocity-depth gradient below the Moho, and further complexity due to arriving secondary pP and sP type phases.

Because of the generally complex tectonic regions traversed by seismic waves from Oregon, California and Alaska to central Alberta, the character variations discussed above and illustrated on Figures 22 and 23 are more likely associated with a complex travel path than with effects local to the stations.

6-3 Comparison of Radial Records

The RAD records show a generally higher background noise contamination than do the VERT records. This is because both microseismic and cultural noise have a greater proportion of their displacement in horizontal plane, and because of the low horizontal signal level for phases arriving at a steep angle of incidence. The lower general S/N ratio of RAD components makes comparison of station pairs of RAD signals more difficult.

RAD records for only those events with epicentral distances between about 35 and 55 degrees were compared in this study. This range was chosen for two reasons:

firstly, the distant events have a significant contribution of vertical energy in the RAD component due to the rotation about the transverse, and secondly, there may be complications in RAD records for the near events of a type discussed in the previous section.

There are 16 events in the 35 to 55 degree epicentral distance range, but 9 of these have RAD records contaminated by noise. The remaining 7 RAD pairs divide into two contrasting groups, 4 with relatively short-period motion, and 3 with relatively long-period motion. The four short-period pairs are shown in Figure 24, and the three long-period pairs in Figure 25. Some of these RAD records have a fairly high noise content, although not enough to disguise the signal content. Event 5-1 on Figure 24 has some long-period noise but the signal is strong enough to dominate the record. Events 22-3 and 23-3 on Figure 25 show some short-period noise, but not enough to distort the long-period signal.

It is seen on Figures 24 and 25 that when long- and short-period RAD motion has similar amplitude relative to the background noise, the long-period signal shows greater similarity on the station pairs of records than does the short-period signal. Those segments of the records which, on the basis of the P-D RAD records, are strongly rectilinear P signal are designated by a "P" on Figures 24 and 25. At all of these segments, and for only these

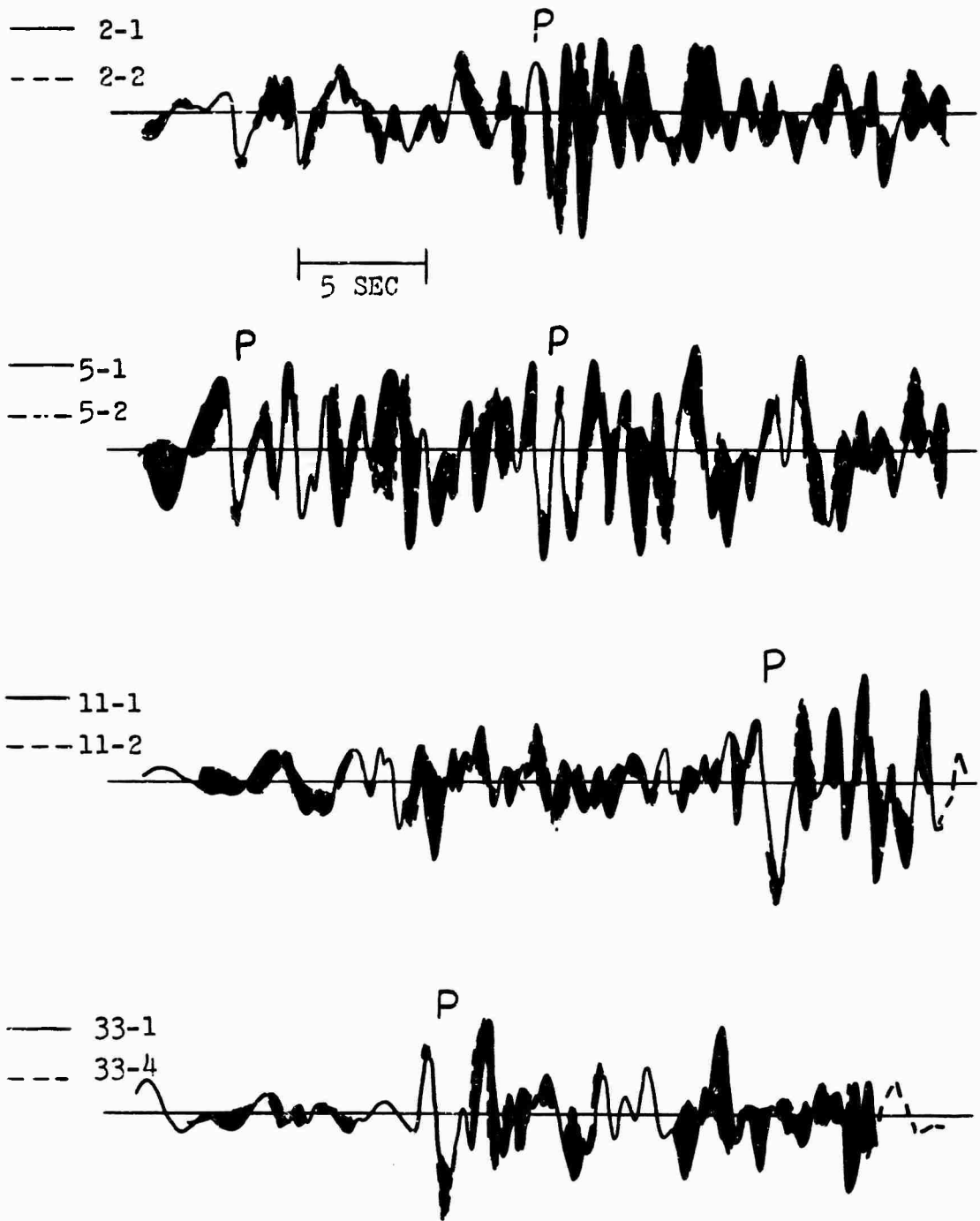


Figure 24. RAD components of four short-period events.

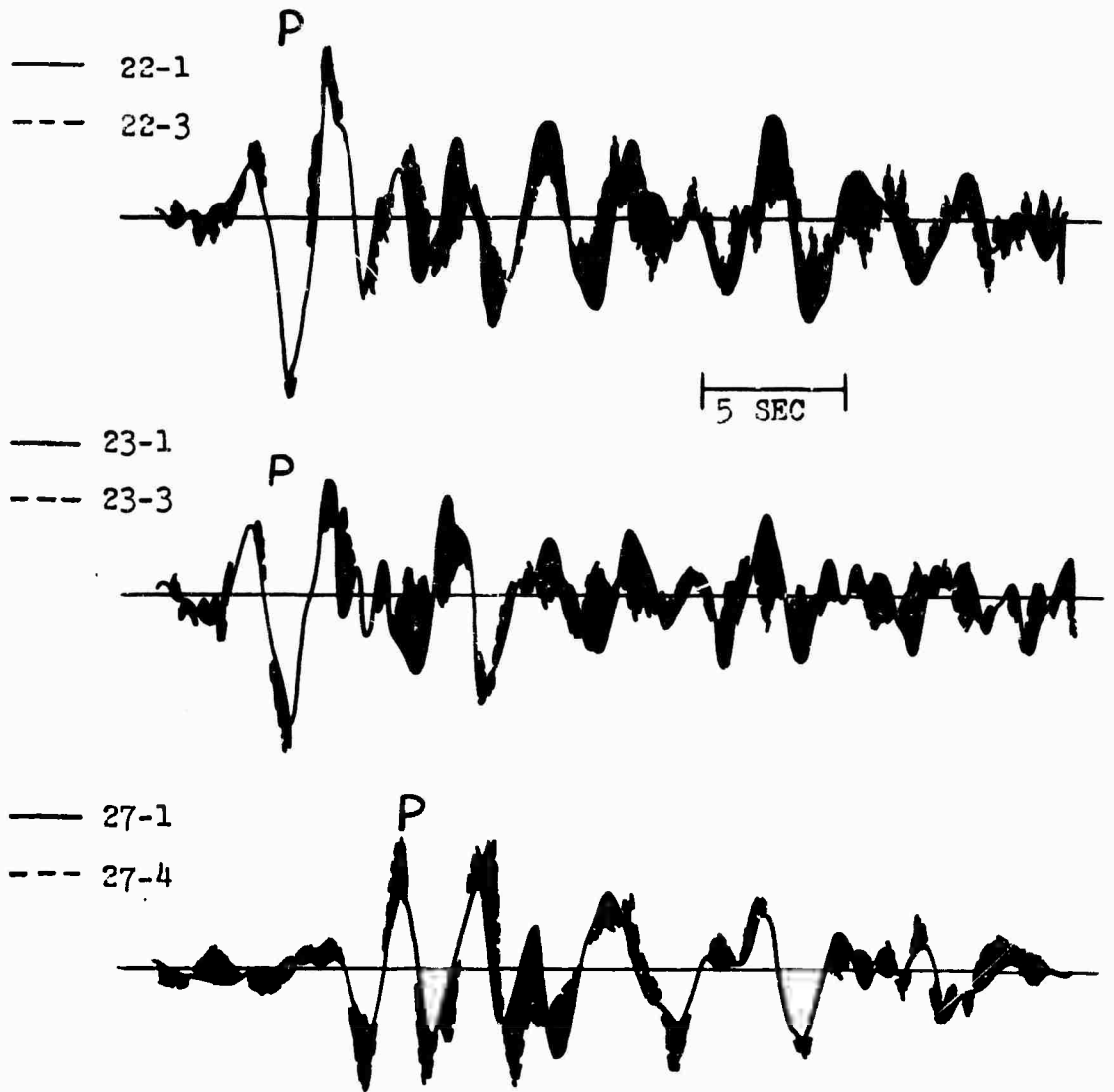


Figure 25. RAD components of three long-period events.

segments, are the RAD records of the stations strongly coincident. This is in contrast to the VERT components which retain a similarity on the station pairs throughout the entire record (see Figures 20 and 23).

6-4 Significance of Results

Some important conclusions can be drawn from this comparison of station records. The remarkable similarity of VERT components (for distances greater than 20 degrees, and when no noise contamination is present) is highly significant in terms of the effect of the crustal structure on records obtained at a station. The differences in station-pair RAD records when a strong P signal is not present is related to S wave generation in the crustal layers. The first of these topics (VERT similarity) will be discussed here, the second (RAD differences) will be included in a more detailed discussion of phase distortion in Chapter VIII.

The Alberta experiment, during which the events of this study were recorded, was specifically planned to test the hypothesis that variations in crustal characteristics beneath stations will be evident in the short-period P phases of teleseismic events. Previous studies (Ichikawa and Basham, 1965, and Utsu, 1966) had indicated that the most dominant effect in the short-period range could be expected from the upper few kilometers of the crust. It

was for this reason that Alberta with a well defined sedimentary section was chosen as a recording site. The stations were located in a line perpendicular to the strike of the regional trend (see Figure 3) to yield a maximum variation in sedimentary section thickness for a station spacing up to about 160 km.

The sedimentary column under each of the four recording sites is shown in Figure 26. The columns were constructed from available deep well control and isopach maps. Each sedimentary sequence in the columns is labelled with the P velocity in km/sec determined from continuous velocity logs from 12 deep wells near the line of section.

The crustal refraction profile nearest to the recording area was that of Richards and Walker (1959). The recording line with a shot point at each end was 140 km long and oriented approximately north-south with the center point about 40 km northeast of Calgary. The profile was not long enough to delineate the Moho and intermediate boundaries at any point except near the center of the line.

The only other refraction profile in the Alberta area is that of Cumming and Kanasewich (1966) between Swift Current, Saskatchewan and Vulcan, Alberta. The western end of this profile is approximately 200 km southeast of the recording area. The interpreted crustal structure on the western end of this profile is used for the recording area, on the assumption that it can be extrapolated along

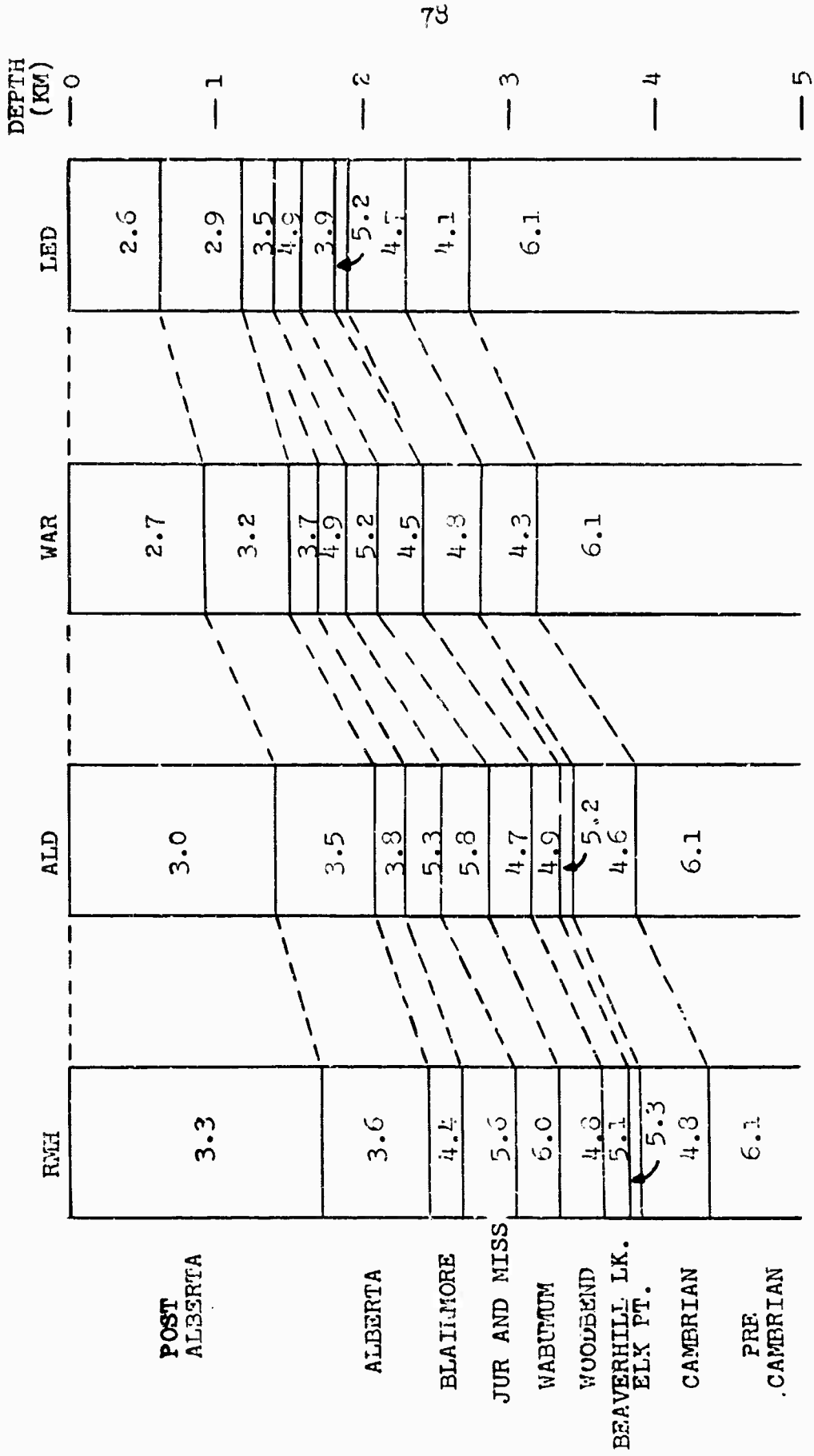
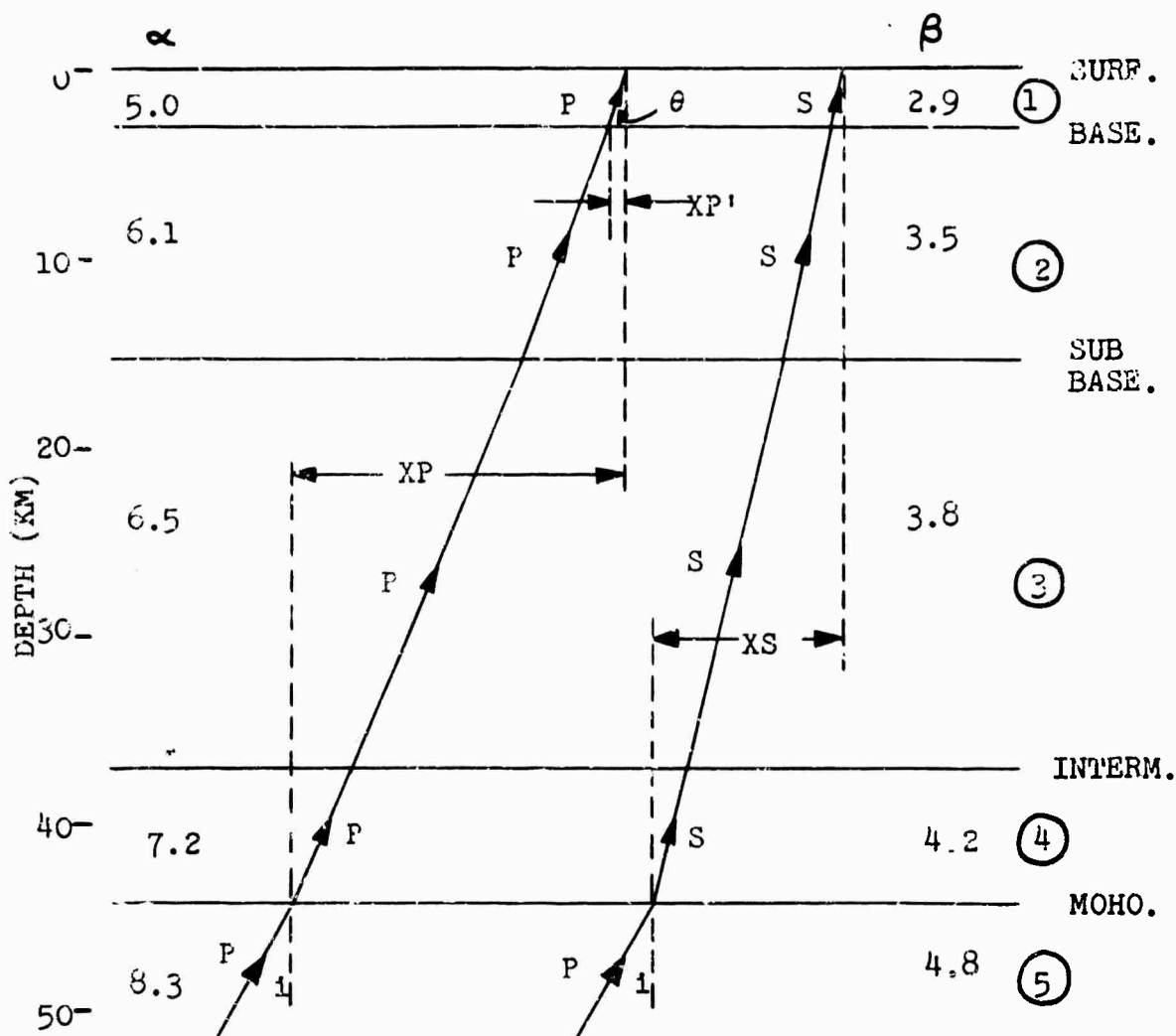


Figure 26. Sedimentary columns under Alberta recording sites showing P velocities in km/sec.

the regional strike. This crustal section, which is shown in Figure 27, is not sufficiently well defined to allow further interpolation to yield a different crustal column under each of the recording stations.

As the incident P wave propagates through these crustal layers, reflected and refracted P and SV waves are generated at each interface, the amplitude of these converted waves depending on the contrast in acoustic impedance across the interface. Acoustic impedance depends on wave velocity and medium density, and velocity is usually assumed to be a linear function of density in the velocity range of interest here. Therefore, it can be assumed that the converted wave amplitudes will depend on the velocity contrast across the interface. References to the numerous investigators who have studied the theoretical problem of the partition of energy incident at an elastic interface and the amplitudes of the resulting reflected and refracted waves are given by Costain et al (1963).

The incident angle used in the seismogram rotation described in Section 3-3 was the angle at the base of the crust. The steepening of the ray path as it propagates through the crust is shown in Figure 27. It can be seen in the table accompanying Figure 27, for example, that an angle of incidence, i , at the Moho of 18° will steepen to 10.7° (θ) at the surface; an i of 42° will steepen to θ of 23.8° .



i (DEG)	XP (KM)	XS (KM)	XP' (KM)	θ (DEG)
18	10.8	6.2	0.59	10.7
24	14.6	8.2	0.78	14.2
30	18.5	10.2	0.98	17.5
36	23.2	12.1	1.22	
42	26.7	14.2	1.36	23.0

Figure 27. Exploded crustal structure under Alberta sites (after Cumming and Kanasewich, 1966) showing P and S ray paths.

For events in the "source window" θ will be between 0° and 40° degrees (see Figure 7), therefore, θ will be between about 11° and 23° degrees. It is apparent then that the greatest proportion of the displacement of direct or converted P waves will be recorded at the surface in the vertical component, the greatest proportion of converted SV displacement in the radial component.

Relating this to the similar station-pair VERT records discussed in Section 6-2, it is concluded that a teleseismic event contributes almost identical amounts of direct and converted P motion to each of the stations, and, if there are significant amounts of converted P motion, it arrived at an identical delay time at each station (within the time resolution of the records shown). The vertical travel time of direct P through, for example, station 1 sediments is about 0.8 seconds; through station 4 sediments it is about 1.1 seconds. A converted P arriving later would have to spend part of its transit time as converted SV or as a multiple reflection among some of the layers. In order to arrive at each of the stations at delay times different enough to be distinguishable on the records shown (say 0.5 seconds) the converted P would lose almost all of its energy in the delaying process. Without more detailed information on the gross crustal structure under each of the stations, it is not possible to determine whether similar effects in the gross crust could produce sufficient amplitude and time-delayed converted P to make

a distinguishable difference to the VERT records on the station pairs. The similarity of VERT records, however, suggests that such an effect does not occur.

The general conclusion to be reached is that although the crustal columns, and particularly the sediments, under the four stations may be different, to the vertical component of a P phase in the period range discussed here they appear identical.

Some additional information concerning the ray paths through the Alberta crust is presented in Figure 27 to show the scale of crustal irregularities required to affect a teleseismic P phase. These are the distances in a horizontal direction between a point directly beneath the station and the point where direct P crosses the base of the Moho (XP), where direct P crosses the base of the sediments (XP'), and where P to SV conversion would occur at the Moho (XS). Values of XP, XP', and XS are listed in the table of Figure 27 for six different angles θ . Irregularities at Moho depth would have to be situated within a circle of radius about 25 km to affect a teleseismic phase arriving at an Alberta station. The radius of a similar circle at basement depth would be about 1.3 km.

The available information on the basement structure under the recording area, after Garland and Burwash (1959), is shown in Figure 28. This basement geology was determined from gravity measurements, magnetic profiles, and petrological

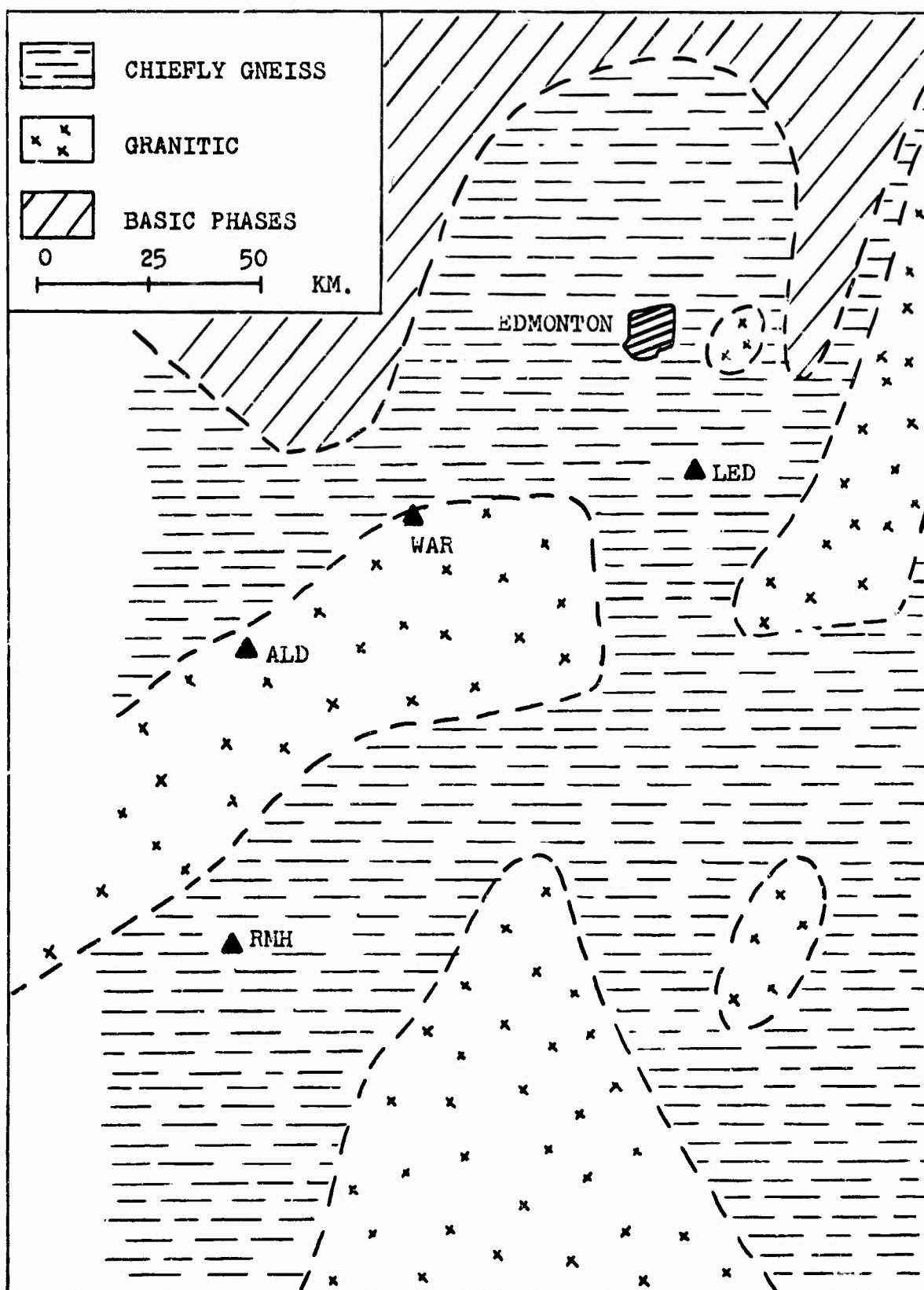


Figure 28. Precambrian basement under recording area (after Garland and Burwash, 1959).

studies of basement well samples. There were no well samples available in the western portion of the map of Figure 28, so the geology represents an interpretation of the geophysical measurements alone. The important feature would appear to be the contact between gneissic and granitic rock passing around the ALD and WAR stations. But, considering the scale of basement irregularities discussed in relation to XP' on Figure 27 and the required amplitude and delay times of converted phases, it is unlikely that this feature would have a noticeable effect on the records. If the feature extended to considerable depth in the basement the incoming ray might pass through it. However, nothing is observed on the records which can be specifically correlated with the contact.

CHAPTER VII

SECONDARY SOURCE PHASES

7-1 Introductory Remarks

It has been indicated in some of the foregoing chapters that complexity in the P phase "coda" results from late arriving secondary source phases. The most dominant of these secondary phases is pP , the reflection of the initial compressional pulse from the surface of the earth above the source. Other secondary phases can be generated near an earthquake source. Theoretical faulting models indicate (A.W.R.E., 1965) that, at the source, shear waves will contain more energy than compressional waves. That this is true in practice is shown by the greater proportion of shear energy on records made near an earthquake source. The source-generated shear waves are strongly attenuated after travelling teleseismic distances, and, because of lower velocities, will arrive of the order of a few minutes after the primary P. However, they are partially converted into compressional waves at the surface and at other elastic discontinuities above the source. The initial compressional wave itself will be partially reflected at elastic discontinuities near

the source. These converted and reflected waves will follow the main P signal to the recording station, and, because of time spent traversing extra paths near the source, will arrive at later times contributing to an extended and complex P coda.

The delay time of these secondary source phases will depend on the depth of the earthquake. The delay times, particularly of pP which is the strongest and hence most easily recognized of the secondary phases, are the most useful criteria in assigning accurate depths to the deeper earthquakes. Because the pP signal will overlap and interfere with the P signal for shallow events, pP is not easily enough recognized to allow its use in depth calculations of earthquakes shallower than about 50 km.

Accurate determination of the focal depth of the shallower events is of practical importance to the detection of underground nuclear explosions. The majority of earthquakes occur at depths greater than 10 km; the detonation of explosions is limited to shallower depths. Therefore, the number of natural earthquakes that might be mistaken for explosions would be greatly reduced if depths could be dependably measured to ± 5 km. Depths of the shallower events reported by U.S.C.G.S. often represent a judgment, or are restrained to "normal" (33 km), with an estimated accuracy of 25 km. Consequently, a number of researchers have attempted to identify pP phases on seismograms of shallow

events and thereby assign to them more accurate focal depths.

Griffin (1966a) describes the application of REMODE 2A and 3A processors (see sections 4-1 and 4-2) to seismograms to enhance secondary depth phases. Those phases which were clearly evident on unprocessed records were made distinctly clearer by processing. For events which showed no sign of a depth phase on the unprocessed records, no enhancement was obtained by processing. Griffin reports considerable improvement in depth phase detection using a more selective processor, REMODE 5, which has not been discussed in Chapter IV. Using REMODE 5, rectilinear waves whose apparent angle of incidence differs from a specified angle can be attenuated as much as desired. This, in effect, requires a focusing of the processor at an apparent angle of incidence determined from the vertical and radial signal amplitudes for each event.

Howell et al (1967) describe a process whereby a seismogram is convolved with an optimum inverse filter. The filter is designed such that its convolution with an entire seismogram, consisting of primary event, plus secondary events, plus noise, should yield the primary seismogram only, thereby simplifying that portion of the original seismogram which contained secondary signals. Howell et al report that the technique is useful in identifying secondary phases, but finds many pulses besides pP and

does not always find pP.

The P-Detection processor described in Chapter IV was applied to the events in this study to detect which portions of the P coda were relatively pure P motion, which portions were P phases more-or-less distorted by shear motions, and which portions were relatively pure SV motion. It became apparent that very strong P signals could be recognized in the P coda of many of the events as distinct secondary arrivals. On the unprocessed records of the deeper events these could be easily identified as pP. On most of the shallower event records the signal level remained high over most of the half-minute record length, but clear arrivals of specific secondary phases could not be discerned. The P-D processor, by enhancing rectilinear P motion, enabled many secondary phases arriving at the station as compressional waves to be accurately timed. See, for example, Figures 11, 12, and 13. In all, pP phases have been tentatively identified for 23 events, and sP phases for 9 events. It has been possible to adjust the focal depth reported by U.S.C.G.S. for some of these events.

7-2 Amplitude Considerations

Before presenting the results of the identification of secondary source phases, a discussion will be given of the amplitudes that can be expected for the secondary phases relative to the primary P phase.

The wave propagating upward from the source will strike the surface inclined to the vertical at an angle depending on the focal depth and epicentral distance. Assume, for the purpose of determining reflection coefficients, that the angle (θ) is 5 degrees.

Ewing et al (1957, p. 30-31) present the square root of the ratio of reflected to incident energy for P and SV waves incident on the free surface of a homogeneous and isotropic half space. For Poisson's ratio equal to $1/4$ and $\theta = 5^\circ$ the above ratio is 0.98 for incident P reflected as P and 0.30 for incident SV reflected as P. In theory, then, pP can contain virtually the same amount of energy as P, and sP about $1/10$ of that amount. But, if the source generates more shear than compressional energy, as seems to be the general case, the relative strength of sP could be considerably larger.

Wu and Hannon (1966) have calculated reflection coefficients for PP as functions of the frequency of the input signal and angle of incidence. Assuming an incident plane wave at the bottom of three different crustal models, the reflection frequency response was computed using the Haskell-Thompson matrix method. Reflection coefficients applicable to pP (assuming the upward-going wave can be considered plane for shallow focus pP phases) appear on the graphs of Wu and Hannon at the smaller angles of incidence. Values applicable to this study appear at the

appropriate frequency. Using $\theta = 5^\circ$ and a frequency of 0.5 Hz, the ratio of incident to reflected P displacement is greater than 0.9 for each of the three crustal models; average central U.S. structure, average oceanic structure, and Peru-Altiplano structure.

Wu and Fannon (1966) also present synthesized PP signals computed on the basis of a delta function input and passing the output through a simulated 30-100 (seismometer-galvanometer periods) seismograph. In addition to the main pulse which reflects from the surface, two additional identifiable pulses are apparent on the synthetic records; a strong, repeated, multiple reflection set up by the incident wave in the water layer of the oceanic crustal model, and a weak early-arriving pulse which is a reflection from the base of the crustal models. Although the frequency range of the signals in these synthetic records is far below that of the events of this study, the relative amplitudes of these additional signals is generally applicable.

An additional factor to be considered in a discussion of amplitudes that can be expected for secondary source phases is the radiation pattern effect discussed in Section 5-2. If the radiation pattern is as strong as the results of Section 5-3 suggest, the amplitude of secondary phases relative to primary P can vary considerably.

7-3 Crustal Columns at the Source

If the delay time of pP and sP after P can be accurately determined from a seismogram the assignment of accurate focal depth to the earthquake requires knowledge of the velocity structure of the earth between the source and the surface. Modern travel-time tables do not include lists of pP-P or sP-P times versus epicentral distance and focal depth. Gutenberg and Richter (1936) do present such a table but it is based on their average velocity-depth information (Gutenberg and Richter, 1935) and is applicable only to focal depths greater than about 100 km. The relative error from assumption of an average velocity-depth relation will be greater for shallower earthquakes.

Since earthquakes occur within a diverse assortment of geological environments, few of which have structures known to an accurate degree, some source-to-surface velocity structure must be assumed for each event. In this study, for purposes of comparing observed pP-P and sP-P times with reported focal depths, four different crustal sections after Menard (1967) were chosen as representative types.

The four crustal columns are shown in Figure 29 with layer thicknesses in km labelled on the left side and P velocities in km/sec on the right side of each layer. The "typical ocean" (T.O.) and "typical continent" (T.C.) are those given by Menard. The "simple island arc" (S.I.A.)

T.O. TYPICAL OCEAN
 S.I.A. SIMPLE ISLAND ARC
 C.I.A. COMPLEX ISLAND ARC
 T.C. TYPICAL CONTINENT

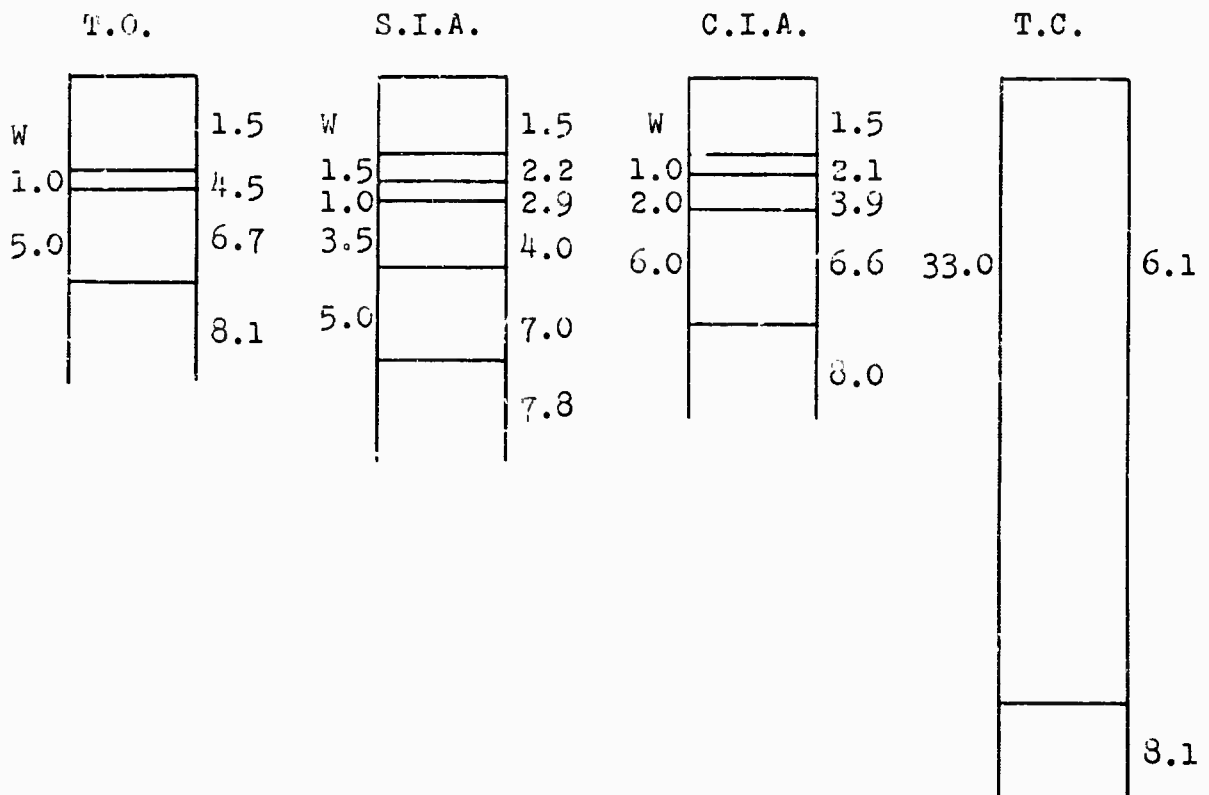


Figure 29. Four crustal columns used for calculating pP-P and sP-P delay times (after Menard, 1967). Thicknesses in km are shown on the left and P velocities in km/sec on the right of each layer. W, the water depth, was determined from bathometric maps for each event.

is Menard's Aleutian Basin structure and the "complex island arc" (C.I.A.), Menard's Yucatan Basin structure. The water depth (W) for the oceanic models was determined for each event in an oceanic environment from bathometric maps for the particular epicenter. With epicenters accurate to a few tenths of a degree in latitude and longitude, the water depths are believed to be accurate to about 1 km.

Although the 4 crustal columns are average ones and cannot be expected to exactly represent the crust above any of the events, the resulting errors in pP-P time calculations will not be large. Two-way travel time error due to erroneous water depth will be about 1 second. If a focal depth is 30 km and the water depth 3 km, the vertical pP-P time for T.O. would be 11.1 seconds, for S.I.A., 13.3 seconds, and for C.I.A., 12.2 seconds. Assuming the crust is well enough represented by one of these models to halve the error, the total expected error in calculated pP-P time will be about 2 seconds, 1 second from an inaccurate water layer and 1 second from inaccurate solid layers.

7-4 The Path of pP Above the Source

In the calculations of this chapter it will be assumed that pP reflects from the surface directly above the source, i.e., travels a vertical path, reflecting

from the surface at the epicenter. In practice the reflection point will be some distance toward the recording station from the epicenter. Using a simulated pP path shown in Figure 30, a measure of the errors involved in assuming vertical reflection for various depths and epicentral distances is shown in Table IV.

It is assumed in Figure 30 that if P leaves the source at an angle i , pP has an angle i of incidence and reflection at the surface and leaves the source depth at an angle i . The material between the source at depth h and the surface has a constant compressional velocity of $\alpha = 8.5$ km/sec. If pP reflected vertically from the surface it would have a travel time, t_0 , given by the equation

$$t_0 = \frac{2h}{\alpha} + t'_0(\Delta, h),$$

where t'_0 is the P travel time from a source at depth h to a station at epicentral distance Δ . If pP travels the inclined path to the surface it will have a travel time given by

$$t_1 = \frac{2h}{\alpha \cos i} + t'_0(\Delta - D, i).$$

The values of $t_0 - t_1$ listed in Table IV are the differences in pP time between a vertical reflection path and this simulated inclined path.

It is seen in Table IV that these time errors have a range from 0.6 to 5.7 seconds for the values of Δ

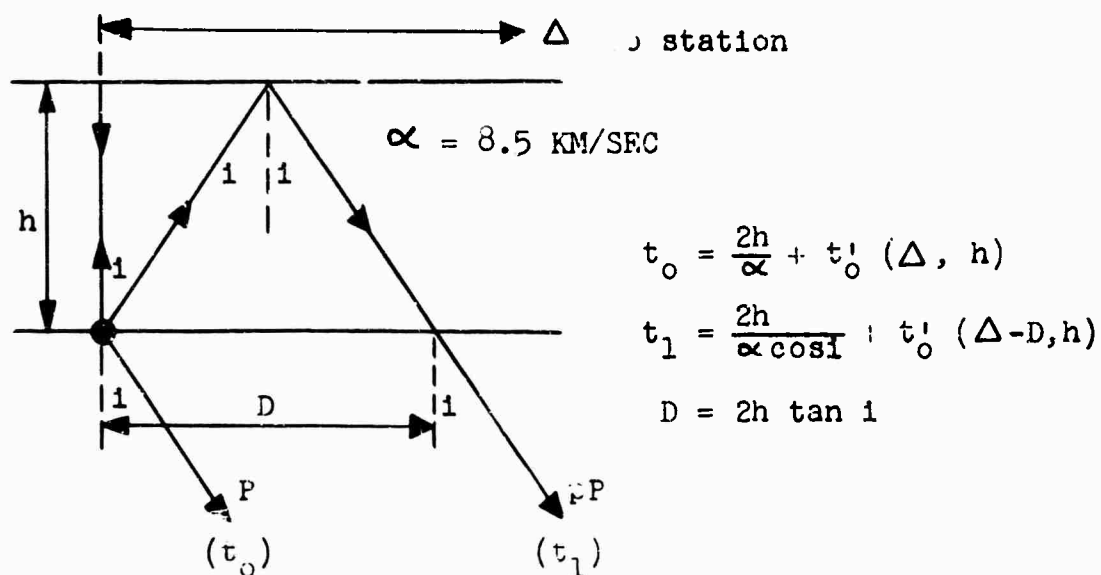


Figure 30. Simulated pP path above the source.

TABLE IV

ERRORS IN pP-P TIME RESULTING FROM
ASSUMPTION OF VERTICAL REFLECTION

Δ (deg)	h (km)	i (deg)	t_0 (Min:Sec)	t_1 (Min:Sec)	$t_0 - t_1$ (sec)
30	25	40	6:14.9	6:13.7	1.2
56	25	30	9:45.9	9:43.8	2.1
88	25	20	12:56.9	12:56.3	0.6
30	60	40	6:21.1	6:18.4	2.7
56	60	30	9:49.1	9:46.3	2.8
88	60	20	13:01.1	13:00.0	1.1
30	100	40	6:29.5	6:23.8	5.7
56	100	30	9:54.5	9:51.1	3.4
88	100	20	13:07.5	13:05.0	2.5

and h chosen; the smaller errors are for large Δ and small h , the larger errors for small Δ and large h . These values of $t_0 - t_1$ are over-estimates of the error. This is because the value of α for the true earth is not constant but generally decreases toward the surface, with the result that the up-going ray, to travel a minimum time path, will bend toward the vertical thereby decreasing the value of D from that assumed in the calculations of Table IV. It is assumed then that except for the worst case (large h and small Δ), the error resulting from the assumption of vertical reflection for pP will be less than 2 seconds.

Since the actual pP-P time will be smaller than the time difference assuming a two-way vertical path from source to surface, use of observed pP-P times in calculating the vertical distance will result in an under-estimate of the focal depth. Using a reported focal depth, the two-way vertical path time will be an over-estimate of the pP-P time.

7-5 Picking and Timing Secondary Phases

Identification of secondary phases was made on the basis of a strong and sharp arrival on the P-D VERT and P-D RAP records at an identical time delay on the records of both stations. Although this criterion was used throughout, the general quality of P-D records varied considerably. An example of high quality P-D records

is shown in Figure 31 for event 18. When aligned on the primary P pulse, the first strong downward motion, the records show two strong secondaries arriving at identical times on both stations. In addition, there is evidence of two weaker secondaries, one about 5 seconds after the primary P and the other about 7 seconds after the second strong secondary. An example of lower quality records can be seen in Figure 13 for event 26. Although this event shows no strong primary P and shows miscellaneous bursts of signal throughout the P-D records, the onset of a strong secondary appears at an almost identical time at both stations.

It can be seen on a number of examples of records shown that a small precursory signal often precedes the onset of strong primary P motion. On event 4 in Figure 11, event 13 in Figure 12, and event 29 in Figure 16 this delay time of the primary P arrival is 1 to 1.5 seconds. Some events exhibit a strong impulsive primary P onset with no precursor. These effects are the azimuthal expression of the orientations of source P wave displacement radiation patterns. At the period of wave motion being considered here, the displacement pattern probably affects only the first half cycle of onset motion. The reader will, no doubt, note that this appears contradictory to the discussions of radiation pattern effects in Section 5-3. In that section it was concluded that the absence of all strong P (or pP) motion, not only of the first half cycle,

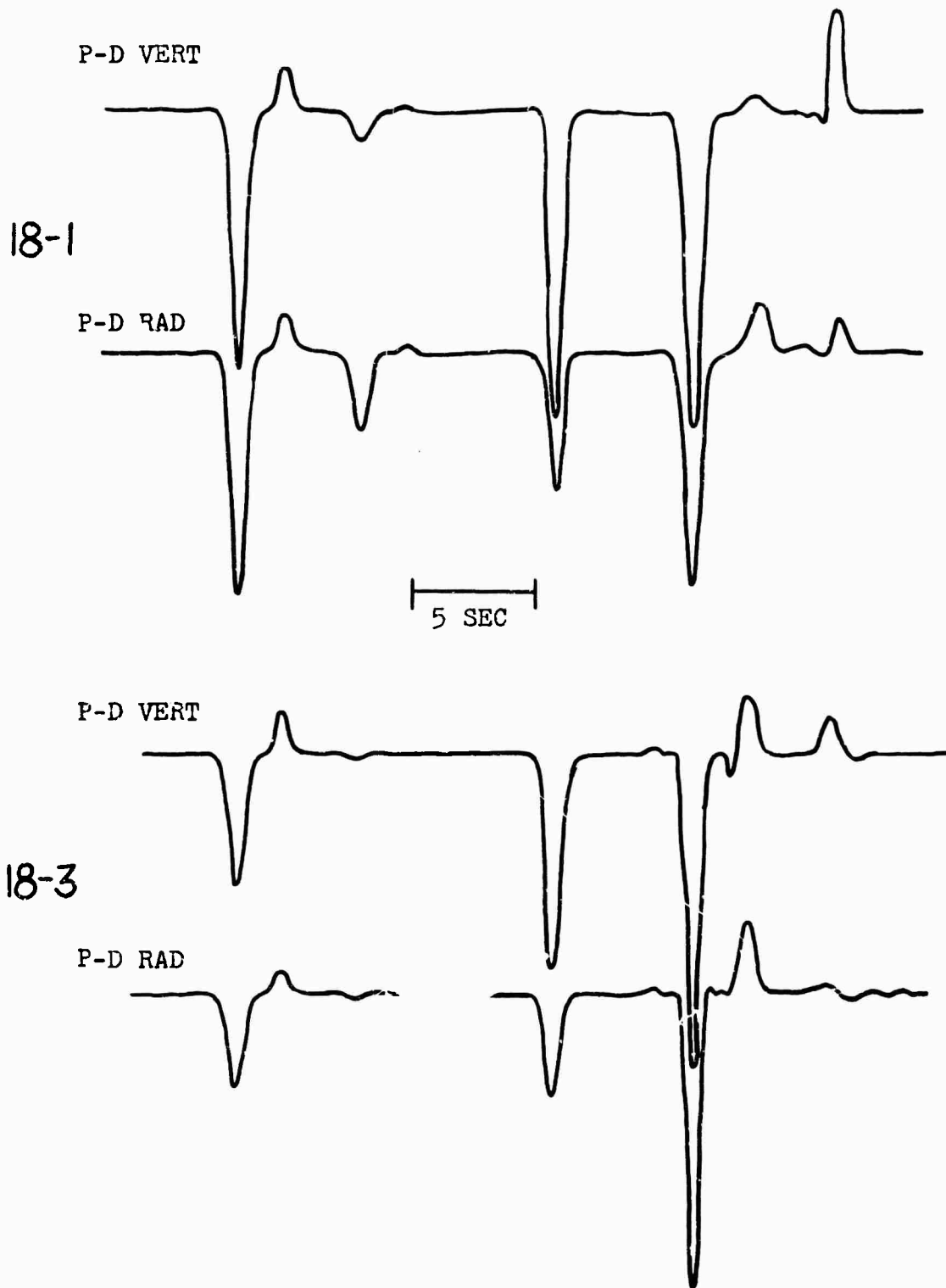


Figure 31. High quality P-D records showing secondary phases arriving at an identical time on two stations.

could be attributed to the radiation pattern. This conflict will be left unresolved, but is probably related in some way to more complex source effects than were discussed in Chapter V.

However, since measurements of secondary phase delay times were made on P-D VERT records, when strong primary P signals were present the measurements were most easily made between the onset of the strong primary and the onset of a strong secondary; when strong primary P was absent, the measurement was made between the arrival pick and the onset of the secondary. This procedure could contribute an error of about 1 second to the pP-P and sP-P times.

A second possible source of timing error is in the secondary onset as displayed on the P-D VERT records for the shallower events. The secondary phase arrives amid the coda of the primary F. Although the P-D processor is surprisingly successful in enhancing the secondary there are suggestions that the first half cycle of the secondary of some events may be lost due to distortion from the P coda. For example, the P-D VERT records of event 4 in Figure 11 and event 12 in Figure 17 show a considerably reduced first half cycle of the secondary. If this half cycle is lost on some of the events, an additional timing error of about 1 second can result.

7-6 Summary of pP Results

On 23 events (events 17 and 41 are omitted from this discussion) the P-D processor detected at least one secondary arrival at an identical time(s) on the records of both stations. The single secondary, or one of the multiple secondaries, of each of these events was interpreted as being pP. On 10 events one or both of the stations showed secondary signal but, because of distortion by background noise or the inability of the P-D processor to enhance the signal, clear secondaries could not be identified at a coincident time on both records. Of the remaining 6 events, 5 exhibited no strong secondary motion and one is discussed as a special case in Section 7-8.

A summary of observed and calculated pP-P times is given in Table V for the 23 events exhibiting pP phases. The presence or absence of a strong primary P onset is designated YES or NO in the second column. The third column is the focal depth for the event reported by U.S.C.G.S., the fourth is the ocean water depth determined for the epicenter from a bathometric map, and the fifth is the type of crustal column used in calculation of the pP-P time (see Figure 29). The calculated pP-P times in Table V are the two-way vertical travel times of a compressional wave between the surface and the source (at the reported focal depth) using the appropriate crust and water layer model. The observed pP-P times were determined as described in

TABLE V
SUMMARY OF PP-P CALCULATIONS

EVENT	STRONG ONSET	REPORTED DEPTH (KM)	WATER DEPTH (KM)	CRUST TYPE	PP-P TIME (SEC)	OBS. CALC	OBS-CALC	ADJUSTED DEPTH (KM)
1	YES	25	1	S.I.A.	9.9	8.5	-1.4	
2	NO	35	3	S.I.A.	14.4	11.4	-3.0	23
3	YES	103	0	T.C.	28.1	27.4	-0.7	
5	YES	54	1	S.I.A.	17.1	12.5	-4.6	36
6	NO	33	4	T.O.	12.9	16.3	+3.4	47
8	NO	36	0	S.I.A.	11.5	9.6	-1.9	
9	YES	33	1	T.O.	9.6	6.0	-3.6	18
11	NO	60	1	S.I.A.	18.6	18.6	0.0	
12	NO	33	2	T.O.	10.8	15.7	+4.9	45
13	YES	28	0	T.C.	9.2	9.5	+0.3	
16	YES	47	0	C.I.A.	13.3	13.4	+0.1	
18	YES	33	2	C.I.A.	12.0	13.0	+1.0	
19	NO	41	0	C.I.A.	11.8	11.3	-0.5	
20	YES	129	0	T.C.	34.5	33.1	-1.4	
21	YES	77	4	T.O.	22.5	19.8	-2.7	66
26	NO	33	1	S.I.A.	11.7	11.2	-0.5	
27	NO	27	2	T.O.	9.3	4.8	-4.5	9
28	NO	67	0	C.I.A.	18.3	18.4	+0.1	
31	NO	22	1	T.O.	.9	4.7	-2.2	13
32	YES	197	1	C.I.A.	51.8	51.5	-0.3	
33	NO	23	4	T.O.	10.4	11.4	+1.0	
34	NO	41	1	S.I.A.	13.3	12.0	-1.3	
39	YES	70	0	T.O.	17.5	17.0	-0.5	

Section 7-5.

The assumption of vertical reflection for pP discussed in Section 7-4 would result in the calculated pP-P time in Table V being too large, and observed-minus-calculated residuals being negative. Most of the obs-calc residuals in Table V are negative, suggesting that the assumption of vertical reflection does contribute significantly to the residuals. Event 6 with a residual of +3.4 seconds has $\Delta = 13^\circ$. In view of the discussion of near events in Section 6-2, the pick of the pP phase itself may be in question. Event 12 with a residual of +4.9 seconds has $\Delta = 45^\circ$. This is probably an event with a large error in the reported focal depth.

Since the observed and calculated pP-P times are estimated to be accurate to about 2 seconds and U.S.C.G.S. reported depths are accurate to ± 25 km, it is appropriate to adjust the focal depths of those events with large residuals. Depths were adjusted for all events in Table V with time residuals larger than 2.0 seconds so that the new depth agreed with the observed pP-F time (again assuming vertical reflection) for the appropriate crustal model; these adjusted depths are listed in the last column in Table V. Care must be taken in assigning accuracy to these adjusted depths because, for example, 1 km of erroneous water depth is equivalent to about 6 km of mantle material. However, considering all of the error estimates

discussed above, the adjusted depths, and those not requiring adjustment, are probably accurate to within about 15 km.

7-7 Summary of sP Results

sP phases will appear on the records delayed after pP a time approximately equal to the difference between one-way compressional and shear travel times from the source to the surface. If a phase was observed on the P-D components at approximately this delay time after pP, it was identified as sP; this occurred on 9 events. The observed and calculated sP-P times for these events are listed in Table VI, along with the absolute difference between observed and calculated time. If the focal depth was adjusted (Table V) the calculated sP-P time in Table VI was based on the adjusted depth. When the source crustal model contained an oceanic water layer it was assumed that sP reflected not from the surface, but from the base of the water layer.

All but two of the events in Table VI have time residuals of 2.0 seconds or smaller, suggesting that for these events the pick of sP is correct. Events 9 and 18 which have large residuals in Table VI, and a number of others requiring further consideration are discussed in the following section.

TABLE VI

SUMMARY OF sP-P CALCULATIONS

EVENT	sP-P TIME (SEC)		OBS-CALC
	CALC	OBS	
3	38.2	37.7	0.5
5 *	15.6	17.5	1.9
9 *	7.9	12.0	4.1
13	12.6	14.0	1.4
16	18.3	19.7	1.4
18	12.8	18.5	5.7
21 *	25.3	25.0	0.3
28	25.1	23.1	2.0
31 *	8.1	10.0	1.9

* Calculated time based on adjusted depth.

7-8 Other Possible Early-Arriving Phases

For a number of the events in Tables V and VI the picking of pP and/or sP may be erroneous because of the possibility that other phases may be arriving within the 25 second record length. Some events show separate phases in addition to those picked as pP and sP.

For certain epicentral distances and focal depths the phase PcP will arrive very soon after P. There are three events with conditions such that, on the basis of Jeffreys-Bullen travel times (Travis, 1965), PcP will arrive 5 or 6 seconds after P. The VERT and P-D VERT records of one station for each of these events (13, 20, and 32) are shown in Figure 32. Event 13 has a focal depth of 28 km; pP and sP picks for it listed in Tables V and VI are shown by arrows on the P-D VERT record in Figure 32. Events 20 and 32 are deep, 129 and 197 km respectively; only the onset P motion is shown in Figure 32 for these events. These three events are among the few which show more than one cycle of strong onset motion. The Jeffreys-Bullen PcP-P times for these events are 6.3, 5.3, and 4.7 seconds for events 13, 20, and 32 respectively. It is probable that the extension of onset motion results from a contribution from PcP, but the overlap with P masks the arrival.

Three events whose late arriving phases might be interpreted as something other than secondary source

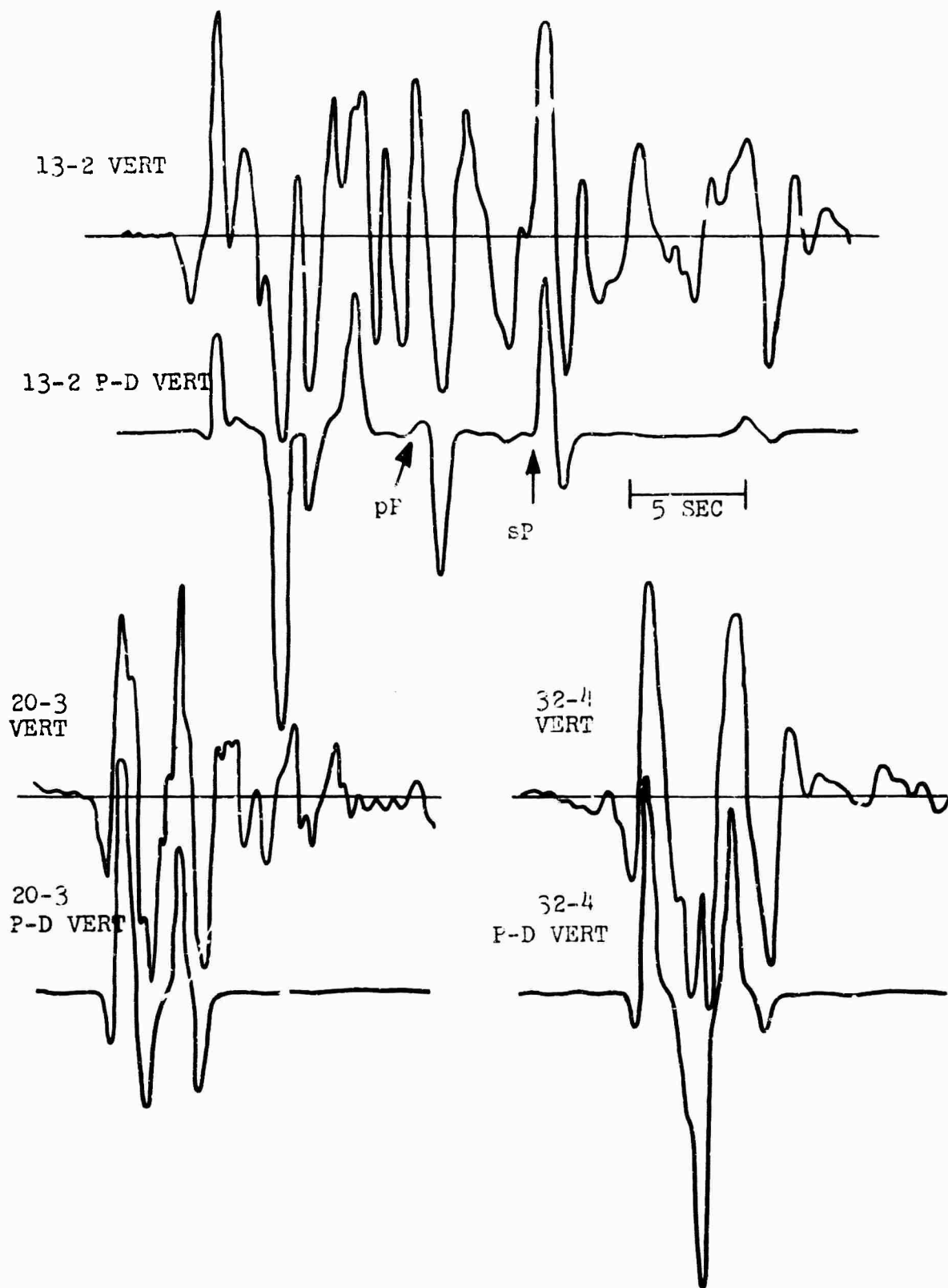


Figure 32. Three events with PcP arriving about 5 seconds after P.

phases are shown in Figure 33. The P-D VERT record of event 5-2 shows three strong secondaries labelled A, B, and C in Figure 33. pP and sP for this event listed in Tables V and VI were phases B and C respectively. This required an adjustment of focal depth from the reported 54 km to 36 km. The U.S.C.G.S. depth was no doubt determined on the basis of event C being pP; observed and calculated pP-P times would then agree quite well. If this is true, what interpretation can be given to phases A and B? The epicentral distance for event 5 is 43 degrees. None of the common phases except pP and sP will arrive within the record length shown. One alternative is to interpret event 5 as a double shock. Considering the amplitude of phase C relative to phases A and B, one possible explanation is as follows: phase C is pP corresponding to the first arriving P phase from a source of focal depth 54 km, while phase B is pP corresponding to the second P phase, A, from a source at a much shallower depth. There are a number of other possibilities one could imagine, including the one originally given on Tables V and VI with phase A interpreted as a second source shock P phase with no strong accompanying pP or sP.

The phases labelled A and B on event 9 in Figure 33 were interpreted as pP and sP respectively in Tables V and VI. This is quite likely in error. Interpreting phase A as pP required depth adjustment from 33 km to 18 km, and

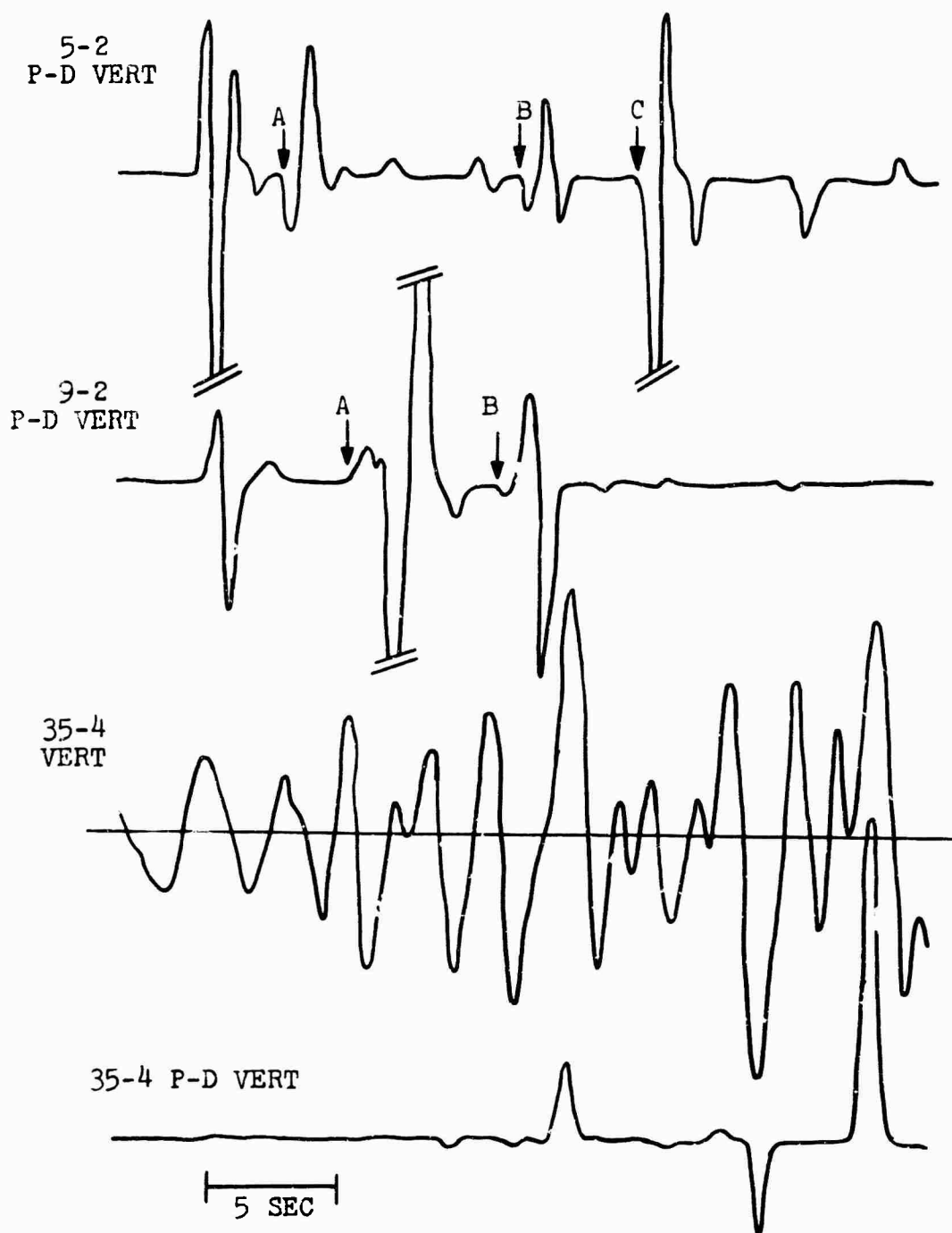


Figure 33. Three events with multiple secondary arrivals.

then interpretation of phase B as sP and using the adjusted depth resulted in a sP-P time residual of 4.1 seconds. The important parameter concerning this event is its large epicentral distance, 139 degrees; the first arriving phase, therefore, is PKP. This distance is very near the "focus" on the PKP travel time curve, the point at which two PKP phases travelling different paths through the earth arrive at the same time. A summary of earlier work and details of some recent theories concerning this complicated phenomena are given by Bolt (1964). No further discussion will be given here except to say that phases A and B on event 9 in Figure 33 are more likely complex PKP type phases than pP and sP phases.

The three secondary phases on event 35 in Figure 33 (they appear equally strong and at identical times on station 1) were not interpreted as secondary source phases. The epicentral distance for this event is 13 degrees, and the later arriving phases are probably related to the complications for near events discussed in Section 6-2.

Event 18 which has the largest sP-P time residual in Table VI requires further consideration. This event has remarkably similar P-D VERT and P-D RAD records on the station pair and was used as an illustration of this in Figure 31. sP is suspiciously strong but no other interpretation seems reasonable. There is some long-

period noise on the VERT and RAD records which may be masking portions of some of the phases resulting in the large sP-P time residual.

Apart from the events discussed in this section, upon which more than one interpretation of the later arriving phases may be placed, the P-D processor is seen to be quite successful in enhancing pP and sP phases. As will be discussed in Chapter X, further improvements can probably be made by appropriate adjustments in filtering and P-D processing.

CHAPTER VIII

SOURCES OF PHASE DISTORTION

8-1 Introductory Remarks

The P-D processor passes P motion in proportion to its amplitude and degree of rectilinearity. From some of the P-D records shown in foregoing chapters the impression might be gained that one does see strongly rectilinear P signals at the surface of the Alberta crust. It will be shown in this chapter that these P signals have, in fact, orbital motions which exhibit a high degree of ellipticity.

Considering the approach angles of these P phases discussed in Section 6-4, the greater proportion of compressional displacement will appear on the recorded vertical component, the greater proportion of crustal generated SV on the radial component. However, it was shown on Figures 24 and 25 that the radial component of a strong P phase will predominate over the SV motion on the radial records, and, although the SV motion is also present on these record segments, the combined vertical and radial P signal is strong enough to be passed by the

P-D processor. But, as will be shown in Section 8-3, the P phase is always highly elliptical because of the SV contribution.

It was stated in an earlier section that, in theory, all signal in the seismogram record lengths discussed here is confined to the vertical and radial components, with no signal remaining in the rotated transverse component. The degree to which the Alberta seismograms conform to this theory will be discussed in Section 8-4. A discussion will also be given concerning the dependence of the amount of transverse motion on the general period of motion.

8-2 Times and Amplitudes of Locally Generated SV

Before presenting some examples of distortion of P phases by locally generated SV and transverse signals, consideration will be given to the time delays and amplitudes which can be expected for SV generated in the Alberta crust.

A notation for PS converted waves used by Costain et al (1963) will be used here. Designation of layer numbers for the five layers of the gross Alberta crust are shown circled to the right of the layers in Figure 27; they are numbered from 1 for the sediments to 5 for the mantle. A converted wave, PS_n , enters the layered system as a P wave, is converted to SV at the interface between

the $n + 1^{\text{st}}$ and n^{th} layer and propagates the remaining distance to the surface as SV.

Calculations of actual SV converted wave amplitudes in the Alberta crust would be arduous and will not be attempted here. Instead, a number of comments given by Costain et al (1963) and Cook et al (1962) (the same group of authors in each case) in detailed summaries of previous investigations of SV converted waves are reproduced here.

- (1) It is supposed that PS converted waves are formed if the thickness of the layer is greater than the wavelength of the compressional wave.
- (2) Strong PS converted waves are found on only those seismograms with wave periods 2 seconds or less.
- (3) The periods of PS converted waves are not usually noticeably different from those of compressional waves found on the same records.
- (4) Whenever a wave changes its character the converted waves show larger decreases in amplitudes than the pure longitudinal waves, and one may suppose, therefore, that the most favorable dynamic conditions for the converted waves are those in which they change only once.
- (5) For the most favorable boundary conditions the amplitudes of the converted waves will theoretically be only slightly smaller than the amplitude of the corresponding P wave.

- (6) The amplitudes of the various PS converted wave arrivals increase with successively increasing depth to the interface where the conversion took place, provided the interface velocity ratios (upper/lower) continually decrease with depth.
- (7) Amplitudes of some PS converted waves are found to be at least twice the value of the corresponding longitudinal wave. It is noted that these large amplitudes are to a certain extent in contradiction with calculated amplitude values and may be attributed to a "partial screening and weakening" of the pure longitudinal wave.

These comments, some of which will prove applicable to the Alberta seismograms, will be referred to in this chapter by statement number.

Table VII showing the wavelengths of compressional waves in the Alberta crust is presented with reference to Statement 1. The layer thicknesses and compressional velocities are from Figures 26 and 27. The calculation was made for the sedimentary layer under both Leduc and Rocky Mountain House using approximate mean velocities for the entire sedimentary column. Because of the variation in period of motion (see Figure 19), wavelengths have been calculated for periods of 1.0 and 2.0 seconds using the simple relationship: wavelength = velocity x period. It will be shown (Section 8-3) that SV is generated at the base of the sediments. Therefore, Statement 1 is

TABLE VII

WAVELENGTHS OF COMPRESSIONAL WAVES IN THE
LAYERS OF THE ALBERTA CRUST.

LAYER	LAYER THICKNESS (KM)	COMPRESSIONAL VELOCITY (KM/SEC)	WAVELENGTH (KM)	
			T = 1.0 SEC	T = 2.0 SEC
1 (LED)	2.7	(4.5)	4.5	9.0
1 (RMH)	4.4	(5.0)	5.0	10.0
2	13	6.1	6.1	12.2
3	22	6.5	6.5	13.0
4	7	7.2	7.2	14.4

TABLE VIII

VELOCITY RATIOS IN THE ALBERTA CRUST

INTERFACE LAYERS	VELOCITY RATIO
1/2 (LED)	0.74
1/2 (RMH)	0.82
2/3	0.94
3/4	0.90
4/5	0.87

not generally valid here, i.e., PS converted waves are formed for layer thicknesses somewhat smaller than the wavelength of the compressional wave.

The velocity ratios in the Alberta crust are shown in Table VIII. The highest velocity contrast (lowest ratio) is at the base of the sediments. Statement 1 notwithstanding it is probably this interface which is most favorable to the generation of converted SV waves, i.e., PS_1 should be a strong phase. Below the 1/2 interface the layering conforms to the requirement of Statement 6, i.e., the velocity ratios decrease with depth. On this basis then PS_4 should be another strong converted phase. Because of the high velocity ratios at interfaces 2/3 and 3/4, converted phases PS_2 and PS_3 will not be considered. There are some low velocity ratios within the sedimentary column (see Figure 26) but, because of the thinness of the layers, PS converted phases generated within the sediments will not be considered.

Attention is now turned to the time delays of PS_1 and PS_4 after P. The shear wave velocities in the crustal layers (β) are shown on the right-hand edge of the layers in Figure 27. On the basis of approximate average velocities in the LED and RMH sediments the PS_1 -P times will be about 0.5 and 0.7 seconds for LED and RMH respectively. Using the shear velocities shown in Figure 27 the PS_4 -P time for the Alberta crust will be about 5.2

seconds with a few tenths of a second variation for different angles of incidence and different stations.

The onset P motion has a duration of a few seconds, depending on the period of motion and other factors. With PS_1 -P times of about half a second, the PS_1 phase with a period similar to that of P (see Statement 3) will be almost entirely coincident with the onset P motion. If this onset motion (now containing both P and PS_1) dies away within 5 seconds, the PS_4 phase should be observed following it very closely.

8-3 Examples of Locally Generated SV

When attempting to identify PS_1 and PS_4 phase motion, which may be very small and often superimposed on P motion, care must be taken to use records with very low background noise level. This also applies to the signals to be discussed in Section 8-4.

The entire suite of records was searched for evidence of the presence of PS_4 phases. The SV motion was identified as described in Section 4-4, i.e., as motion which was completely rejected by the P-D processor but which was of sufficient amplitude and regularity to be distinguishably out-of-phase on the VERT and RAD components. The six examples found are shown in Figure 34. Three, events 16-1, 19-1, and 22-1, show one cycle of clear SV type motion 5 or 6 seconds after the P arrival; these

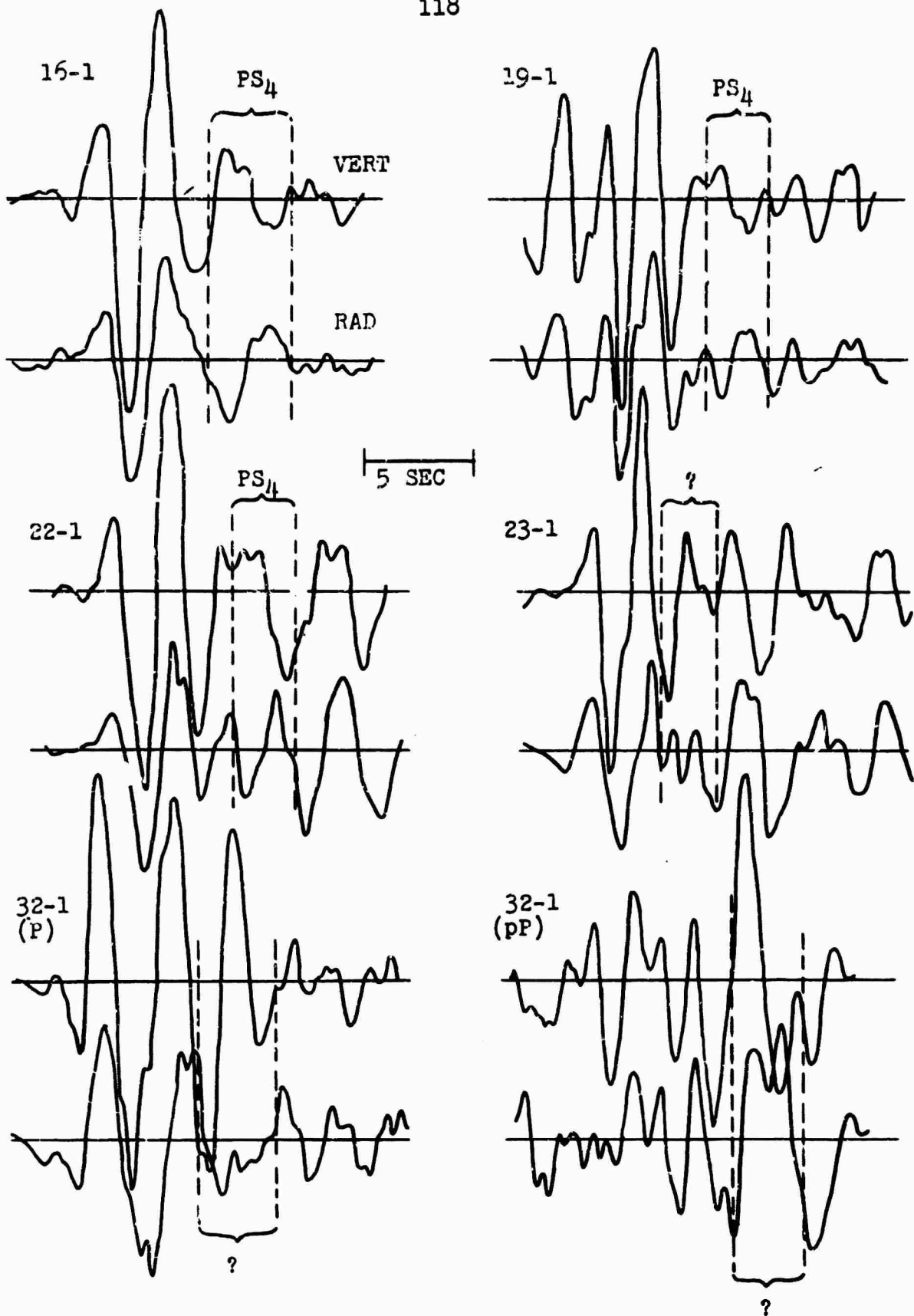


Figure 34. Examples of possible PS₄ phases.

segments have been labelled as PS_4 in Figure 34. Three others, events 23-1, 32-1 (P phase), and 32-1 (pP phase) show less distinct SV motion which is really only an out-of-phase distortion of the in-phase P motion; these segments have been labelled with a question mark in Figure 34. In none of the other events could SV motion be identified at the appropriate time as well as shown in the examples of Figure 34. This was generally due to background noise contamination or to a longer duration of the primary P phase. On the basis of these results the amplitude of PS_4 is judged to be approximately 0.2 to 0.3 that of P.

Four representative sets of vertical-radial P phase particle motion plots are shown in Figure 35. These plots were constructed from bandpass filtered (BP-1, Figure 4) original vertical and singly-rotated radial (see Figure 5(a)) seismograms. Seven plots, each showing 2.4 seconds of motion, consisting of two preceding background noise plots and five signal plots are shown for each event. The total signal represented is then 12 seconds. A heavy dot is shown at the beginning of each separate plot so that the orbital motion can easily be followed throughout the 12 seconds of signal.

Here the general ellipticity of the P motion, even at the very onset of the signal, is strikingly apparent. Although only four events with good signal-to-noise level are shown in Figure 35, this is a feature

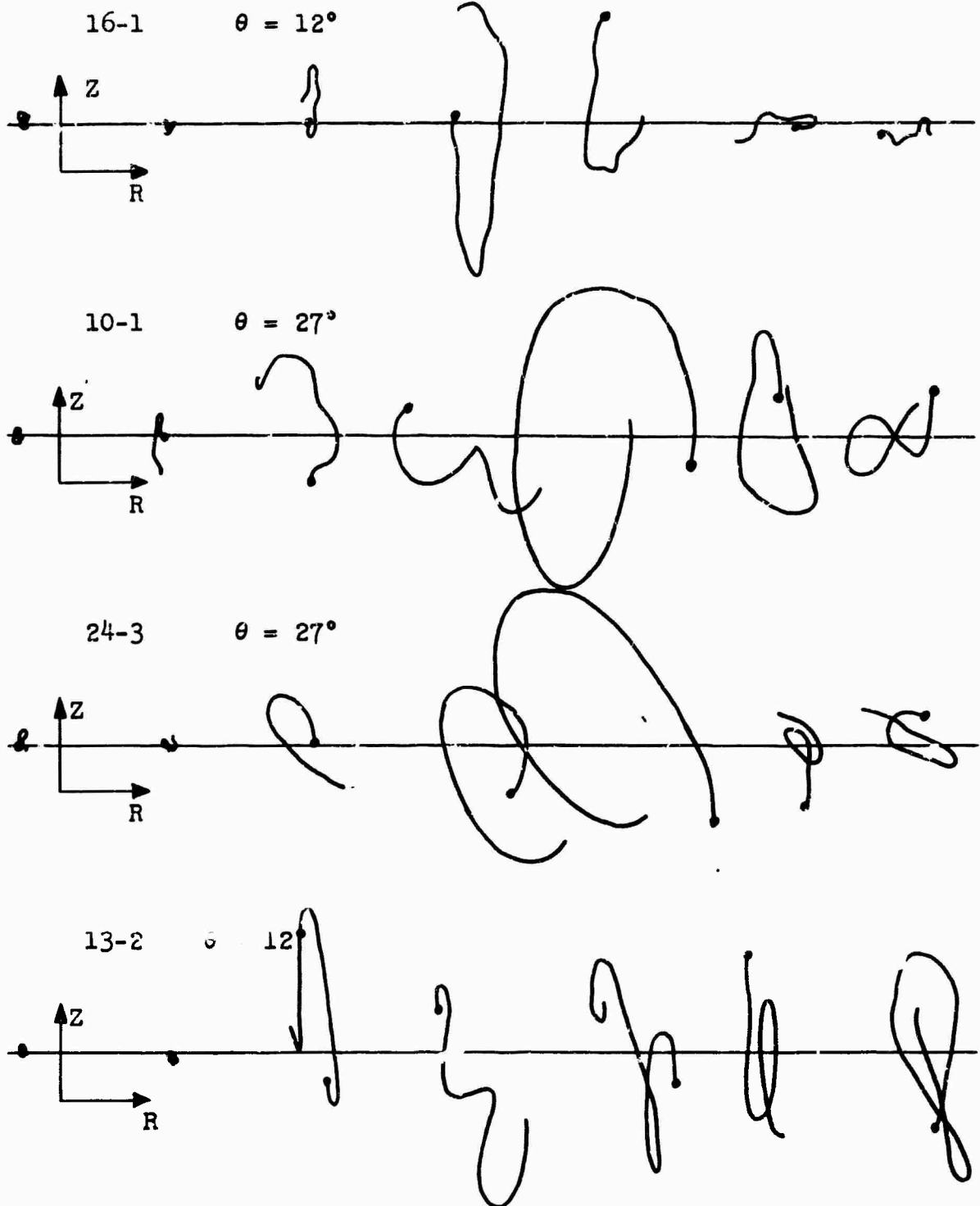


Figure 35. Vertical-radial particle motion plots of P phases. Each plot contains 2.4 seconds of motion. The beginning of each plot is denoted by a heavy dot. θ is the approximate angle of incidence at the surface.

common to all events. The first three signal plots correspond generally to the P signal burst. In events 10-1 and 13-2 the signal level remains high in the last two plots; the reasons for this can be seen in Figure 6 for event 10 which was very shallow and exhibits long duration of P motion, and in Figure 32 for event 13 which has pP arriving at approximately 9 seconds (within the fourth signal plot). The distortion of the primary P motion away from rectilinearity toward ellipticity is interpreted as due to the presence of strong PS_1 motion (with the possible addition of some motion due to PS_2 and PS generated within the sediments, although this is unlikely in view of the discussions in Section 8-2).

The angle of incidence (θ) at which the signal approaches the surface, determined for these events from Figure 7 and the table in Figure 27, is shown in Figure 35. The greater degree of ellipticity exhibited for events with the greater angle θ is a generally observed feature. This is in agreement with a theoretical PS_1/P_4 amplitude curve presented by Costain et al (1963) for a similar crustal model. In their model P_4 is the P wave which is incident on the bottom of the model, and the PS_1/P_4 amplitude ratio has a maximum at $i = 60$ degrees, and drops to zero at $i = 0$.

On the basis of the results shown a judgement can be made of the PS_1/P amplitude ratio. PS_1/P for

events 13-1 and 16-1 is about 0.2, for event 10 about 0.6, and for event 24 about 1.5. The latter value appears to be an example of the phenomena mentioned in Statement 7 in Section 8-2.

It should be noted that the effects of the free surface have not been accounted for in the orbital motion plots of Figure 35. The general conclusions should remain the same, however, with the amplitudes of both P and PS being approximately halved (see Costain et al, 1963).

The particle motion in the larger amplitude plots of Figure 35 forms ellipses which are quite regular. This is an indication that the period of SV signal forming the horizontal trajectory is very nearly equal to the period of the P signal forming the vertical trajectory, i.e., these events are in general agreement with Statement 3 in Section 8-2. Event 13-2 in Figure 35 diverges slightly from this trend, particularly in the 2nd to 4th signal plot, where the P motion describes 1 1/2 to 2 cycles while the SV describes less than 1 cycle, i.e., the period of SV is slightly longer than that of P.

The PS_4 phase seen on event 16-1 in Figure 34 is also apparent in Figure 35, where event 16-1 exhibits mainly horizontal (SV) motion in the last two signal plots.

8-4 Examples of Transverse Motion

One transverse seismogram has been shown previously, event 10-1 in Figure 6. The gradual buildup of transverse signal over the 30 second record is a general feature of the events of this study. This is a commonly observed phenomena which becomes more dominant as the frequency band becomes higher. For example, in high-frequency refraction seismology transverse signals similar in amplitude to the vertical and radial signals are not uncommon (A.M. Bancroft, personal communication). At the other end of the seismic body wave frequency band, for example in teleseismic seismology, transverse distortions of this type are seldom observed for signal periods greater than about 10 seconds (Key, 1967).

This, and other types of signals which cannot be explained in terms of the transmission of plane waves through horizontal layering have been termed "signal-generated-noise". It is generally believed to be due to scattering (i.e., reflection, refraction, and diffraction) by the elastic and density discontinuities commonly present at shallow depths in the crust of the earth. The shorter wavelengths (higher frequencies) can "see" these small inhomogeneities, the longer wavelengths (longer periods) cannot. Key (1967) by applying velocity-filtering techniques to array records was, in addition, able to identify dominant topographic features within about 100 km

of the station as sources of signal-generated-noise (probably surface waves). It is unlikely that similar effects are occurring at the Alberta sites where the topographic relief is usually very small.

Ellis and Basham (1967) have presented and discussed a number of examples of transverse signal-generated-noise on the Alberta records in relation to the problems of crustal deconvolution; no further discussion will be given here.

Before leaving this topic, however, a number of examples of a puzzling, but possibly related, phenomena will be presented. This concerns the distortion of the horizontal rectilinearity of the P signal immediately at its onset on some of the events. Although, because of the low signal level, the horizontal motion is usually distorted by background noise, on some of those events with high horizontal signal-to-noise ratio the horizontal orbital motion exhibits a high degree of ellipticity. Six examples of the horizontal orbital motion of the P onset are shown in Figure 36. These have been constructed from bandpass filtered (BP-1, Figure 4) north-south and east-west components. Each plot shows 3.0 seconds of onset motion beginning at the arrival pick for the particular event. The direction of approach of the P phase is shown by a large arrow near each plot.

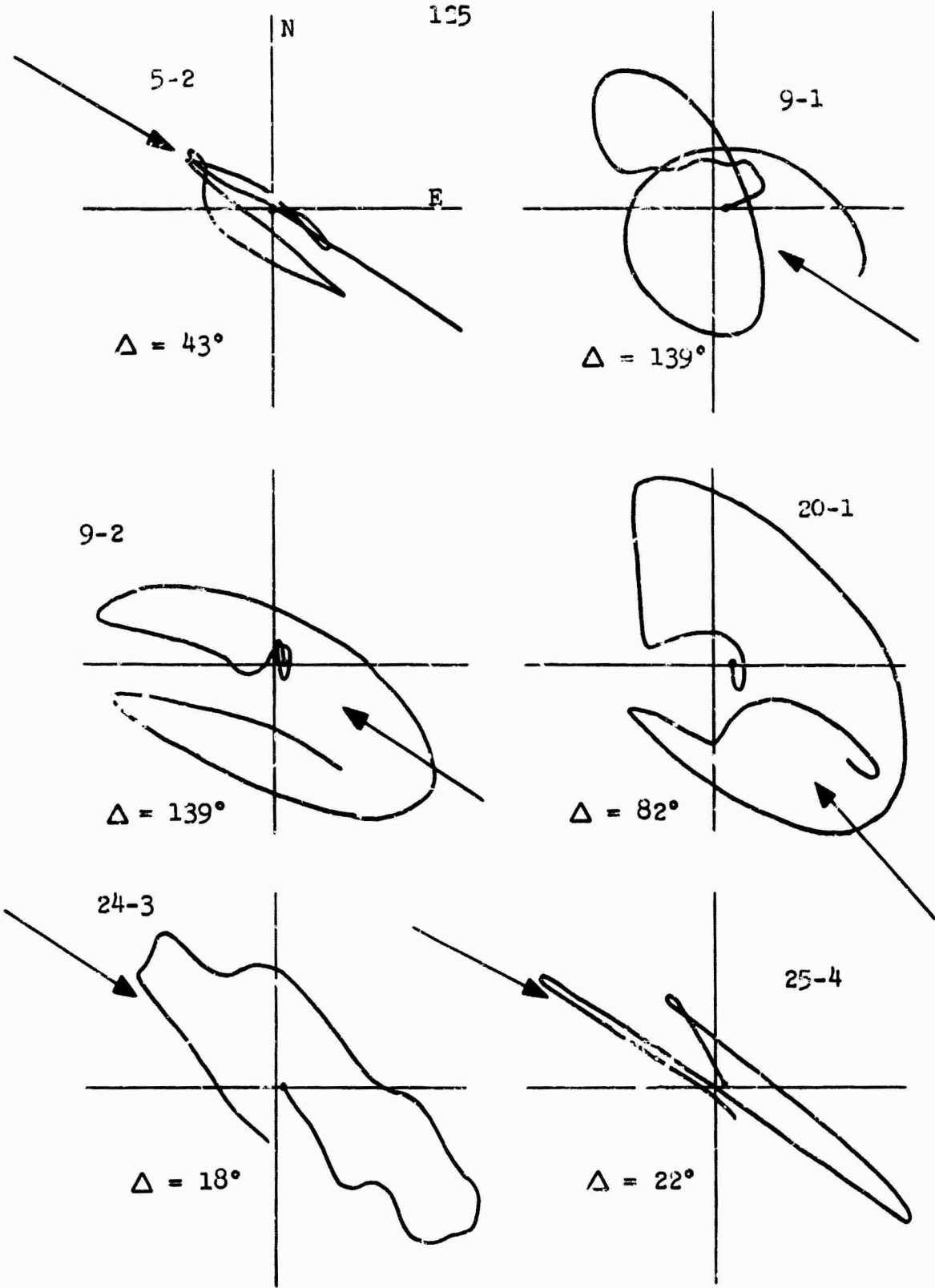


Figure 36. Horizontal onlet orbital motion.

A clue to the source of ellipticity of the horizontal orbital motion may be found in the epicentral distance (Δ) which is shown for each event in Figure 36. Events with the larger epicentral distances exhibit a greater degree of ellipticity than do the nearer events. Much of the horizontal motion, particularly for the distant events where the signal is arriving almost vertically, results from the PS converted phases (PS_1 for the case of onset motion). Niazi (1966) in a study of deviations of apparent azimuth due to refraction at a tilted interface showed that the azimuth deviation for a particular dip and velocity contrast depends on the azimuth but is larger for the smaller angles of incidence, i.e., for larger Δ 's. An SV wave incident on an inclined interface at some azimuth different from the dip direction will have its polarization direction shifted out of the vertical plane. The projection of the rectilinear motion on to a horizontal plane (say, the surface) will then be elliptical, the semi-minor axes of the ellipses being larger for larger Δ 's.

The dip of the Alberta sediments is less than 1° toward the SSW. The gross crust is not well enough known to determine a possible dip on the Moho. and intermediate interfaces, although it might be expected that the crust would thicken slightly toward the root of the Rocky Mountains. The ellipses with the larger semi-minor axes shown in Figure 36 would require dips of the order

of 10° . Although such dips cannot be postulated for the Alberta crust, Ellis and Basham (1967) do observe azimuth deviations for some of the events as large as 15° . The azimuth deviations, if interpreted entirely in terms of dipping interfaces, would also require dips of the order of 10° . Niazi (1966) does report localized Moho dips of about 8° under Arizona. Recently Kanasevich and Jones (1967) have reported dips of 20° on a reflecting horizon at a depth of 30 km in southern Alberta.

An additional contributing factor to elliptical trajectories during onset would be the generation of SH by small scale inhomogeneities at the interfaces or within the upper layers.

CHAPTER IX

SUMMARY AND CONCLUSIONS

9-1 Summary

The events recorded during the Alberta Experiment have been subjected to a detailed study in the time domain using both visual observation and polarization filtering of the records to identify the types of seismic motion present in the P phase and about 25 seconds of its coda. A P-detection polarization filter of the REMODE class has been designed and shown successful in enhancing segments of the records containing strong P motions. The principal findings can be summarized as follows.

1. The general appearance of a P phase at a distant station depends on the nature of the source of the event. Although the more distant events show slightly longer period wave motion, most of the variation in period among events is probably related to variations in source functions. The length of duration of strong signal after the P onset depends on the depth of focus of the event, the main contribution to extended strong motion resulting from early arriving secondary phases for the shallow events.

2. The P displacement radiation pattern of a fault-

type earthquake mechanism governs the pP/P amplitude ratio. Appropriate orientations of the displacement pattern can, in theory, explain much of the observed pP/P amplitude ratios.

3. Except for those events distorted by background noise all station pairs of vertical records of teleseismic events show very similar wave motion throughout the 25 second P coda.

4. The station pairs of radial records show a general similarity only in those record segments containing strong P motion.

5. pP phases have been identified for 23 of the 40 earthquakes. On the basis of observed pP-P times and using source crustal columns of Menard (1967), the focal depth of 8 of these events has been adjusted. The adjusted depths and those not requiring adjustment are believed to be accurate to better than ± 15 km.

6. sP phases have been identified on 9 events.

7. The PS_4 converted phase has been observed at the calculated time following six strong P phases. The PS_4/P amplitude ratio is found to be between 0.2 and 0.3.

8. SV motion, and particularly the PS_1 converted phase, is present on all records of the suite. The PS_1/P amplitude ratios are observed to vary between 0.2 and 1.5. The strongest PS_1 phases appear on the records of the nearest events.

9. Transverse motion attributed to scattering by

crustal inhomogeneities appears as a slow buildup on all seismograms.

10. Some events have unidentified transverse motion distorting the horizontal particle trajectories very soon after the P onset.

9-2 Conclusions

Conclusions which relate to three fields of seismology can be drawn from the results of this study. These three fields are: crustal deconvolution in the short period range, distinguishing underground explosions from natural seismic events, and the fundamental problem of P coda composition.

During the Alberta experiment recordings were made of teleseismic events over a varying crustal section. Ellis and Basham (1967) show the numerous difficulties inherent in relating the theoretical response of the crustal layering at each station to observed P phase spectra. The results of Chapter VI suggest that, within the resolution of visual inspection of the seismograms of this suite, the different crustal layering beneath each of the four stations makes a very similar contribution to the vertical component of the recorded signal for teleseismic events. The radial components of the recorded signals show considerable variation among the stations. The major contribution to the radial differences can be

related to different amplitudes and different time-delayed SV waves generated within the crustal layering. This alone, however, does not explain the frequency domain difficulties because the theoretical transfer function used takes into account all P and SV reflected and refracted waves generated within the assumed crustal model. But two other factors which have been observed here in the time domain may complicate the frequency domain studies. The first is the excessive amplitude of some PS converted phases which is not predicted theoretically; this will contribute principally radial motion which is not included in the horizontal transfer function. The second factor is the presence of large amplitude pP and sP phases for the shallow events within the record segment used in the frequency domain calculation. Although the extra compressional phases themselves should not contribute difficulties (they will make an additive contribution to both components of the transfer function), each will have its associated PS converted phases making contributions discussed as factor one. In addition, if the frequency-analysed record segment contains a strong pP or sP phase near the end of the segment the complete wave transfer may not be represented in the segment, i.e., some important reverberations and refractions which will be included in the theoretical record will be omitted from the experimental record.

If the depth of occurrence of all seismic events could be determined accurately the problem of distinguishing

underground explosions from earthquakes would be greatly simplified. The accuracy of focal depth assignment (± 15 km) for shallow events discussed in Chapter VII is an improvement of significance to explosion detection studies. Most underground explosions have been, and in the future probably will be, detonated on land masses, either islands or continents. This means that the error due to estimated ocean depth discussed in Section 7-3 will not apply. Further, the crustal column at the source, particularly for continental epicenters, will be known to a higher degree of accuracy than those used in Chapter VII. Careful attention to these details might improve the accuracy of calculated pP-P times to within ± 0.5 seconds. The observed pP-P times were assumed accurate to within ± 2 seconds. Improvements in the P-detection processor (suggestions for which will be made in Chapter X) may bring these limits down to about ± 0.5 seconds. If these limits of accuracy were attainable focal depths of earthquakes exhibiting pP phases could be determined to within ± 5 km, an accuracy sufficient to distinguish all but the very small earthquakes from underground explosions. However, there is a theoretical consideration which has not been discussed here. In dealing with pP, consideration has to be given to the curvature of the wave front for the upward passage of the compressional wave from a shallow source. If the plane wave assumption is not valid in the frequency range of the recording the amplitude of pP phases may be greatly reduced.

PS converted waves have been utilized for crustal studies by a number of Russian and American researchers (see Cook et al, 1962) using both explosive and natural seismic sources. In theory the thickness of a single crustal layer can be determined by observing the difference in time of the arrival of the primary P wave and the arrival of the PS converted wave, provided the compressional velocity in the layer is known approximately. The Alberta records were shown in Chapter VIII to be composed in part of large amplitude PS converted phases, which suggests the feasibility of similar studies in Alberta and elsewhere using teleseismic recordings. The difficulty in accurately timing the PS converted phases shown in Figures 34 and 35 would be the limiting factor. PS_4 is often weak and distorted by the coda of the primary P signal burst; PS_1 , although strong, is completely superimposed on the primary P signal. Careful observation of particle motion trajectories might enable accurate timing of the PS converted phases.

CHAPTER X

SUGGESTIONS FOR FURTHER RESEARCH

10-1 Bandpass and Polarization Filtering

Prior to each of the studies reported in this thesis the records were bandpass filtered using BP-1 shown in Figure 4. On many of the events the filter was not sufficiently narrow to eliminate all of the background noise. If further studies are to be conducted using the records of the Alberta Experiment it is suggested that a group of bandpass filters be designed for application to the records as required. In some cases to provide good signal records the pass band may have to be very narrow, but only signal which is inseparable from the noise will be lost.

The P-D polarization filter described in Chapter IV requires much additional study. The effect on the output of varying the window length and maximum lag should be considered in more detail. Considerable improvement in processing might be made if an optimum window length and maximum lag were chosen on the basis of the dominant period of motion in each event. The theoretical response of all

of the polarization filters in the REMODE class requires further consideration.

The REMODE 5 filter with variable selectivity has not been discussed in Chapter IV but this filter may prove to be the most useful in the REMODE class. The important difference between it and the P-D processor is its ability to detect rectilinear signals arriving from within a narrow arc. The most important suggestion for further research to appear in this chapter is that the REMODE 5 be programmed and applied to the events of the Alberta Experiment or others of similar quality.

10-2 pP and Focal Depth Assignment

Improvement in signal quality using the suggested changes in bandpass and polarization filtering would no doubt enable identification of pP phases to be made on some of the events considered too noisy in this study. Application of a REMODE 5 type processor might improve the pP-timing accuracy to an extent which would enable considerable improvement in focal depth assignment to the shallower earthquakes. The possible improvement in focal depth determination suggested in Section 9-2 should be attempted using a suite of shallow earthquakes from a continental or oceanic region with a well defined crustal structure.

10-3 PS Converted Phases

PS converted phases make a significant contribution to seismograms of teleseismic events. The importance of these events on the Alberta records has not been adequately explored; the observed amplitudes in particular should be compared to theoretically expected values.

Particle motion plots showing PS_1 motion have been presented for four of the quietest events (Figure 35). PS_1 motion of similar amplitude is present on all events, although some of the events will require narrow bandpass filtering to remove background noise. The Alberta records are available in digital form and provide the opportunity of studying PS converted phases for a wide range of epicentral distances.

REFERENCES

- Atomic Weapons Research Establishment, The detection and recognition of underground explosions, A special report to the United Kingdom Atomic Energy Authority, December, 1965.
- Bancroft, A.M., and P.W. Basham, An FM magnetic tape recording seismograph, Pub. Dom. Obs., 35, 195-217, 1967.
- Polt, B.A., The velocity of seismic waves near the earth's center, Bull. Seism. Soc. Am., 54, 191-208, 1964.
- Cook, K.L., S.T. Algermissen, and J.K. Costain, The status of PS converted waves in crustal studies, J.G.R., 67, 4769-4778, 1962.
- Costain, J.K., K.L. Cook, and S.T. Algermissen, Amplitude, energy, and phase angles of plane SV waves and their application to earth crustal studies, Bull. Seism. Soc. Am., 53, 1039-1074, 1963.
- Cumming, G.L., and E.R. Kanasewich, Crustal structure in western Canada, Final report for AFCRL-66-519, Department of Physics, University of Alberta, June, 1965.
- Ellis, A.M., and P.W. Basham, Crustal characteristics from short period P waves (provisional title), in preparation, 1967.
- Ewing, J.M., W.S. Jardetzky, and F. Press, Elastic waves in layered media, McGraw-Hill, 1957.
- Garland, G.D., and R.A. Burwash, Geophysical and petrological study of the Precambrian of central Alberta, Canada, Bull. Am. Assoc. Pet. Geol., 43, 700-806, 1959.
- Griffin, J.N., Application and development of polarization (REMODE) filters, Seismic Data Laboratory Report No. 141, Earth Sciences Division, Teledyne, Inc., April, 1966a.

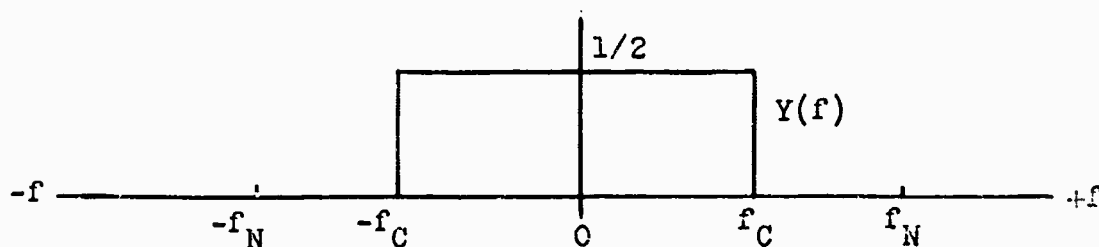
- Griffin, J.N., REMODE signal/noise tests in polarized noise, Seismic Data Laboratory Report No. 162, Earth Sciences Division, Teledyne, Inc., September, 1966b.
- Gutenberg, B., and C.F. Richter, On seismic waves, Gerlands Beitr. z. Geophys., 45, 280-350, 1935.
- Gutenberg, B., and C.F. Richter, Materials for the study of deep-focus earthquakes, Bull. Seism. Soc. Am., 26, 341-390, 1936.
- Heezen, B.C., and M. Tharp, Tectonic fabric of the Atlantic and Indian Oceans and continental drift, Phil. Trans. Roy. Soc. London, A, 258, 90-106, 1965.
- Howell, B.F., P.M. Lavin, R.J. Watson, Y.Y. Cheng, and J.L. Lin, Method for recognizing repeated pulse sequences in a seismogram, J.G.R., 72, 3225-3232, 1967.
- Ichikawa, M., and P.W. Basham, Variations in short-period records from Canadian seismograph stations, Can. J. Earth Sci., 2, 510-542, 1965.
- Kanasewich, E.R. and R.M. Clowes, Geophysical investigation of the earth's crust and upper mantle in Alberta (abstract), Physics in Canada, 23, 106.
- Key, F.A., Signal-generated-noise recorded at the Eskdalemuir seismometer array station, Bull. Seism. Soc. Am., 57, 27-37, 1967.
- Lanczos, C., Numerical analysis, Pitman, 1957.
- Lehmann, I., The travel times of the longitudinal waves of the Logan and Blanca atomic explosions and their velocities in the upper mantle, Bull. Seism. Soc. Am., 52, 519-526, 1962.
- Menard, H.W., Transitional types of crust under small ocean basins, J.G.R., 72, 3061-3073, 1967.
- Mims, C.H., and R.L. Sax, Rectilinear motion detection (REMODE), Seismic Data Laboratory Report No. 118, Earth Sciences Division, Teledyne, Inc., March, 1965.
- Niazi, M., Corrections to apparent azimuths and travel-time gradients for a dipping Mohorovicic discontinuity, Bull. Seism. Soc. Am., 56, 491-509, 1966.
- Richards, T.C., and D.J. Walker, Measurement of the thickness of the earth's crust in the Alberta plains of western Canada, Geophysics, 24, 252-284, 1959.

- Sax, R.L., Feasibility of linear polarization measurements for detecting and measuring seismic body waves, Seismic Data Laboratory Report No. 163, Earth Sciences Division, Teledyne, Inc., September, 1966.
- Shimshoni, M., and S.W. Smith, Seismic signal enhancement with three-component detectors, *Geophysics*, 29, 664-671, 1964.
- Stevens, A.E., S-wave focal mechanism studies of the Hindu Kush earthquake of July 6, 1962, *Can. J. Earth Sci.*, 3, 367-387, 1966.
- Sykes, L.R., Mechanism of earthquakes and nature of faulting on the mid-oceanic ridges, *J.G.R.*, 72, 2131-2153, 1967.
- Travis, H.S., Interpolated Jeffreys and Bullen seismological tables, Technical Report No. 65-35, The Geotechnical Corporation, May, 1965.
- Utsu, T., Variations in spectra of P waves recorded at Canadian Arctic seismograph stations, *Can. J. Earth Sci.*, 3, 597-621, 1966.
- Wu, F.T., and W.J. Hannon, PP and crustal structure, *Bull. Seism. Soc. Am.*, 56, 733-747, 1966.

APPENDIX A

THE LANCZOS NUMERICAL FILTER

Ideally, one would like a numerical filter which, in the frequency domain, is infinitely sharp. For example, for a low-pass filter the desired response, $Y(f)$, is illustrated in the following diagram,



where f_N is the Nyquist frequency and f_C is the corner frequency of the low-pass filter. The time domain filter function, $W(t)$, is given by the Fourier transform of $Y(f)$, i.e.,

$$W(t) = \int_{-\infty}^{+\infty} Y(f) e^{i\omega t} df = 1/2 \int_{-f_C}^{+f_C} e^{i\omega t} df.$$

This reduces to

$$W(t) = \frac{\sin 2\pi f_C t}{2\pi t}, \quad (A1)$$

which is the "diffraction function". If the filter function, $W(t)$, is truncated to a finite length with a "boxcar", ripples (Gibbs oscillations) will appear on the corresponding response, $Y_{\Omega}(f)$. Lanczos^{*} (1957) devised a method by which the Gibbs oscillations can be smoothed.

Consider the expansion of an even function $A(f)$ in the interval $(-\pi, \pi)$, i.e., let

$$f_N = \pi = \frac{1}{2\Delta t},$$

then
$$\Delta t = \frac{1}{2\pi}$$

and
$$2\pi f t = 2\pi f k \Delta t = f k,$$

where k is the time sample index. Truncating the expansion at n terms with a length $T = n\Delta t$ yields

$$A_n(f) = \sum_{k=-n}^n a_k \cos kf \tag{A2}$$

where a_k , the expansion coefficients, are given by

$$a_k = \frac{1}{2\pi} \int_{-\pi}^{\pi} A(f) \cos(kf) df.$$

Since $A_n(f)$ is $A(f)$ truncated at n terms, the ripple remaining on $A_n(f)$ will be due to the highest order term, i.e., the

^{*}Lanczos, C., Numerical Analysis, Pitman, 1957.

n^{th} term. If Δf is the "period" of the n^{th} term ripple then

$$\Delta f = \frac{2\pi}{n} .$$

Therefore, if $A_n(f)$ is to be smoothed, it should be smoothed over the interval $\Delta f = \frac{2\pi}{n}$. The smoothed frequency response is given by

$$\overline{A}_n(f) = \frac{n}{2\pi} \int_{f - \frac{\pi}{n}}^{f + \frac{\pi}{n}} A_n(\xi) d\xi . \quad (A3)$$

Substituting (A2) into (A3), integration and simplification yields

$$\overline{A}_n(f) = \sum_{k=-n}^n \left[a_k \frac{\sin k \frac{\pi}{n}}{k \frac{\pi}{n}} \right] \cos kf ,$$

i.e., the coefficients in the expansion of $A_n(f)$ when multiplied by a second diffraction function become the coefficients in the expansion of $\overline{A}_n(f)$.

This smoothing process can be applied to the low-pass filter. If $W(t)$ given by (A1) is truncated at $\tau = n\Delta t$, the ripple on $Y_G(f)$ will have a "period" of $\Delta f = \frac{2\tau}{n}$. Putting (A1) in digital form, i.e., $t = k\Delta t$, and defining f_C in units of a fraction of the Nyquist frequency, f_K , the filter function \overline{W}_k which will produce a smoothed frequency response $\overline{Y}_G(f)$ will be given by

$$\overline{W}_k = \frac{\sin \pi k f_K}{2\pi k \Delta t} \left(\frac{\sin k \Delta t}{k \Delta t} \right), \quad |k| \leq n. \quad (\text{A4})$$

That is, the original diffraction function, (A1), is truncated with the center lobe of another diffraction function.

The bandpass filter shown in Figure 4 is the response of a filter constructed from the convolution of a high-pass and a low-pass filter function, both designed on the basis of equation (A4). The Gibbs oscillations on the corners are almost non-existent and the first side lobe rises to about 1 per cent of the peak.

Truncating functions other than a diffraction function center lobe can be used to produce a smoothed frequency response. For example, the center lobe of both a Hamming and Hanning^{*} window have been tested. Both Hamming and Hanning truncation produce slightly less sharp cut-off than the Lanczos truncation, but have a smaller first side lobe. In any particular application the corner sharpness requirement should be weighed against the side lobe height to decide which truncation function should be used.

^{*}for definitions see, for example, Blackman, R.B., and J.W. Tukey, The measurement of power spectra, Dover, 1959.

APPENDIX B

LISTING OF FORTRAN IV SUBROUTINE "REMODE"

```

SUBROUTINE REMODE (LAGS,LWIN,NTOT,Z,R,FZ,FR,KEY)
C
C GENERAL ROUTINE FOR REMODE 2, 2A, 3, 3A
C
C RESTRICTED TO 610 DATA POINTS PER SERIES AND
C 15 CROSS-CORRELATION LAGS
C
C LAGS = NUMBER OF LAGS
C LWIN = WINDOW LENGTH IN SAMPLES
C NTOT = TOTAL NUMBER OF DATA POINTS PER SERIES
C Z = VERTICAL INPUT SIGNAL
C R = RADIAL INPUT SIGNAL
C FZ = VERTICAL OUTPUT SIGNAL
C FR = RADIAL OUTPUT SIGNAL
C
C KEY DETERMINS TYPE OF REMODE FILTER--
C KEY=1..... REMODE 2
C KEY=2..... REMODE 2A
C KEY=3..... REMODE 3
C KEY=4..... REMODE 3A
C
DIMENSION Z(610),R(610),FZ(610),FR(610),RR(610),ZZ(610),
1RZ(15,610)
DO 10 L=1,LAGS
NT=NTOT-L+1
K=L-1
DO 10 I=1,NT
J=K+I
10 RZ(L,I)=R(I)*Z(J)
LEND=NTOT-LAGS
LW2=LWIN/2
GO TO (30,30,20,20),KEY
20 L2=LEND-LW2
DO 25 I=LAGS,L2
ZZ(I)=Z(I)*Z(I)
25 RR(I)=R(I)*R(I)
30 DO 70 II=LAGS,LEND
SUM=0.
J3=II+LW2
J1=II-LW2

```

```

GO TO (34,33,34,33),KEY
33 IF (RZ(1,II).GE.0.) GO TO 34
    FZ(II)=0.
    FR(II)=0.
    TO TO 70
34 GO TO (37,37,35,35),KEY
35 Z1=0.
    R1=0.
    DO 36 J=II,J3
        Z1=Z1+ZZ(J)
36 R1=R1+RR(J)
    SIG=SQRT(1./(Z1*R1))
37 DO 40 K=J1,J3
40 SUM=SUM+RZ(1,K)
    SZ=Z(II)*SUM
    SR=R(II)*SUM
    LLL=LAGS-1
    DO 60 I=1, LLL
        I2=II-I
        I3=II+I
        SSZ=Z(I2)+Z(I3)
        SSR=R(I2)+R(I3)
        I1=I+1
        J2=J3-I
        RED=0.
        DO 50 J=J1,J2
50 RED=RED+RZ(I1,J)
        SZ=SZ+SSZ*RED
50 SR=SR+SSR*RED
    GO TO (65,65,66,66),KEY
65 FZ(II)=SZ
    FR(II)=SR
    GO TO 70
66 FZ(II)=SZ/SIG
    FR(II)=SR/SIG
70 CONTINUE
    I1=LAGS-1
    I2=LEND+1
    DO 80 I=1, I1
        FZ(I)=0.
80 FR(I)=0.
    DO 90 I=I2,NTOT
        FZ(I)=0.
90 FR(I)=0.
    RETURN
    END

```

DOCUMENT CONTROL DATA - R & D

(Security classification of title, body of abstract and indexing annotation must be entered when the overall report is classified)

1. ORIGINATING ACTIVITY (Corporate author) Arctic Institute of North America 3458 Redpath Street, Montreal 25, P.Q.	2a. REPORT SECURITY CLASSIFICATION Unclassified
	2b. GROUP

1. REPORT TITLE
TIME DOMAIN STUDIES OF SHORT PERIOD TELESEISMIC P PHASES

4. DESCRIPTIVE NOTES (Type of report and inclusive dates)
Scientific Final

5. AUTHOR(S) (First name, middle initial, last name)
Basham, Peter W.

8. REPORT DATE September 1967	7a. TOTAL NO. OF PAGES 145	7b. NO. OF REFS 30
---	--------------------------------------	------------------------------

8a. CONTRACT OR GRANT NO. AF-AFOSR-702-67 b. PROJECT NO. 8652 c. 6250601R d.	9a. ORIGINATOR'S REPORT NUMBER(S)
	9b. OTHER REPORT NO(S) (Any other numbers that may be assigned this report) AFOSR 67-2519

10. DISTRIBUTION STATEMENT
Distribution of this Document is Unlimited

11. SUPPLEMENTARY NOTES TECH, OTHER	12. SPONSORING MILITARY ACTIVITY Air Force Office of Scientific Research (SREG) 1400 Wilson Blvd. Arlington, Virginia 22209
---	---

13. ABSTRACT

Forty-one seismic events recorded on the plains of western Alberta are subjected to a detailed study in the time domain. A "P-detection" time-varying polarization filter is described and applied to the events to detect segments of strong P motion in the first 25 seconds of the P phase coda.

On seismograms of 23 events, 12 of which have reported depths shallower than 40 km, pP phases have been identified; sP phases have been identified on 9 of the events. Considering estimated accuracies of observed and calculated pP-P times, assigned focal depths are accurate to within ± 15 km.

A varying upper crustal structure is found to make a similar contribution to the vertical components of the P phase for stations at separations up to 160 km. The radial components at these stations are similar only during time segments of strong P motion. The dissimilarity in other time segments of the radial components is attributed to different amplitudes and time-delays for PS converted phases generated at crustal layer interfaces. The largest PS converted phase, with amplitude up to about 1.5 that of P, is generated at the base of the sediments. A small number of PS converted phases generated at the base of the crust have been identified.

14 KEY WORDS	LINK A		LINK B		LINK C	
	HOLE	WT	HOLE	WT	HOLE	WT
Short period P phases bandpass filtering polarization filtering source radiation pattern pP and sP phases PS converted phases transverse motion						